

UNIVERSITÉ DE LILLE



Thèse en cotutelle

Présentée en vue
d'obtenir le grade de

DOCTEUR

En

Spécialité : Informatique, Automatique

Par

Deyao SHEN

DOCTORAT délivré par l'Université de Lille et l'Université de Donghua

Titre de la thèse :

**AI based fatigue assessment system for athletes using smart textile
wearables**

**Système d'évaluation de la fatigue basé sur l'IA pour les athlètes
utilisant des vêtements intelligents**

Soutenue le 23/09/2024 devant le jury d'examen :

Imed KACEM	Professeur	Université de Lorraine	Rapporteur
Florence RAZAN	Professeure	École Normale Supérieure de Rennes	Rapportrice
Marie-Ange BUENO	Professeure	ENSISA-Université de Haute-Alsace	Examinatrice et présidente
Hayriye GIDIK	Maître de Conférences, HDR	JUNIA Grande école d'ingénieurs	Examinateur
Xuyuan TAO	Maître de Conférences, HDR	ENSAIT-Université de Lille	Directeur de thèse
Jianping WANG	Professeure	Université de Donghua	Co-directrice de thèse
Vladan KONCAR	Professeur	ENSAIT-Université de Lille	Invité

Thèse préparée dans le Laboratoire **GEMTEX** – Laboratoire de Génie et Matériaux Textiles

École Doctorale : MADIS - Science Pour l'Ingénieur Lille Nord-de-France

Acknowledgments

As I reflect on the past two years at GEMTEX Laboratory, I am struck by how swiftly time has flown. This journey has been one of immense growth, both professionally and personally. Through my chosen research topic, I have had the opportunity to delve into diverse fields of knowledge and acquire valuable practical skills. Moreover, I have gained a deep appreciation for the unique characteristics of French higher education.

First, I would like to express my profound gratitude to my doctoral advisors, Associate Professor Tao and Professor Koncar. Your rigorous scientific approach and unwavering commitment to excellence have been instrumental in guiding me through this challenging doctoral project. Your vast knowledge and dedication to the pursuit of truth have set an inspiring example that I will carry with me throughout my career.

I am also deeply indebted to my co-supervisor, Professor Wang, from Donghua University. It was your recommendation and steadfast support that enabled me to apply for and receive the scholarship from the China Scholarship Council, granting me this invaluable opportunity to pursue my doctoral studies in France. Your patience and encouragement have been a constant source of strength, and I will forever cherish your mentorship.

To my parents, words cannot express my gratitude. You have given me life, nurtured me through the years, and selflessly supported me in times of difficulty. Your unconditional love and support have been the foundation upon which I have built my achievements.

Lastly, I would like to extend my heartfelt thanks to my fellow doctoral candidates at GEMTEX Laboratory: Dr. Wang Zhujun, Dr. Xing Bo, Mr. Marc-Junior Nkengue, Miss. Wu Hanhan, Mr. Hu Jian, Miss. Yang Wen, and Dr. Zhang Mengyun. Your assistance and camaraderie over these past two years have been invaluable, and I am deeply appreciative of the support you have provided throughout my studies.

This journey would not have been possible without the collective support of all those mentioned above. Thank you for being an integral part of this significant chapter in my life.

Abstract

This doctoral dissertation report presents an innovative fatigue assessment system for athletes, leveraging advancements in smart textile wearables to develop an intelligent garment monitoring system (IGS). The primary focus was on the design, fabrication, and evaluation of 3D textile biopotential electrodes, seamlessly integrated into compression garments, enabling real-time monitoring of electrocardiography (ECG) and electromyography (EMG) signals during physical activities.

A meticulous parametric design process was employed to optimize electrode design and configuration, considering critical factors such as diameter, height, and applied pressure, to ensure high-quality signal acquisition while prioritizing user comfort. The intelligent garment system incorporates strategically positioned electrodes, pioneering conductive channel designs, and adjustable fastening mechanisms to maintain a stable electrode-skin interface position and pressure throughout dynamic movements.

The report is structured into five comprehensive chapters. The introductory chapter outlines the background, motivation, objectives, and scope of the study, emphasizing the significance of wearable technology in sports science and biomedical engineering. Chapter 2 provides a thorough review of the current state-of-the-art, covering bioelectric signals, fatigue assessment methods, smart textiles, and AI techniques in sports applications.

Chapter 3 is dedicated to the design, fabrication, and evaluation processes of the intelligent garment system, including impedance tests using PVA artificial skin and real-world evaluations in cycling sports. Chapter 4 focuses on the rigorous testing and analysis of the system, describing the experimental setup, data preparation processes, and the application of advanced AI algorithms. State-of-the-art deep learning models, including Temporal Convolutional Networks (TCN), Gated Recurrent Units (GRU),

Long Short-Term Memory (LSTM), and Transformer architectures, were meticulously applied to the processed data to accurately predict fatigue levels.

Chapter 5 summarizes the key findings, contributions, and implications of the research, discusses limitations, and proposes directions for future research. The study underscores the importance of continuous improvement and adaptation in enhancing intelligent garment systems for sports monitoring.

The findings demonstrate the efficiency of the proposed fatigue assessment system in providing reliable, real-time insights into an athlete's fatigue state, offering invaluable information for optimizing training regimens, preventing injuries, and enhancing overall athletic performance. This research marks a significant breakthrough by integrating advanced textile engineering, sensor technology, and machine learning techniques into a unified smart compression cycling garment. For the first time, it enables synchronized monitoring of ECG and EMG signals during cycling. This advancement is supposed to help coaches and athletes adjust training plans in real-time, reducing the risk of fatigue-related injuries.

Résumé

Ce rapport de thèse de doctorat présente un système innovant d'évaluation de la fatigue pour les athlètes, en s'appuyant sur les avancées en matière de textiles intelligents pour développer un système intelligent de surveillance des vêtements (IGS). L'accent a été mis sur la conception, la fabrication et l'évaluation d'électrodes biopotentielles textiles 3D, intégrées de manière transparente dans des vêtements de compression, permettant une surveillance en temps réel des signaux d'électrocardiographie (ECG) et d'électromyographie (EMG) pendant les activités physiques.

Un processus de conception paramétrique méticuleux a été utilisé pour optimiser la conception et la configuration des électrodes, en tenant compte de facteurs critiques tels que le diamètre, la hauteur et la pression appliquée, afin de garantir une acquisition de signaux de haute qualité tout en privilégiant le confort de l'utilisateur. Le système de vêtement intelligent intègre des électrodes stratégiquement positionnées, des canaux conducteurs de conception novatrice et des mécanismes de fixation réglables afin de maintenir une position et une pression stables de l'interface électrode-peau tout au long des mouvements dynamiques.

Le rapport est structuré en cinq chapitres détaillés. Le chapitre d'introduction présente le contexte, la motivation, les objectifs et la portée de l'étude, en soulignant l'importance de la technologie portable dans les sciences du sport et l'ingénierie biomédicale. Le chapitre 2 présente un examen approfondi de l'état actuel des connaissances, couvrant les signaux bioélectriques, les méthodes d'évaluation de la fatigue, les textiles intelligents et les techniques d'intelligence artificielle dans les applications sportives.

Le chapitre 3 est consacré aux processus de conception, de fabrication et d'évaluation du système de vêtement intelligent, y compris les tests d'impédance utilisant la peau artificielle PVA et les évaluations en situation réelle dans les sports

cyclistes. Le chapitre 4 se concentre sur les tests rigoureux et l'analyse du système, décrivant la configuration expérimentale, les processus de préparation des données et l'application d'algorithmes d'IA avancés. Des modèles d'apprentissage profond de pointe, notamment des réseaux convolutifs temporels (TCN), des unités récurrentes gérées (GRU), des mémoires longues à court terme (LSTM) et des architectures Transformer, ont été méticuleusement appliqués aux données traitées afin de prédire avec précision les niveaux de fatigue.

Le chapitre 5 résume les principales conclusions, contributions et implications de la recherche, discute des limites et propose des orientations pour la recherche future. L'étude souligne l'importance d'une amélioration et d'une adaptation continues pour améliorer les systèmes de vêtements intelligents destinés à la surveillance du sport.

Les résultats démontrent l'efficacité du système d'évaluation de la fatigue proposé, qui fournit des informations fiables et en temps réel sur l'état de fatigue d'un athlète, informations précieuses pour optimiser les programmes d'entraînement, prévenir les blessures et améliorer les performances athlétiques globales. Cette recherche marque une avancée significative en intégrant l'ingénierie textile avancée, la technologie des capteurs et les techniques d'apprentissage automatique dans un vêtement cycliste de compression intelligent unifié. Pour la première fois, ce vêtement permet une surveillance synchronisée des signaux ECG et EMG pendant le cyclisme. Cette avancée est censée aider les entraîneurs et les athlètes à ajuster les plans d'entraînement en temps réel, réduisant ainsi le risque de blessures liées à la fatigue.

Contents

CHAPTER 1 Introduction.....	1
1.1 Context.....	1
1.2 Objectives and Scope of the Study	6
1.3 Strategy to achieve the objectives.....	8
1.4 Structure of the Thesis.....	9
CHAPTER 2 State of the Art	12
2.1 Bioelectric Signals.....	12
2.1.1 Electrocardiography (ECG)	14
2.1.2 Electromyography (EMG).....	17
2.2 Fatigue Assessment.....	20
2.2.1 Fatigue Definition.....	20
2.2.2 Borg Scale	21
2.2.3 Fatigue Evaluation for Sports Activities	22
2.3 Smart Textiles for Sports Activities	23
2.3.1 Bioelectric Textile Electrodes.....	23
2.3.2 Data Treatment System for E-textile.....	31
2.4 AI Methods for Bioelectric signals.....	33
2.5 Overview of Current Sports Monitoring Commercial Intelligent Garment System.....	37
2.6 Conclusion.....	41
CHAPTER 3 Design, Fabrication, and Evaluation of Intelligent Garment Systems	45
3.1 Design, Fabrication, and Evaluation of 3D Textile Biopotential Electrodes	48
3.1.1 Design and Fabrication of Textile Electrodes	48
3.1.2 Evaluation of Textile Electrodes	56
3.2 Fabrication of the Intelligent Garment.....	72
3.2.1 Garment Design and Fabrication.....	72
3.2.2 Hardware Integration	77
3.2.2 Software Development	80
CHAPTER 4 Testing and Analysis of Intelligent Garment System in Cycling Sport.....	83

4.1 Test Setup and Methodology	83
4.2 Data Processing and Analysis	86
4.3 Data Preparation for Deep Learning Model	97
4.3.1 ECG Data.....	97
4.3.2 EMG Data.....	99
4.3.3 Input data for machine learning.....	101
4.4 Application of Deep Learning Model for Predicting.....	103
4.4.1 Temporal Convolutional Network (TCN).....	103
4.4.3 Transformer.....	112
4.4.4 Long Short-Term Memory (LSTM).....	117
4.5 Results and Discussion	122
CHAPTER 5 Conclusion.....	124
5.1 Summary of Finding	124
5.2 Contributions of the Study	125
5.3 Limitations and Future Work.....	127

CHAPTER 1 Introduction

1.1 Context

In recent years, the sportswear industry has experienced significant growth due to increasing health awareness and rising participation in sports activities. The trend towards worldwide fitness has become a major driver of the sports garment market, with consumer demand increasingly favoring more specialized and personalized sportswear. Statistics indicates that the popularization of nationwide fitness has catalyzed the emergence of activities such as trail running and road cycling. Furthermore, the expansion of sporting events and the corresponding increase in the number of subjects are anticipated to sustain and potentially amplify the market demand for sports apparel continuously.

Due to the characteristics of certain long-duration sports, such as road cycling and marathon running, involving extended periods of activity and high-intensity exertion, athletes are at risk of experiencing muscle cramps that lead to muscle fatigue and sometimes serious injuries. Muscle fatigue can negatively impact athletic performance and grade, and in severe cases, can cause musculoskeletal injuries. These potential issues present significant concerns for sports enthusiasts. To address these risks, wearable monitoring garment has become an essential solution. These intelligent garments can provide real-time tracking of bioelectric signals and other key indicators of athletes during exercise, helping athletes and coaches identify the exact timing of muscle fatigue. This enables the creation of more effective training plans and better energy management, preventing sports injuries caused by excessive fatigue. By continuously monitoring physiological data, this technology can alert athletes to early signs of fatigue, allowing them to make timely adjustments to their activity levels. The application of wearable monitoring garment not only improves performance, but also plays a critical role in injury prevention, ensuring that athletes can train and compete more safely and effectively.

Based on the aforementioned context, athletes and sports enthusiasts require flexible wearable devices to effectively monitor their exercise fatigue and performance in real-time, providing timely feedback on physical conditions to prevent sports injuries. The advent and rapid development of smart wearable technology offers new avenues for real-time monitoring of athletic status for both, professional athletes and sports amateurs. However, traditional wearable monitoring devices, such as smartwatches, fitness trackers, and chest strap heart rate monitors, are often rigid or external, lacking portability, resulting in discomfort during use and a disconnect with the actual feeling of motion during competition. These devices fail to achieve seamless, unobtrusive monitoring and suffer from poor real-time adherence between sensors and muscles during activity, affecting signal stability. In the field of scientific sports training and sports medicine, traditional sports physiological monitoring equipment had problems such as significant material rigidity, poor portability, and low stability of fit. These issues made it more challenging to achieve the function of real-time acquisition of human bioelectric signals during long-time sports and had been a problem that needed to be solved. In addition, problems such as signal noise and motion artifacts also vastly reduce the reliability of physiological exercise monitoring.

Increasingly sophisticated textiles, materials, and microelectronics have enabled wearable technology to be widely accessible and used in diverse ways in recent years[1, 2]. Latest advancements in the field have introduced novel materials and structures that significantly enhance the capabilities of wearable technologies. These include metamaterials for advanced sensing[3], near-zero-index materials for enhanced sensor performance[4], nanoparticles for medical diagnostic applications[5], multi-functional structures offering a metamaterial perspective[6], metasurfaces for surface wave manipulation[7], plasmonics for optical and chiroptical response[8], and graphene-based field-effect transistors for DNA detection[9]. Meanwhile, the miniaturization and integration of signal-monitoring devices into wearable systems are some future development trends[10]. Wearable technologies refer to intelligent electronic devices worn on the body to analyze and transmit various forms of data, such as signals

connected to human bodies and physical activities[11].

As advanced electronic technologies with a real-time signal sensing function, wearable technology can monitor various human bioelectric signals using multiple sensors integrated into the device. In addition to these sensors, wearable technology utilizes advanced algorithms and tools, such as machine learning to process and analyze the collected bioelectric signals. By providing real-time feedback, these algorithms enable the device to influence the wearer's physical and mental state[12], such as heart rate variability, stress levels, and sleep quality. As human bioelectric signals are consistently detected and monitored, and valuable information is abundantly generated, wearable technology allows individuals to track their progress, make informed decisions, and maintain a healthy lifestyle.

Intelligent garment systems (IGS) are a subcategory of wearable technology. IGS are specialized wearables that integrate information technology and microelectronics into clothing. The evolution of IGS has been marked by significant milestones, such as the integration of IoT (Internet of Things) for seamless data transfer and the use of advanced materials like conductive textiles for improved comfort and functionality[13].

IGS refer to clothing or accessories with built-in sensors, electronics, and software to monitor, track or enhance various aspects of human physiology, such as health, performance, or comfort, as shown in Figure 1-1. The architecture of an IGS primarily consists of embedded sensors designed to monitor bioelectric signals. These sensors are interfaced with a controller unit responsible for initial data acquisition and processing. Following initial processing, the acquired data are transmitted to user-specific devices like mobile phones or desktop computers. This transmission can occur through a variety of communication channels, both wired and wireless, with Bluetooth being a commonly employed protocol. Once received, the data can be further uploaded to cloud storage systems for advanced analytical procedures. Examples of IGS products range from smart watches and smart compression garments to smart shoes and smart wristbands. Over the past few years, intelligent garment systems have been one of the hottest research topics as an emerging wearable technology. Among the different IGS, smart

textile wearables in compression garment form containing elastic fibers and yarns, become a promising candidate. These garments are particularly advantageous due to their gradient compression characteristics. They can apply specific mechanical pressure to targeted body areas as needed, stabilizing and supporting underlying tissues, and helping to alleviate discomfort caused by exercise or medical conditions. They offer benefits such as reducing muscle micro-damage, promoting blood circulation, accelerating the removal of metabolic waste, and enhancing comfort. As the applications of compression garments continue to expand, the functional development and application of smart compression garments for physiological monitoring will become a research focus in the future.

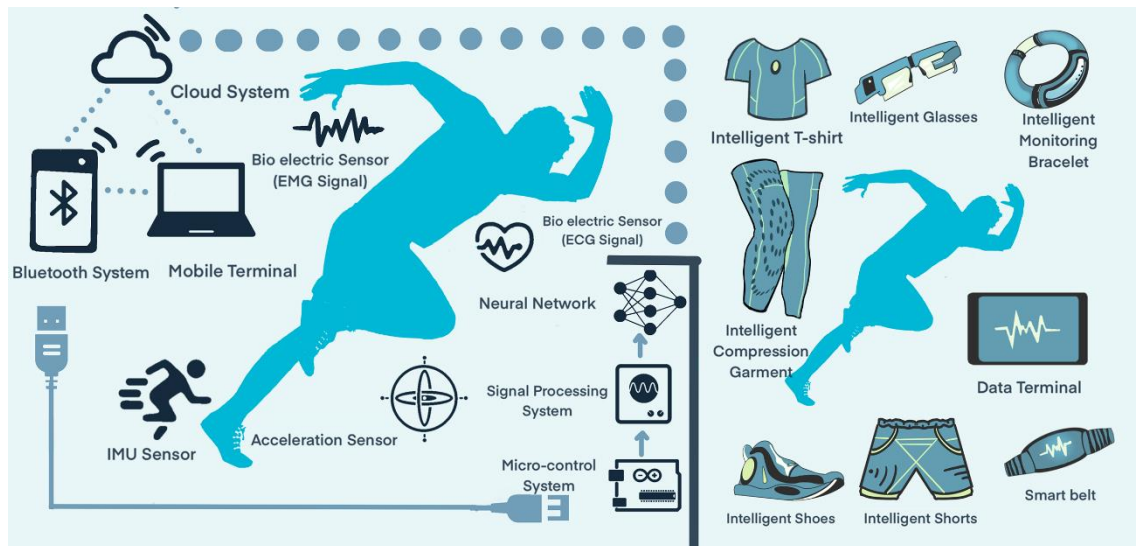


Figure 1-1 Intelligent Garment System (IGS)

The popularity of long-duration sports such as road cycling and marathon running, which involve prolonged periods of high-intensity exertion, underscores the necessity for effective solutions to monitor and prevent exercise-induced muscle fatigue. Traditional fatigue monitoring methods, such as the Borg Scale, rely on subjective self-assessment and lack the precision and real-time feedback essential for optimizing performance and preventing injuries. Furthermore, conventional wearable monitoring devices are often rigid, bulky, and poorly integrated with the body, resulting in discomfort and unreliable data collection during dynamic sports activities. These limitations have impeded the widespread adoption of real-time fatigue monitoring in

sports. The advent of IGS has opened new avenues for the seamless and unobtrusive monitoring of physiological parameters during exercise. By integrating sensors, electronics, and data processing capabilities directly into garments, IGS present a promising solution for real-time fatigue assessment in sports. However, the development of reliable and effective IGS for sports applications faces several challenges, including the need for flexible and comfortable materials, robust sensor integration, and advanced data analysis techniques to extract meaningful insights from complex bioelectric signals.

The objective of this thesis is to develop an intelligent knitted compression garment capable of real-time ECG and EMG monitoring during cycling activities. Additionally, an AI-based predictive model integrated to the IGS will forecast fatigue from physiological signals generated by the IGS sensors is developed. This is aimed at protecting athletes from fatigue-induced injuries and assisting coaches and athletes in designing training programs tailored to the athlete's individual condition.

The study of development of an AI-based fatigue assessment system for athletes using smart textile wearables concerns several interconnected domains:

1. Sports science and performance optimization: Understanding the physiological mechanisms of muscle fatigue and its impact on athletic performance is crucial for developing effective strategies to monitor, prevent, and manage fatigue in sports. The study aims to leverage advanced wearable technologies and data analytics to provide objective, real-time insights into an athlete's fatigue status, enabling evidence-based training and recovery interventions.
2. Biomedical engineering: The development of intelligent garment monitoring systems relies on the integration of textile engineering, sensor technology, and biomedical signal processing. My research explores the design and fabrication of comfortable, high-performance textile electrodes for capturing ECG and EMG signals, as well as the development of hardware and software components for data acquisition, transmission, and analysis.
3. Artificial intelligence and machine learning: AI-based methods, such as deep learning,

have shown great promise in analyzing complex physiological signals and extracting relevant features for fatigue assessment. By applying state-of-the-art AI techniques to the data collected by the intelligent garment system, my study aims to develop accurate and personalized fatigue prediction models that can adapt to individual athletes' characteristics and sport-specific requirements.

4. Wearable technology and IoT: The proliferation of wearable devices and the Internet of Things (IoT) has created new opportunities for continuous, remote monitoring of health and performance metrics. My research leverages these advancements to create a connected, user-friendly system that can seamlessly integrate into an athlete's training routine and provide actionable insights to athletes, coaches, and sports scientists.

1.2 Objectives and Scope of the Study

The main goal of this research is to create an advanced AI-based fatigue assessment system that is built into intelligent garment. This system will provide real-time monitoring of athletes' bioelectric signals, particularly focusing on electrocardiography (ECG) and electromyography (EMG). By using intelligent garment systems (IGS), this study aims to improve the precision and ease of fatigue prediction, which will help boost athletic performance and prevent injuries.

Specific Objectives:

1. 3D textile electrodes developments:

- (1) Design and creation of 3D textile biopotential electrodes.
- (2) Characterization of the skin-to electrode impedance of 3D knitted silver electrodes.

2. Design and Creation of Intelligent Garment System:

- (1) Development of integration of 3D knitted silver electrodes in compression garments and to make sure the garments are comfortable, flexible, and able to collect high-quality signals during physical activity.
- (2) Development of hardware and software systems for data acquisition, transmission and storage.

3. Development of Advanced AI Algorithms for fatigue assessments:

- (1) Realization of fatigue assessments by using developed intelligent garment system for cycling sports.
- (2) Development of AI-based algorithms, such as deep learning models, to process and analyze physiological signals (ECG and EMG).
- (3) Development of predictive models that can accurately predict fatigue levels based on real-time data acquisition.
- (4) Discussion on the challenges related to the stability, comfort, and accuracy of intelligent garment systems during extended physical activities.

Scope of the Study:

1. Sports Science and Performance Optimization:

- (1) Understanding the physiological mechanisms of muscle fatigue and how it affects athletic performance.
- (2) Using wearable technology to provide objective, real-time insights into an athlete's fatigue status, enabling evidence-based training and recovery interventions.

2. Biomedical Engineering:

- (1) Combining textile engineering, sensor technology, and biomedical signal processing to create high-performance reliable textile electrodes.
- (2) Developing the necessary hardware and software components for effective data collection, transmission, and analysis.

3. Artificial Intelligence and Machine Learning:

- (1) Applying cutting-edge AI techniques to analyze complex physiological signals and extract relevant features for fatigue assessment.
- (2) Developing personalized predictive models that can adapt to individual athletes' characteristics and sport-specific requirements.

1.3 Strategy to achieve the objectives

To achieve the objectives of developing an AI-based fatigue assessment system for athletes using smart textile wearables, a detailed and multi-pronged strategy will be employed. This approach integrates advanced materials, innovative design, rigorous testing, and the application of cutting-edge artificial intelligence techniques to ensure the development of a comprehensive and reliable system.

1. Design and Fabrication of Intelligent Garment Systems

(1) Development of 3D knitted silver-plated electrodes:

Electrode Design and Material Selection: Advanced textile engineering methods will be employed to develop 3D knitted silver electrodes. These electrodes will be designed to offer optimal electrical conductivity and mechanical durability. The aim is to integrate these electrodes seamlessly into compression garments, ensuring comfort and flexibility for the user.

Optimization and Testing: A systematic design process will be followed to fine-tune electrode parameters such as height, size, and pressure. Comprehensive testing will be conducted to ensure that the electrodes provide high-quality ECG and EMG signal acquisition under various conditions.

(2) Integration of textile electrodes:

Garment Integration: The developed 3D knitted silver electrodes will be strategically integrated into the intelligent garment. This integration will focus on maintaining wearer comfort and ensuring stable skin contact during physical activity.

Electrical Connectivity: Low-resistance silver conductive wires will be incorporated into the garment to establish robust connections between the electrodes and the electronic components, ensuring reliable signal transmission.

2. Real-Time Testing in Cycling Sports

(1) Experimental Setup:

Extensive testing of the intelligent garment system will be conducted in real-time sports scenarios, with a focus on cycling. Controlled experiments will be set up to

collect data on athletes' physiological responses during cycling sessions.

(2) Performance Analysis:

The performance of the intelligent garment system in capturing accurate bioelectric signals and providing reliable fatigue assessments will be thoroughly analyzed.

3. Data Preparation and Processing

(1) Data Collection and Preprocessing:

A comprehensive data preparation process will be established, encompassing the collection, cleaning, and preprocessing of ECG and EMG data. This ensures the quality and consistency of the data used for training the AI models.

(2) Hybrid Model Development:

Hybrid models that combine ECG and EMG data will be developed to enhance the accuracy and reliability of fatigue predictions. These models will leverage the strengths of both data types to provide more comprehensive assessments.

4. Application of Advanced AI Algorithms

(1) Development of Deep Learning Models:

Model Selection and Implementation: Various deep learning models, including Temporal Convolutional Networks (TCN), Gated Recurrent Units (GRU), Transformer models and Long Short-Term Memory (LSTM), will be developed to analyze the collected physiological data.

(2) Training and Optimization:

These models will be trained using data acquired from the intelligent garment system. The goal is to develop predictive algorithms that can accurately forecast fatigue levels based on real-time ECG and EMG signals.

1.4 Structure of the Thesis

This thesis is organized into five main chapters, each focusing on a specific aspect of developing and evaluating an AI-based fatigue assessment system for athletes using

smart textile wearables.

Chapter 2 presents a comprehensive review of current knowledge and technologies in the relevant fields. It begins by discussing the principles and importance of bioelectric signals, specifically electrocardiography (ECG) and electromyography (EMG), in sports monitoring. Various methods for assessing fatigue are then explored, including the Borg Scale and other techniques used in sports activities. This chapter also examines smart textiles designed for sports applications, focusing on bioelectric textile electrodes and data processing systems for e-textiles. It concludes with an overview of AI methods for analyzing bioelectric signals and a survey of current commercial intelligent garment systems for sports monitoring.

Chapter 3 explains the design, fabrication, and evaluation of the intelligent garment system developed in this study. It starts with the design and fabrication process for 3D textile biopotential electrodes. Their electrical performance is evaluated using impedance tests on PVA reference artificial skin. This chapter then outlines the fabrication of the complete intelligent garment, including garment design, hardware integration, and software development. It also discusses the integration of 3D knitted silver electrodes to ensure optimal signal quality and user comfort.

Chapter 4 focuses on testing and analyzing the intelligent garment system in the context of cycling sports. It begins by describing the experiment setup and methodology used in real-world cycling scenarios. This is followed by a detailed explanation of the data preparation process for ECG, EMG, and hybrid ECG + EMG data. This chapter then presents the application of various deep learning models, including Temporal Convolutional Networks (TCN), Gated Recurrent Units (GRU), Long Short-Term Memory (LSTM), and Transformer models, for predicting fatigue based on the collected data. Finally, the results obtained are discussed, highlighting their implications for the effectiveness of the system in providing accurate and timely fatigue assessments.

Chapter 5 summarizes the main findings of the research and highlights the study's contributions to the field of AI-based fatigue assessment in sports. It acknowledges the

limitations of the current work and suggests potential avenues for future research and development. The chapter also underscores the importance of continuous improvement and adaptation to enhance the system's capabilities and applications.

CHAPTER 2 State of the Art

This chapter presents a comprehensive review of the current state of the art in bioelectric signal monitoring, fatigue assessment, and intelligent garment systems for sports applications. We begin by examining the fundamental aspects of bioelectric signals, with a focus on electrocardiography (ECG) and electromyography (EMG), and their relevance in sports monitoring. The chapter then explores various fatigue assessment methodologies, including the widely used Borg Scale, and discusses their applications in sports activities.

A significant portion of this chapter is dedicated to the advancements in smart textiles for sports, particularly the development of bioelectric textile electrodes and data treatment systems. We analyze different electrode preparation techniques and their integration into intelligent garment systems. Furthermore, we investigate the application of artificial intelligence methods in processing bioelectric signals, highlighting recent innovations that have enhanced the accuracy and efficiency of signal analysis in sports contexts. The chapter concludes with an overview of current commercial intelligent garment systems, providing insights into their features, capabilities, and limitations.

2.1 Bioelectric Signals

Bioelectric signals refer to electrical signals produced by biological systems during biological events[14]. As shown in Figure 2-1, typical human bioelectric signals include electrocardiography (ECG), electromyography (EMG), electroencephalography (EEG), and electrooculography (EOG). Among these signals, electrocardiograms (ECGs), electromyograms (EMGs) and galvanic skin response (GSR) are the most commonly used bioelectric signals in human sport monitoring. These signals are pivotal in sports monitoring, giving precious information about an athlete's physiological state. By measuring these signals, experimenters and coaches can gain insight into an athlete's physical performance, fatigue, and overall health.

Recent advancements in Internet of Things (IoT) technologies have facilitated the real-time collection and analysis of these bioelectric signals, particularly in sports environments. Wearable sensor devices can now monitor ECG patterns along with body acceleration, providing a comprehensive view of an athlete's physiological and physical state[15].

These bioelectric signals give precious perceptivity into an athlete's performance, health, and well-being and can help trainers, coaches, and athletes optimize training programs, help injury, and ameliorate athletic performance. For illustration, by measuring EMG, ECG, and GSR during a training session, coaches can adjust the drill's intensity. This can help to prevent overtraining and reduce the threat of injury. Also, by covering bioelectric signals during competition, trainers can make real-time adaptations to an athlete's strategy grounded on changes in their physiological state. In addition, advances in wearable technology have enabled the nonstop monitoring of bioelectric signals, allowing for the real-time analysis and interpretation of the data.

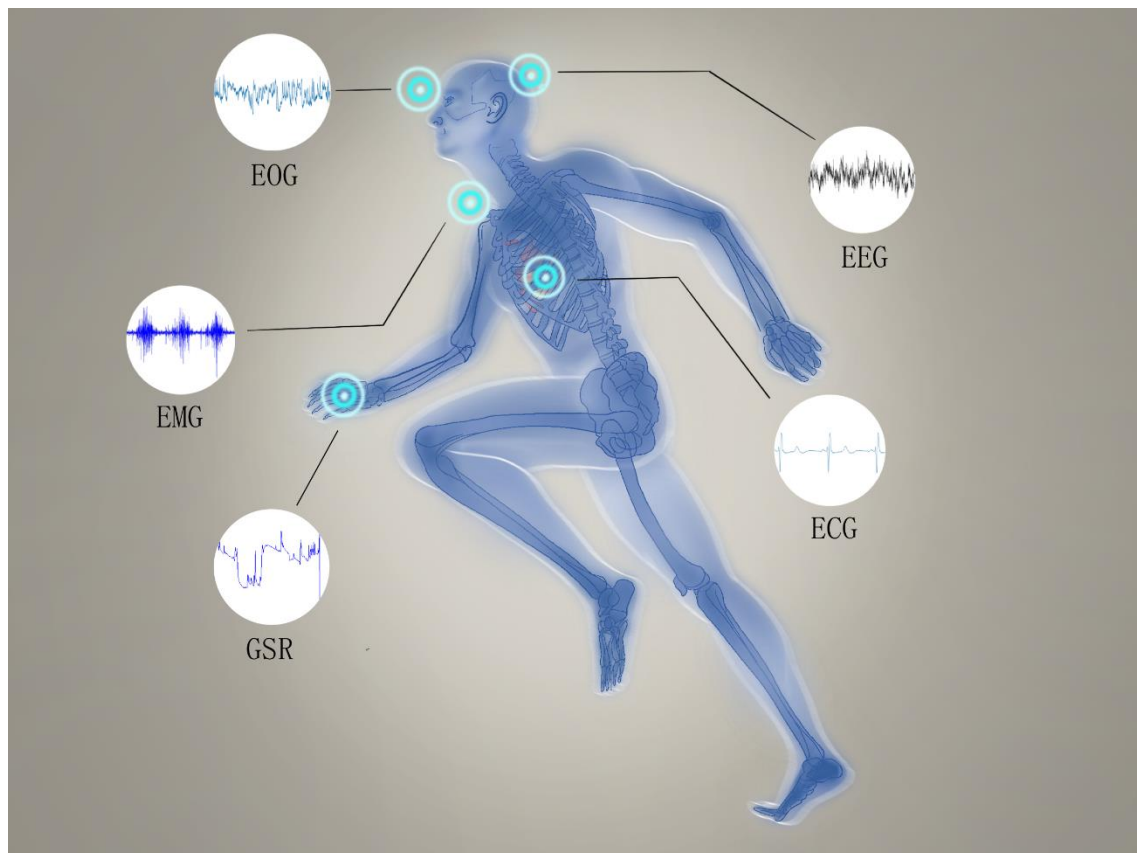


Figure 2-1 Bioelectric Signals.

2.1.1 Electrocardiography (ECG)

Electrocardiogram (ECG) is a bioelectric signal used for vital sign sensing and health monitoring methods and can provide information regarding the electrical activity of the heart[16, 17]. As an efficient non-invasive tool, it can measure the heart rate, examine the rhythm of heartbeats, diagnose heart abnormalities, recognize emotions, and identify biometric information[18]. ECG can be used to collect information about an athlete's heart health in long-last sports monitoring.

As shown in Figure 2-2 (a), the left and right atria, the left and right ventricles, veins and arteries, and the ECG pathway constitute a simplified diagram of the heart. An electrocardiogram (ECG) records the heart's electrical signals as it contracts and relaxes. Figure 2-2 (b) shows that each beat is represented on an ECG as a series of moves called P, Q, R, S, and T. A period of ECG generally lasts 10-20 seconds and consists of several beats. The P wave represents the electrical activity of the atria as they contract to pump blood into the ventricles. The QRS complex represents the ventricles' rapid and synchronized electrical activity employed as they contract to pump blood out of the heart. The T wave represents the ventricles as they relax and refill with blood. These heights, ranges, and shapes can give important information about the heart's electrical exertion. It can help diagnose heart-meter diseases, heart attacks, and other heart problems.

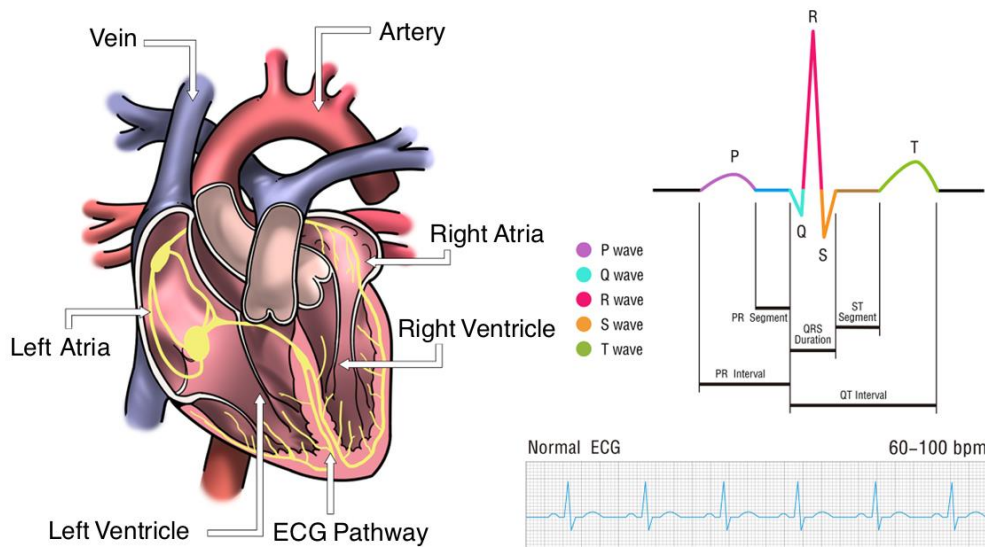


Figure 2-2. (a) Diagram of heart structure; (b) Schematic diagram of ECG signal wave combination.

The electrocardiogram (ECG) is pivotal in sports monitoring, furnishing precious information about an athlete's cardiovascular health and performance. The integration of ECG into wearable technology has enabled nonstop monitoring and real-time data analysis, allowing for optimized training programs and injury forestallment. The ECG monitors heart rate and detects implicit heart problems during physical exertion, like abnormal heart measures or arrhythmias, which may indicate heart conditions. This information is essential for athletes engaged in high-intensity conditioning, as it helps identify implicit health pitfalls and helps prevent severe injury or illness. Also, ECG can track changes in heart rate and meter during physical exertion, furnishing perceptivity into the athlete's heart response to different situations of exertion and the impact of training programs on performance.

Multitudinous experimenters have tried to develop wearable systems that capture and dissect real-time ECG signals. These systems include the Tele-ECG monitoring system with textile electrodes[19], the wireless sensorized belt for simultaneous respiratory and cardiac signal acquisition[20], and the wearable exercise fatigue detection technology utilizing ECG and inertial sensor signals[21]. The significance of ECG signals in sports and physical activity lies in their potential to provide healthcare

professionals with crucial information for health management. However, current wearable systems need a better quality of bioelectric signal acquisition electrodes, which can limit their usefulness in practice. Several studies have been conducted to address these limitations to improve the quality of ECG signals, such as modifying textile electrodes[22]. In this context, a novel ECG classification algorithm has been developed specifically for wearable devices with limited computational resources[23]. The algorithm could greatly improve the feasibility of ECG monitoring in sports.

A multimodal biosensing System-on-a-Chip (SoC) has also been developed to reliably acquire ECG, photoplethysmography, and bio-impedance signals[24]. This innovation could significantly enhance the reliability of wearable systems for ECG monitoring. Furthermore, the feasibility of using sportswear-type wearables for evaluating physical and physiological exercise intensity has been demonstrated[25], indicating the potential for ECG applications in sports to provide valuable insights into athletic performance.

In the field of sports bioelectric monitoring, Electrocardiogram (ECG) sensors play a pivotal role in capturing cardiac electrical activities. These sensors predominantly operate through a mechanism that involves the use of electrodes to detect the electrical potential generated by the heart. The electrodes are often made of conductive materials like silver or gold to ensure high signal fidelity. The signal acquisition ICs in these sensors are designed to amplify the captured signals, providing a gain of around 32 dB and a bandwidth of 370 Hz[26]. Moreover, advancements in electrode structures have been made to suppress motion artifacts, thereby maintaining the stability of the signal quality during non-contact ECG acquisition[27]. It's worth noting that the energy efficiency and transmission delay are also critical factors in the operation of these sensors[28]. The integration of machine learning algorithms has further enhanced the capability to reconstruct ECG signals even under conditions of low to heavy movements[29].

The recent advancements in ECG applications in sports have shown the potential to enhance ECG signals and enable multi-dimensional monitoring. Building on recent

advancements in wearable technology, ECG monitoring in sports has undergone significant transformations. Notably, sports environments are now benefiting from IoT-based systems specifically designed for real-time heartbeat tracking, employing advanced data classification techniques such as Radial-basis Function Network and Levenberg-Marquardt with Probabilistic Neural Network[15]. Complementing this, a recent study has underscored the diagnostic utility of ECG in sports cardiology, offering a comprehensive review of tailored electrocardiographic monitoring solutions[30]. However, limitations such as processing capacity and movement artifacts remain to be addressed. Future research should focus on improving the stability and reliability of ECG signals, increasing subject comfort, and developing advanced signal processing techniques to maximize the potential of wearable ECG systems. By doing so, it will enhance the ability to detect arrhythmias and accurately estimate exercise fatigue and improve the overall accuracy and practicality of wearable ECG devices.

2.1.2 Electromyography (EMG)

Electromyography (EMG) is a technique for recording biomedical electrical signals obtained from neuromuscular activities[31]. In long-last sports monitoring, EMG can be used to gather information about an athlete's muscle health and performance. In addition, EMG signals are further divided into nEMG and sEMG grounded on the system of accession. Needle EMG involves the insertion of a fine line electrode into the muscle to measure the electrical exertion of individual muscle fibers, while the other involves the use of electrodes placed on the skin to measure the electrical exertion of muscles. In comparison with nEMG, sEMG is better suited to the monitoring of sports and recreational activities. As illustrated in Figure 2-3, the contraction or activation of human muscles induces the generation of electrical impulses through muscle fibers and neurons, a phenomenon meticulously recorded through electrodes strategically positioned on the muscle surface. These impulses, innately composed of electrical signals emanated from muscle fibers, are reflective of the intricate dynamics encompassing both the muscles and the governing nervous

system, with the intensity and pattern of these impulses providing insightful information into their underlying operational mechanics. Following the acquisition of the Electromyography (EMG) signals, a subsequent step entails the execution of a series of analytical processes including smoothing, rectification, filtering, and root mean square of the raw signals, which are pivotal in delineating the precise status of the muscle condition. These procedural steps aid in the refinement of the data, enhancing the accuracy in understanding the complex interplay of muscular and neural activities, thereby facilitating a more nuanced interpretation of muscle states. In the field of sports science, sEMG has been increasingly adopted for real-time evaluation of muscle state and forecasting of future fatigue trends. Advanced sEMG systems have been developed that are cost-effective, portable, and wearable, specifically designed for sports and healthcare applications[32].

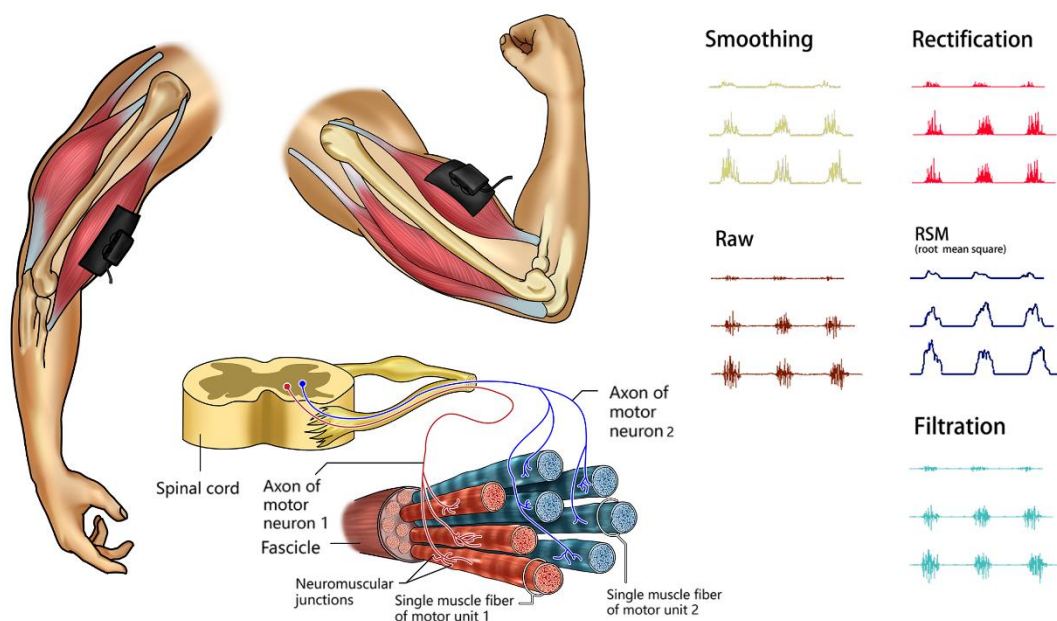


Figure 2-3 Schematic diagram of EMG signal generation and processing flow.

Surface electromyography (sEMG) is increasingly used in sports science to monitor and assess muscular fatigue. By recording and analyzing the electrical activity produced by muscles during contraction via surface electrodes, sEMG enables real-time evaluation of muscle state and forecasting of future fatigue trends. This information is useful for optimizing training and injury prevention strategies. The position of muscle

activation measured by sEMG can be used to track changes and give precious feedback to athletes and trainers on areas that bear enhancement. The measurement of muscle activation over time also provides information on muscle fatigue, allowing for timely adjustments in training to prevent further fatigue. In addition to monitoring muscle activation and fatigue, sEMG is also used to assess muscle symmetry and balance, which is essential for optimizing performance by addressing any imbalances or asymmetries in muscle activation. Also, sEMG is used to cover muscle activation during specific exercises and movements, furnishing precious information to optimize training and ameliorate performance.

In parallel to ECG sensors, Electromyography (EMG) sensors are instrumental in the realm of sports bioelectric monitoring, particularly for assessing muscle activities. These sensors primarily function through the detection of electrical potentials generated by muscle contractions. The electrodes in EMG sensors are often fabricated from conductive materials like silver chloride (Ag/AgCl) to ensure high signal fidelity[33]. Advanced signal processing techniques, have been employed to enhance real-time EMG signal interpretation, thereby improving the functionality of upper-limb artificial body[34]. Recent innovations have focused on the robustness of human-machine interactive control for myoelectric prosthetic hands, especially during arm position changes[35]. Moreover, pattern recognition algorithms have been increasingly integrated into EMG sensors to discern user intentions more accurately, thereby enhancing the human-machine interaction[36].

In recent times, there have been significant advancements in the field of sEMG signal accession for sports monitoring operations. Several studies have concentrated on developing cost-effective, movable, and wearable sEMG systems that can be used to cover human exertion during sports and in healthcare application[37-39]. Another study investigated the extent to which sEMG is adopted by professionals in the field of exercise and human movement[40]. Additionally, Spanu et al. made a significant contribution by developing and validating cost-effective and robust electrodes that provide adequate signal quality in dynamic conditions[41]. Campanini et al. presented

educational tools for teaching sEMG detection using electrode pairs and grids[42].

Despite these advancements, there are still limitations and challenges associated with the use of sEMG in wearable applications. One of the key challenges is improving the accuracy and reliability of sEMG signal acquisition in dynamic conditions. Furthermore, current sEMG systems can improve user-friendliness and comfort for long-term wear. Incorporating advanced signal processing techniques and electrode design could improve performance and increase the adoption of sEMG technology in the healthcare and sports industries. To achieve this, further research is needed to address the current limitations of sEMG in wearable applications.

2.2 Fatigue Assessment

2.2.1 Fatigue Definition

Fatigue is a complex concept that involves a wide range of disciplines such as physiology, psychology and medicine. In the field of human performance, fatigue is defined as a symptom of decreased physical and cognitive function caused by the interaction of performance fatigability and perceived fatigability [43, 44]. Sport fatigue performance refers to a decrease in objective performance indicators over a specific period of time, whereas perceived fatigability includes sensory changes that regulate the integrity of the individual [43, 45].

This definition emphasizes the complex essence of fatigue, recognizing the interaction of physiological and psychological factors [46]. Sport fatigue performance is influenced by a variety of physiological processes, such as metabolite accumulation, energy substrate depletion, and altered neuromuscular function [47, 48]. The perceived fatigue performance, on the other hand, is characterized by an individual's sensory, emotional and cognitive processes, and can be modified by factors such as motivation, expectations and prior experiences [49, 50].

This fatigue definition framework provides a comprehensive approach to understanding the effects of fatigue on human performance, integrating findings from

different research areas [43]. By considering both motor and perceptual aspects of fatigue performance, researchers and practitioners can develop targeted interventions to mitigate the negative effects of fatigue on physical and cognitive function [44].

2.2.2 Borg Scale

The Borg Scale or the Realized Perceived Exercise Intensity (RPE) scale is a widely used tool for assessing perceived fatigue performance during physical activity [51]. The scale was originally developed by Gunnar Borg to provide a subjective measure of an individual's perceived exercise intensity during exercise [52]. As shown in Table 2-1, The Borg Rating of Perceived Exertion (RPE) Scale ranges from 6 to 20, with 6 indicating "no exertion at all" and 20 representing "maximal exertion" [51]. The scale values are intended to correspond to heart rate values, with a score of 12 corresponding to 120 beats per minute [53].

Table 2-1
Borg rating of perceived exertion (RPE) scale

Rating	Description
6	No exertion at all
7	Extremely light
8	
9	Very light
10	
11	Light
12	
13	Somewhat hard
14	
15	Hard
16	
17	Very hard
18	
19	Extremely hard
20	Maximal exertion

The Borg scale has been widely used and has shown strong correlations with a large number of physiological indicators such as heart rate, oxygen consumption and blood lactate levels [54, 55]. It is consequently a useful tool for monitoring perceived exercise intensity and assessing perceived fatigue performance of individuals during

exercise [56], and has been applied in a multitude of settings, including athletic training, recovery, and clinical exercise testing [57, 58].

However, it is important to recognize that the Borg scale is a subjective measure that can be influenced by various psychological factors [59]. Individuals' RPE values may be influenced by their motivation, mood, and prior experiences, leading to variability in the relationship between RPE and physiological indicators [60]. In addition, the sensitivity of the scale to changes in exercise intensity may vary depending on the type and intensity of the activity performed [61].

Despite these limitations, the Borg scale is a widely used and practical tool for assessing perceived fatigue performance in sport [62]. Combined with objective measures of exercise fatigue performance, the Borg scale can provide valuable insights into an individual's overall fatigue experience and inform strategies to optimize human performance.

2.2.3 Fatigue Evaluation for Sports Activities

In the field of sports science, fatigue assessment plays a key role in optimizing performance and preventing overtraining syndromes [63]. A comprehensive assessment of fatigue in sports activities usually combines objective and subjective measures, taking into account both motor and perceived fatigue performance [64].

Objective measures of exercise fatigue performance can provide important insights into an athlete's physical capabilities and the extent of fatigue-induced performance decrements [65], and may include assessments of muscular strength, power output, endurance, and sport-specific skills [66, 67]. For example, a critical power test for a 3-minute all-out ride has been shown to be a reliable predictor of endurance performance in cyclists [68, 69]. Similarly, jump tests such as the following squat jump can be used to assess lower extremity strength and neuromuscular fatigue in a variety of sports [70, 71].

In addition to laboratory tests, field-based assessments of athletic fatigue performance can provide physiological valid measures of fatigue during sports

activities [72]. Time trials, sprint tests and sport-specific drills can be used to assess athlete performance under fatigue conditions [73, 74]. These assessments can help both coaches and sport scientists to identify weaknesses and develop training plans to increase an athlete's resistance to fatigue [75].

Subjective measures of perceived fatigue performance such as the Borg scale and questionnaires such as the Profile of Mood States (POMS) or the Recovery-Stress Questionnaire for Athletes (RESTQ-Sport) can provide valuable information about athletes' psychological state and subjective fatigue levels [76]. These measures can be useful in detecting overtraining, burnout, or other fatigue-related problems that may affect athletes' health and performance [77, 78].

Assessment of fatigue in sports activities requires a combination of objective and subjective measures of fatigue [43]. By monitoring changes in exercise and perceived fatigue performance over time, coaches and sport scientists can optimize training loads, prevent overtraining, and ensure that athletes recover adequately prior to competition [79, 80]. This holistic approach to fatigue management can improve athletic performance, reduce the risk of injury, and enhance overall athlete health [81].

2.3 Smart Textiles for Sports Activities

2.3.1 Bioelectric Textile Electrodes

Textile electrodes, a flexible and intelligent skin-friendly textile, can be closely integrated with intelligent clothing systems. Compared to traditional electrodes, textile electrodes offer many benefits when incorporated into intelligent garment systems, including comfort, flexibility, durability, concealment, skin-friendly contact, stability in time, and washability.

Textile dry electrodes are a better alternative to traditional wet electrodes for bioelectric signal monitoring. Unlike traditional wet electrodes, which rely on a conductive gel to provide electrical connectivity to the skin, dry textile electrodes utilize conductive fibers integrated into the textile material. The skin equivalent circuit and

skin-electrode contact structure of the conventional wet electrode and textile dry electrode is shown in Figure 2-4. Compared with the gel medium of the conventional wet electrode, the dry textile electrode achieves signal transmission with the help of sweat[82], which has advantages in long-term sports. This results in a more comfortable, flexible, and interactive electrode that can be worn for a long time without causing skin vexation or discomfort. Also, the lack of gel reduces the setup time and minimizes the threat of impurity, making the monitoring process more effective and aseptic. These advantages make dry textile electrodes attractive for various bioelectric signal monitoring. In the field of wearable health monitoring, E-textile electrodes have surfaced as a pivotal innovation, harmonizing with the fabric of clothing for unintrusive and continuous bioelectric signal capture. These electrodes are engineered through sophisticated textile technologies, employing conductive fibers and polymers to ensure a high signal-to-noise ratio, rivaling that of conventional gel-based electrodes. The design philosophy behind E-textile electrodes is anchored in biocompatibility, flexibility, and resilience, offering a marked advantage over traditional electrodes that often necessitate skin preparation and are susceptible to motion artifacts. This adaptability renders them particularly invaluable in sports and healthcare scenarios where sustained, long-term monitoring is imperative. As we look to the future, the trajectory of wearable health monitoring is set to be influenced by advancements in sensor miniaturization, energy-efficient technologies, and real-time data analytics. These forthcoming innovations hold the potential to revolutionize both sports training and healthcare by facilitating more precise performance evaluations and enabling timely medical interventions.

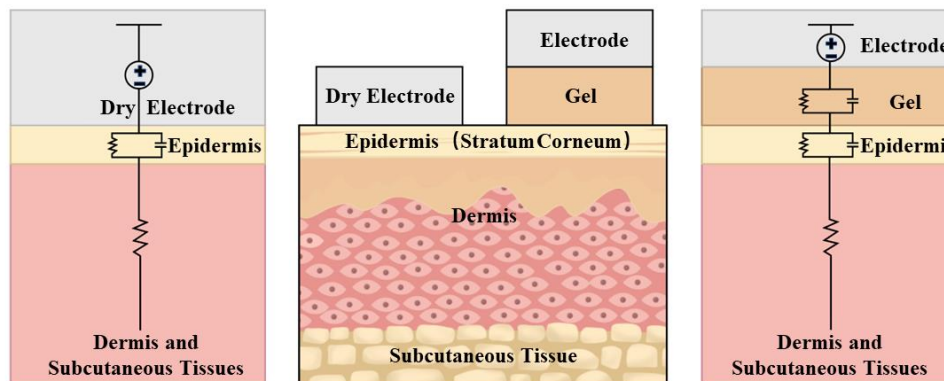


Figure 2-4 Schematic diagram of skin equivalent circuit with the conventional wet electrode and dry textile electrode.

Textile dry electrodes can be prepared using various techniques, including stitching, knitting, embroidering, electroplating, and chemical plating. The preparation method is chosen based on the desired properties and applications of the electrode, each offering advantages and challenges. The most common approach is stitching, where conductive yarns are sewn directly onto the textile substrate. For example, Arquilla et al. used silver nanoparticle-coated nylon yarns in an overlapping serrated pattern to create 3 cm x 3 cm textile electrodes with a resistance of 0.3Ω (Figure 2-5. (a)), which were capable of recording ECG signals with distinguishable R and S peaks[83]. Milad et al. applied STOLL flat machine to knit plane textile dry electrodes and 3D textile dry electrodes with silver and carbon yarns (Figure 2-5. (b)) and evaluated the performance of these electrodes in long-term electrocardiographic monitoring[84]. Rajanna et al. created knitwear and silver textile electrodes by knitting silver and copper-nickel yarns onto a foam sponge substrate[85]. Both electrodes had a skin contact impedance of less than $1 \text{ M}\Omega/\text{cm}^2$, with the knitwear electrode having a square resistance of $46 \Omega/\text{sq}$ and the silver textile electrode having a much lower square resistance of less than $1 \Omega/\text{sq}$.

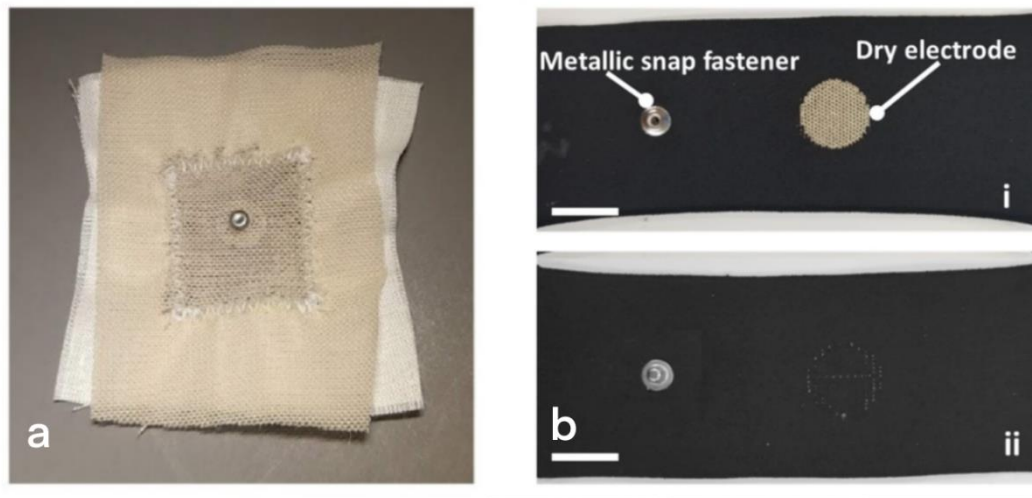


Figure 2-5 (a) Silver nanoparticle-coated nylon electrodes. [83] (b) Schematic diagram of the (i) front and (ii) back of a sample dry electrode[84].

Further preparation involves embroidering the conductive yarn on the fabric surface to reduce the skin-electrode interface impedance. The research team of Zhao et al. presented a knitted electrode with a mixture of reduced graphene oxide (RGO), sericin, and a water-retention polymer (Figure 2-6) that is capable of monitoring the bioelectric signals of the human body during long-lasting sport[86]. This electrode effectively reduces the electrode-skin interface impedance due to its unique 3D structure and water-retention material properties. Lee et al. used two conductive yarns, stainless steel, and silver, to embroider fabric dry electrodes on the compression garment. At the same time, silicone was applied to the designed embroidery pattern to increase the adhesion between the electrodes and the skin, thereby increasing the effective contact area. His study showed that the application of this method, combined with the appropriate garment pressure, could improve the accuracy of sEMG signal acquisition while increasing the comfort level[87].

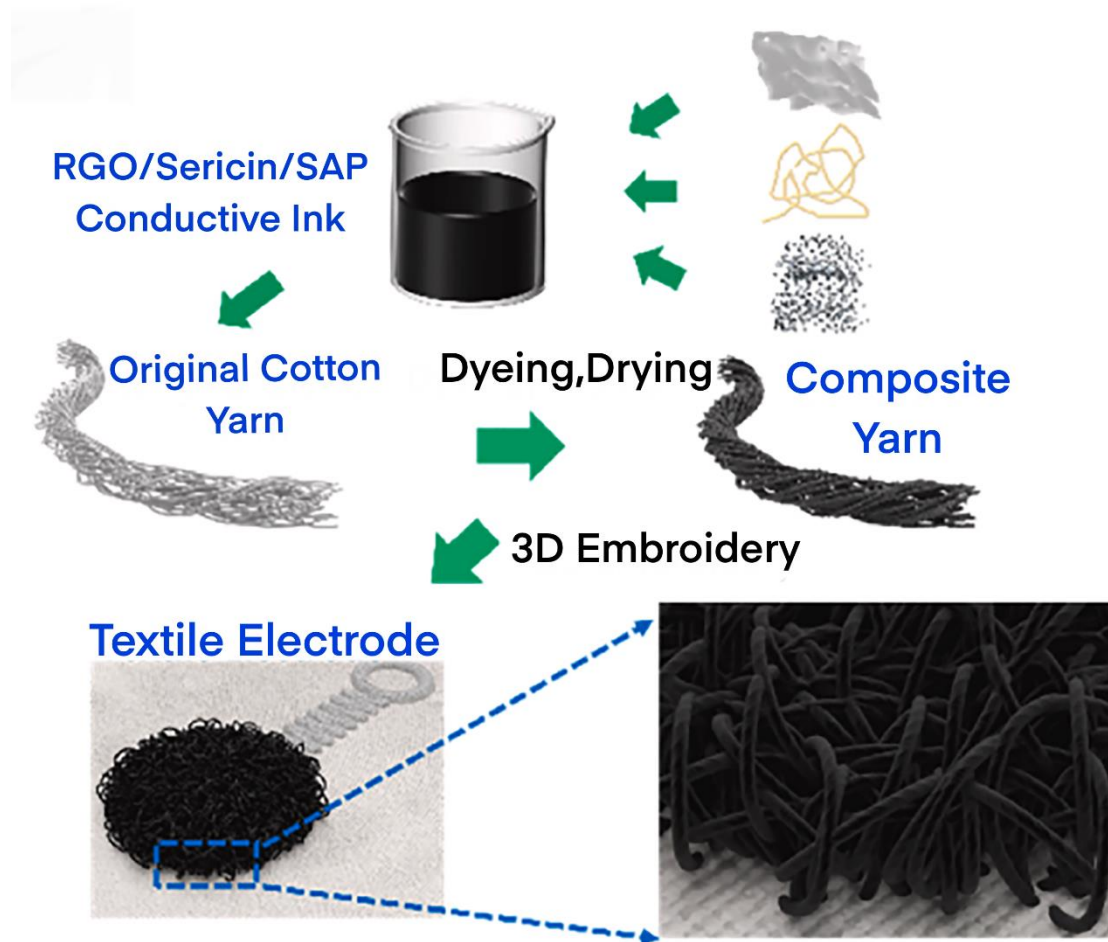


Figure 2-6 Schematic illustration of the 3D textile electrode fabrication process. [86]

Another method of generating electrodes directly on the fabric is electroplating. This surface coverage method enables the deposition of conductive metals directly on the textile surface to generate electrodes. Plating technology mainly covers electroplating and chemical plating, the principles of electrolysis and redox respectively[88]. Electroplating allows for control over the thickness of the metallic coating, while chemical plating provides conductivity in all directions of the textile surface and uniformly deposited metallic coatings on complex geometries[89]. Ladan et al. applied silver-plated and carbon-containing nylon yarn to knit electrocardiographic electrodes by electroplating and carbon suffusion methods (Figure 2-7(a)), respectively, and compared them with gold standard hydrogel electrodes for skin impedance before and after washing. The results showed that the performance of these two electrodes is comparable to that of gold-standard hydrogel electrodes and can

be effectively used for continuous monitoring of human bioelectric signals[90]. Das et al. fabricated conductive textiles through a chemical plating process, depositing nickel/copper/nickel/gold layers on polyester textiles, resulting in textiles with high electrical conductivity and stability[91]. Wu et al. metalized the "dye bath" by using a method based on chemical nickel-impregnated gold (ENIG), which allows complete penetration of metal ions into the textile structure and deposition of metal coatings on the surface of individual textile fibers (Figure 2-7(b)). This method helps maintain the textile's inherent structure and abrasion resistance and gives e-textiles high electrical conductivity, flexibility, and stretchability[92].

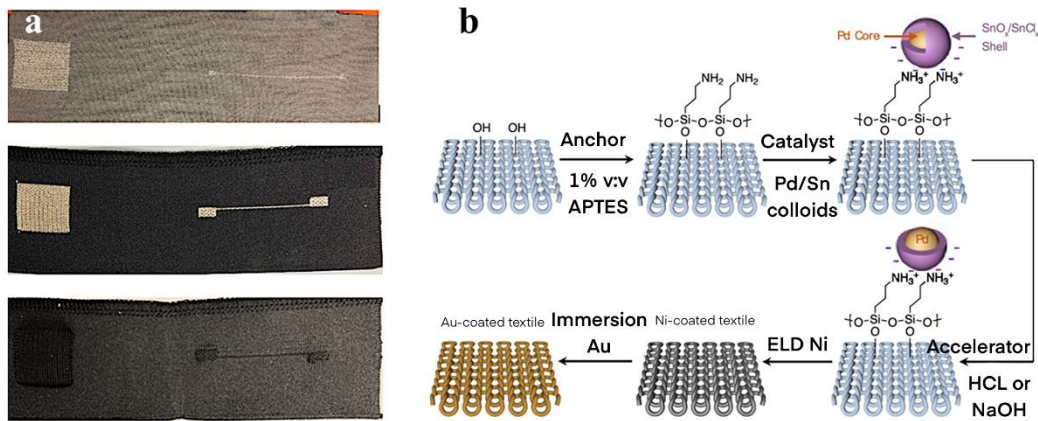


Figure 2-7 (a) Square and line patterns on the circular knitted silver yarn sample, flatbed knitted silver yarn sample, and flatbed knitted carbon yarn sample. [90] (b) Schematic of the ENIG process on textiles. [92]

Screen printing, which involves applying carbon-based inks to textile substrates to create conductive patterns, is another common approach. Zhang et al. applied the chemical silver-plating method to assemble ECG fabric electrodes from conductive cloth, space wool, and double-sided adhesive conductive foam (Figure 2-8(a)). They discussed the effect of the fabric electrode surface on static and dynamic ECG quality after the conductive media coating. The results showed that the fabric electrode coated with conductive paste could effectively reduce the electrode-skin contact impedance

and acquire ECG signals more clearly[93]. Xu et al. used screen printing to apply aqueous graphene ink on cotton textiles(Figure 2-8(b)) and achieved a high Pearson correlation coefficient of 99.47% between the graphene electrode and the commercial Ag/AgCl wet electrode[94].

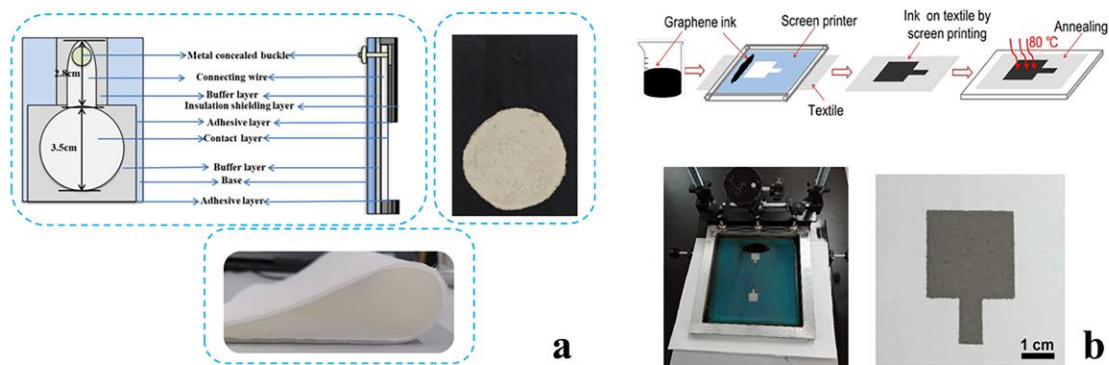


Figure 2-8 (a) Schematic diagram of the structure of the silver-plated fabric electrode. [93] (b) Preparation process of screen-printed graphene electrodes, the experimental setup for the screen printing, and photo of the fabricated graphene-coated electrode. [94]

The interconnection of sensors with intelligent garment systems has garnered significant attention within e-textiles research. To attain the desired level of integration and functionality, a multitude of techniques have been employed for connecting sensors to these systems. Amongst the most widely employed methods, adhesive bonding, snap fasteners, pogo pins, and magnets are the four most prominent.

Adhesive bonding, the most used method in e-textiles, encompasses several types of bonding, including non-conductive adhesive bonding (NCA), isotropic electrically conductive adhesives (ICA), and anisotropic conductive adhesives (ACA), as shown in Figure 2-9. The NCA bonding method has been adapted to create a connection between rigid circuit modules, and conductive textile interconnects using a thermoplastic film that is sandwiched between the two[95, 96]. ICA bonding involves the addition of a

conductive filler to an adhesive material. In contrast, ACA bonding is similar but employs a lower concentration of conductive filler, making it more suitable for fine-pitch connectors[97-99].

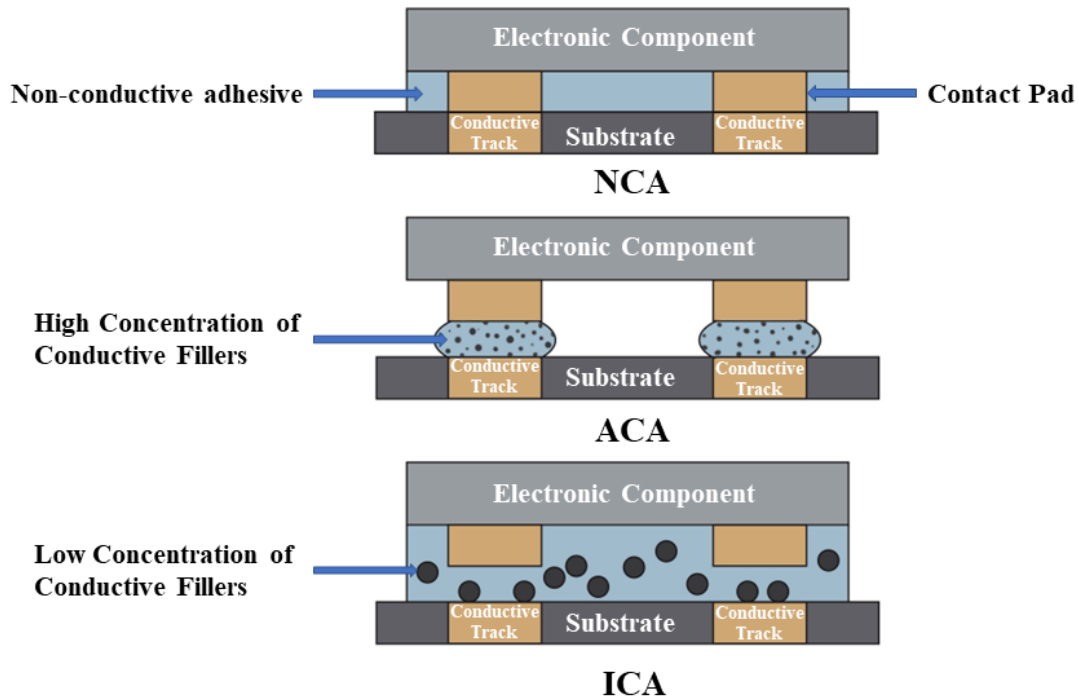


Figure 2-9 Diagram of NCA, ECA, and ICA bonding.

Snap fasteners, also called press studs or poppers, have been extensively employed as connectors in e-textiles. Despite their widespread usage, there is a need for further research to determine their viability as electronic connectors[100, 101]. Ozberk et al. demonstrated that snap fasteners could be used as an electrical interface for graphene-coated fabric electrodes to monitor the sEMG signal in the dynamic state of the human body[102]. For long-lasting sport monitoring, however, we need to assess snap fasteners' durability, reliability, and performance under various conditions to determine whether and how well they are suited for use as electronic fabric connectors.

Pogo pins, typically with a diameter ranging from 1-2 millimeters, have emerged as a standard solution for connecting rigid circuit modules with flexible circuitry in a garment. These pins offer a reliable and efficient way to connect within e-textile systems and have been widely used in various applications. Another method for connecting sensors to intelligent garment systems is to use magnets. Magnets have been

used either for alignment or as electrical contacts themselves[103]. This approach presents a unique solution for connecting sensors in e-textile systems, offering a non-contact method for making electrical connections. Further research is needed to explore this approach's feasibility and limitations, particularly its ability to withstand various environmental conditions and its long-term performance.

2.3.2 Data Treatment System for E-textile

ECG signal processing involves preprocessing and feature engineering steps to reduce noise and interference in recorded ECG signals and extract relevant features for analysis. Preprocessing utilizes bandpass, low-pass, high-pass, notch, and median filters to eliminate various types of noise. Feature engineering involves extracting temporal, morphological, and statistical features in the spatial, frequency, or time-frequency domains. Traditional methods use denoising and fiducial point extraction through direct or transform processes, while recent techniques employ mathematical computations and neural networks for faster processing. The accuracy of the extracted features significantly impacts the analysis performance, with the QRS complex being the most predominant feature.

Preprocessing is essential in electrocardiogram (ECG) signal analysis to reduce interference and determine signal features[104]. Preprocessing aims to minimize noise and artifacts in the recorded ECG signals to prepare them for further analysis. Bandpass filters are commonly used for this purpose and effectively reduce noise sources like muscular noise, movement-related artifacts, power-line interference, baseline wandering, and high/low-frequency noise signals[105-113]. Low-pass filters (LPF) eliminate high-frequency components of the signals, while high-pass filters (HPF) eliminate low-frequency components[114, 115]. Notch filters eliminate DC offsets in signals[107, 114, 116, 117]. Median filters remove special effects and arbitrary or baseline wander noise[113, 118-121]. Other techniques, such as adaptive noise cancellation and leaky-based normalization, have also been proposed for noise reduction[122-124].

Feature engineering (FE) is crucial for ECG signal analysis and consists of extracting different temporal, morphological, and statistical features from the periodic ECG signal pattern[125]. The accuracy of the extracted features impacts the analysis performance. These features can be acquired in the spatial, frequency, or time-frequency domains[126]. Conventional signal processing techniques and machine learning models have been introduced to find ECG features such as the R-R interval, QRS complex, and others[127]. Traditional FE methods involve denoising the ECG signal and extracting fiducial points through direct or transformation methods like wavelet transform (WT) and discrete wavelet transform (DWT). However, current limitations in terms of processing time and computational constraints have resulted in the development of faster techniques using mathematical computations and neural networks[128]. These techniques rely heavily on accurately identifying features, with the QRS complex being the most predominant.

Effective signal processing of sEMG signals is crucial for accurately assessing muscle fatigue in the sports domain. The preprocessing and feature extraction of sEMG signals are vital in obtaining accurate results. Recently, a multitude of techniques and features have been utilized to monitor changes in muscle activation and state over time, providing crucial information for sports training and rehabilitation.

Raw sEMG data often contain power line interference and motion artifacts. Therefore, preprocessing techniques such as detrending, filtering, normalization, and windowing mitigate these issues[129-131]. For example, detrending removes trends (both linear and nonlinear slow shifts of the signal from zero level) on EMG. Detrending is typically performed as an initial step to reduce artifacts and improve the quality of the sEMG signal for further processing and analysis. It is essential for obtaining accurate measurements of muscle activation patterns and identifying changes in muscle function during physical exertion. Other methods used for preprocessing include Independent Component Analysis (ICA) and empirical mode decomposition (EMD)[132], Ensemble Empirical Mode Decomposition (EEMD) with Hilbert Transform (HT)[133], and Discrete Wavelet Transform (DWT)[134]. In estimating

muscle activity onsets, methods such as visual and automated methods[135], sample entropy (SampEn) analysis[136], and sequential Gaussian mixture model (GMM) have been proposed[137]. Regarding feature extraction, four main types of features are extracted from sEMG signals time-domain, frequency-domain, time-frequency domain, and nonlinear parameters[138-140]. Time-domain features include root mean square (RMS), integrated EMG (iEMG), zero-crossing rate (ZCR), waveform length (WL), the variance of electromyography (VAR), and mean absolute value (MAV)[141-145]. The RMS and iEMG values increase over time as muscle fatigue sets in, indicating changes in muscle activation intensity and human motion state[133, 146-148]. In the frequency domain, mean frequency (MF) and median frequency (MDF) represent the frequency of measured muscle CV and provide information about muscle fatigue, with MDF being more sensitive to muscle activity[149-151]. The time-frequency distribution of sEMG signals is also analyzed to provide comprehensive information about physiological muscle changes during exercise.

2.4 AI Methods for Bioelectric signals

The rapid advancement and integration of artificial intelligence (AI) into bioelectric signal processing, particularly in sports-related contexts, have unveiled a host of transformative developments. AI has significantly refined our ability to evaluate muscle activation, fatigue, and overall athletic performance by bolstering the efficiency and accuracy of preprocessing and feature extraction from sport-related bioelectric signals such as electrocardiograms (ECGs) and sEMG. Consequently, this has placed AI at the crux of applications spanning sports training, rehabilitation, and injury prevention, providing a robust foundation for more tailored and potent interventions.

A summary of key research contributions in the field of AI-enhanced bioelectric signal processing in sports is presented in Table 2-2:

Table 2-2

AI approaches in bioelectric signal processing across diverse applications

Author	Application	Metrics Measured	AI Methods
--------	-------------	------------------	------------

Emma Farago et al. [152]	Wearable Smart Devices	ECG and EMG	Autoregressive, Markov Chain, Recurrent Neural Network Models
Ali Raza et al. [153]	Digital Healthcare	ECG	Transformer-based Autoencoders, Support Vector Data Description, Federated Learning
Ali Raza et al. [154]	ECG-based Healthcare	ECG	Deep Convolutional Neural Networks (CNN), Explainable Artificial Intelligence (XAI), Federated Learning
Bruce Hopenfeld et al. [155]	Sports Activities	ECG	Temporal Pattern Search (TEPS), Methodology to Mitigate Motion Artifacts
Duan Na et al. [156]	Accurate Recognition of Action Modes	EMG	Convolutional Neural Networks (CNN)
Chengyu Liu et al.[157]	Wearable ECG SmartVest System	ECG	Machine Learning (SVM)
Alejandro Castillo-Atoche et al.[158]	Sports Activities Monitoring	ECG	Convolutional Neural Network (CNN)
Xiao Sun et al[159].	Sentiment Classification	GSR	Convolutional Neural Network, Long Short-Term Memory, Self-Attention Mechanism
Shuvodeep Saha et al[160].	Cognitive State Change Classification	GSR, PPG	General Linear Chirplet Transform, Random Forest, Decision Tree, k-Nearest Neighbours

In the field of motion artifact data processing, Emma Farago et al. delved into the application of three distinct AI-based methods: autoregressive models, Markov chain models, and recurrent neural network (RNN) models[152], Autoregressive models employ a linear combination of past observations to predict future values, offering simplicity and computational efficiency. Markov chain models, on the other hand, rely on the principle of “memorylessness”, where the future state depends solely on the current state, making them suitable for systems with short-term dependencies. However, it was the RNN models that stood out for their ability to capture long-term dependencies in the data, thereby proving to be the most effective in generating diverse motion artifact

data that closely emulated experimental data properties. While RNN models have shown superior performance, they are not without limitations. For instance, they are computationally more intensive and may require larger datasets for training. In scenarios where computational resources or data availability are constrained, autoregressive or Markov chain models may offer a more practical alternative. Emerging innovations in the field of artificial intelligence, including the advent of optimized recurrent neural network architectures and the application of transfer learning techniques, offer promising avenues for refining and augmenting the existing methods used in motion artifact data generation.

In response to the limitations of existing simulation techniques, Farago's team introduced and compared three AI-based methods for generating motion artifact data—autoregressive, Markov chain, and recurrent neural network models. Their work substantiated the recurrent neural network model as the most effective in generating diverse motion artifact data that closely emulated experimental data properties, thus enhancing the reliability of bioelectric signal quality analysis in sports applications. In a parallel vein, Ali Raza et al. from ENSAIT-GEMTEX Laboratory presented AnoFed, a pioneering federated learning framework that incorporated transformer-based Autoencoders and Support Vector Data Description[153]. This framework was developed to address the challenges of efficient and privacy-minded anomaly detection in bioelectric signals during sports activities. Notably, AnoFed leverages transformer-based Autoencoders for feature extraction and Support Vector Data Description for anomaly detection, offering a comprehensive solution for ECG analysis in sports settings. The framework has shown promise for broader applications, including other types of bioelectric signals and healthcare scenarios outside of sports. This integration facilitated efficient, privacy-minded anomaly detection in bioelectric signals during sports activities. When applied to ECG analysis, the approach exhibited exceptional performance and computational efficiency, effectively tackling data privacy issues inherent to healthcare applications. In addition, Raza's team proposed an innovative federated learning framework that harmonized explainable artificial intelligence (XAI)

and deep convolutional neural networks (CNN) for ECG-based arrhythmia classification during sports, offering promising applicability across various healthcare and sports scenarios[154]. Furthermore, Bruce Hopenfeld et al. introduced a novel methodology that employs autocorrelation and TEPS for the extraction of persistent rhythms in the motion artifact record of the NSTDB. Their work has significant implications for enhancing the accuracy and reliability of ECG analysis in sports performance evaluation, especially in noisy environments.[155, 161, 162]. Focusing on the unique challenges of ECG data, they introduced the highly constrained temporal pattern search for multi-channel heartbeat detection during sports activities and proposed an innovative methodology to mitigate motion artifacts in waist-based ECGs. Their work has contributed to enhancing the accuracy and reliability of ECG analysis in sports performance evaluation.

In a similar endeavor, Duan et al. adopted convolutional neural networks for efficient feature extraction and action classification in sEMG signals during sports activities[156]. Their approach of treating sEMG signal spectrograms as images demonstrated the efficacy of deep convolutional networks in gesture motion recognition during sports, underlining the promising potential of AI methods in sEMG signal processing for athletic performance assessment. On another front, Chengyu Liu et al. devised an innovative IoT-based wearable 12-lead ECG SmartVest system for real-time, continuous cardiovascular disease monitoring[157]. By confronting the real-time signal quality assessment and lightweight QRS detection challenges, their novel methodology combining multiple signal quality indices and machine learning techniques improved the efficiency and reliability of ECG recordings, opening new possibilities for broad population monitoring. Moreover, Alejandro Castillo-Atoche et al. developed an integrated energy-aware technique and a CNN for a cardiac arrhythmia detection system wearable during sports training[158]. Their introduction of an ultra-low-power microcontroller programmed with a dynamic power management strategy, coupled with a photovoltaic energy harvesting circuit, resulted in a significant extension

of battery life. With an arrhythmia detection precision of 98.6%, their proposed system exemplifies the potential of AI in effectively monitoring athletes' conditions.

Innovations in AI-driven bioelectric signal processing have revolutionized sports-related applications, providing enhanced efficiency, accuracy, and privacy in muscle activation, fatigue and performance assessment. The adoption of advanced methods including autoregressive, Markov chain, and recurrent neural networks, as well as federated learning and convolutional neural networks, has enabled breakthroughs in mitigating motion artifact contamination, ECG analysis, sEMG signal processing, and real-time monitoring. These advancements underscore the vital role of AI in sports training, rehabilitation, injury prevention, and healthcare scenarios, and pave the way for further research and development in this domain.

2.5 Overview of Current Sports Monitoring Commercial Intelligent Garment System

With adding fitness and health monitoring demand, the request for intelligent garment systems has recently seen significant growth. These systems use advanced cloth detectors and wearable technology to cover biometric data such as heart rate, respiration rate, and physical exertion. The data collected can be fluently transferred to a mobile operation, furnishing real-time feedback to athletes on their health and fitness. This section will present an overview of a selection of presently available intelligent garment systems that have commercial viability.

Xiaomi Mijia Cardiogram T-shirt is an industry-leading intelligent garment system designed to enhance athletic performance with monitoring systems[163]. One of its primary functions is the capability to conduct electrocardiogram (ECG) monitoring, which involves the assessment of the electrical exertion of the heart. This capability is accomplished by the incorporation of technical sensors within the fabric of the t-shirt. The ECG data attained from these detectors offer discerning information about the heart rate and other parameters, enabling the monitoring of physical exertion and detecting any possible heart-related issues. Likewise, this ECG data can be transferred to a mobile

operation, furnishing athletes with immediate feedback and enabling them to make well-informed opinions regarding their exercise routines. This system distinguishes itself by focusing on cardiac health, making it particularly useful for athletes concerned with cardiovascular performance.

Athos Shirt is an exemplar in intelligent garments designed to enhance athletic performance[164]. This shirt is equipped with muscle-tracking detectors that can cover the activation of muscle groups during exercise. The data collected by the detectors is transferred to a mobile operation, so the athletes can receive real-time feedback on their performance and identify areas for enhancement. The Athos Shirts are designed for comfort and are made from feather-light, porous materials, equipped with sweat-wicking technology to keep the wearer cool and dry during intensive exercises. Unlike the Xiaomi Mijia, the Athos Shirt specializes in muscle activity, offering a unique set of data valuable for strength training and muscle development.

Tymewear Smart Shirt is a novel intelligent garment system that optimizes athletic performance with monitoring systems[165]. It can measure breathing rate, which reflects the respiratory exertion of the runner. This system is unique in its ability to measure respiratory metrics, offering athletes insights into their aerobic capacity and stamina. The shirt has technical sensors embedded in the fabric that collect breathing data. This data reveals the runner's metabolic thresholds, training load, and VO_2 max. Runners can use these parameters to adjust their training intensity, duration, and frequency according to their fitness goals and needs. The shirt also transfers the breathing data to a mobile application, which gives runners immediate feedback and helps them make informed decisions about their exercise routines. A visual representation of the TymeWear Smart Shirt is provided in Figure 2-10.

Moreover, the shirt measures running power, force production, ground contact time, and cadence from sensors embedded in the fabric. These parameters help runners analyze their biomechanics and gait patterns and improve their running efficiency, performance, and injury prevention. Aaron H. et al. conducted two graded exercise test (GXT) trials to verify the reliability of the TymeWear Smart Shirt[166].

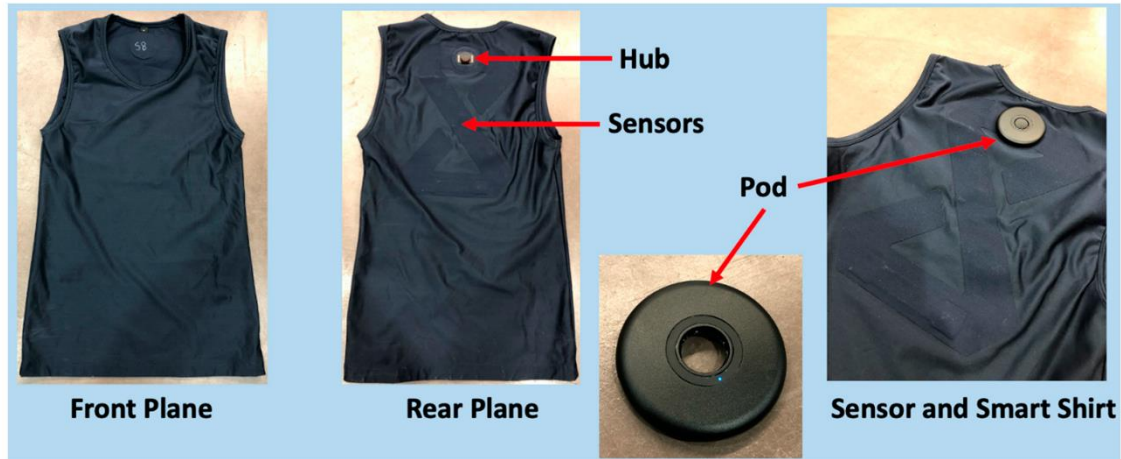


Figure 2-10 External Layout of Tyme Wear Smart Shirt and Pod[166]

OM Signal Bra (Figure 2-11) is an intelligent garment technology designed explicitly for women. OM Signal Bra incorporates advanced cloth detectors into a comfortable and protective sports bra and can track biometric data, including heart rate, respiration rate, and physical exertion situations. The data collected by the OM Signal Bra can be fluently transferred to a mobile operation, so users are informed about their health and fitness progress in real-time. The OM Signal Bra is designed with comfort and functionality and is made from high-quality, sweat-wicking material.

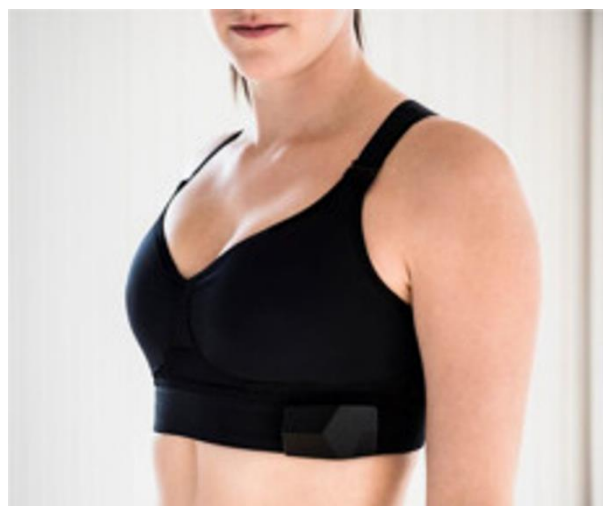


Figure 2-11 OM Signal Bra.[167]

Another product utilizing intelligent garment technology is the Hexoskin Smart[168]. As shown in Figure 2-12, this shirt has advanced cloth detectors knitted into the fabric that can cover various biometric data, including ECG, blood pressure,

activity level, skin temperature, etc.[169]. The data collected can be fluently transferred to a mobile operation, allowing users to cover their health and fitness progress in real-time. The Hexoskin Smart Shirt is designed to be durable and accessible, with the capability to be washed and worn like a regular garment. Hexoskin Smart Shirt takes a more holistic approach by incorporating a range of biometric data, including ECG, blood pressure, activity level, and skin temperature. This makes it a versatile choice for athletes looking for comprehensive health monitoring.



Figure 2-12 Hexoskin Smart Shirt. [169]

In addition to these commercial intelligent garment systems, several other analogous products are also available. While this overview highlights some of the key commercial IGS available, it's worth noting that the wearable technology spectrum in sports is broad and continually expanding. These include Whoop Strap[170] and Nadi X Yoga Pants[171]. These products use advanced wearable technology to cover biometric data and give real-time feedback via a mobile app. They're designed to be comfortable and discreet, allowing individuals to cover their health and fitness without demanding a separate wearable device. Details of the representative commercial intelligent garment systems are shown in Table 2-3.

Table 2-3

Details of the representative commercial intelligent garment system.

Commercial Products	Biometric data	Washability	Machine Wash	Availability / Price
Xiaomi Mijia Cardiogram T-shirt[163]	ECG	Yes	No	€35.43
Athos shirt[164]	sEMG	Yes	Not recommended	\$298
Tymewear[165]	VO ₂ Max & Heart Rate	Yes	Yes	\$35/ Month
OM Signal Bra[167]	ECG	Yes	Yes	\$150
Hexoskin Smart Shirt[168]	ECG	Yes	Yes	\$499
Whoop Strap[170]	ECG	Yes	Yes	\$264/Year
Nadi X Yoga Pants[171]	sEMG	Yes	Yes	\$65

While the table highlights some of the paramount commercial IGS available in the market, it's worth noting that the wearable technology spectrum in sports is broad and continually expanding. Beyond the field of Intelligent Garment Systems, the athletic domain has embraced a slew of other wearable devices. Activity trackers such as Fitbit and Garmin have gained immense traction for their role in optimizing athletes' daily physical activities. Intelligent shoes, with Under Armour's HOVR series as a notable example, have revolutionized footwear by embedding sensors that monitor crucial parameters like pace and stride length. Additionally, innovative sportswear, like Sensoria's heart rate monitoring sports bra, has bridged the gap between apparel and technology. Even minimalist devices, such as the Oura Ring, pack a punch by providing insights into metrics like body temperature and heart rate, aiding athletes in understanding recovery patterns. As the convergence between technology and sportswear deepens, athletes and trainers are better equipped than ever to harness data for performance enhancement.

2.6 Conclusion

The detailed review of the latest research in bioelectric signal monitoring, fatigue assessment, smart textiles and AI methods for sport revealed great progress and

opportunities for further study. ECG and EMG signals have been widely accepted as useful signs of an athlete's physical state, giving insight into heart health, muscle activity, and fatigue. New developments in wearable technology, especially in textile electrodes and smart garment systems, have allowed for non-stop, real-time tracking of these bioelectric signals during sports.

However, the current state of wearable ECG and EMG monitoring systems still has some issues. Traditional gel-based electrodes, while giving reliable signal collection, are not ideal for long-term use due to problems like skin irritation and signal quality getting worse over time. Dry textile electrodes have come up as a promising option, offering better comfort and ease of use. But, the stability and signal quality of these electrodes can be affected by things like motion, different skin conditions, and how much pressure is between the electrode and skin.

Fatigue assessment methods, such as the Borg scale and regular EMG analysis techniques, have been widely used to measure an athlete's perceived effort and muscle fatigue. While these methods give valuable insights, they often depend on subjective ratings or need data processing after exercise, limiting their use for real-time fatigue monitoring during sports.

Putting smart textiles and intelligent garment systems together has opened up new ways for comfortable, non-stop monitoring of bioelectric signals. Commercial products like the Xiaomi Mijia Cardiogram T-shirt, Athos Shirt, and Hexoskin Smart Shirt have shown the potential of seamlessly adding sensors into clothing for ECG and EMG monitoring. However, these systems often face challenges in terms of signal quality, durability, and user comfort, especially during long-term use in active sports settings.

Recent progress in AI methods, such as deep learning techniques, has shown promise in improving the accuracy and strength of bioelectric signal analysis for sports applications. Convolutional neural networks, recurrent neural networks, and transformer models have been used to pull out meaningful features and sort fatigue levels based on ECG and EMG data. However, the performance of these AI models can

be limited by things like data quality, differences between individuals, and the need for large, diverse training datasets.

In this context, my study aims to address the shortcomings of existing wearable ECG and EMG monitoring systems by developing a new intelligent garment system designed specifically for real-time fatigue assessment in sports. The key innovations of my approach include:

(1) The design and creation of 3D knitted silver electrodes that provide better comfort, durability, and signal quality compared to traditional textile electrodes. The detailed design process, considering factors such as electrode size, height, and pressure, ensures the best electrode-skin contact and minimizes motion-related signal noise.

(2) The seamless integration of these electrodes into a compression garment, along with carefully designed conductive channels and adjustable fastening mechanisms, enables stable and reliable signal collection during dynamic sports activities.

(3) The development of advanced AI algorithms, such as the LSTM model, that use the unique combination of ECG and EMG features to accurately predict fatigue levels in real-time. By including both time-based and static features, the model captures the complex interaction between heart and muscle factors contributing to fatigue.

(4) The thorough testing and validation of the intelligent garment system in a realistic cycling sport scenario, showing its effectiveness in monitoring fatigue progression and providing personalized insights for athletes and coaches.

By addressing the limitations of current wearable ECG and EMG monitoring systems and applying advanced textile engineering, sensor technology, and AI methods, my study aims to contribute to the development of practical, reliable, and user-friendly fatigue assessment tools for sports applications. The proposed intelligent garment system is designed to provide personalized fatigue predictions based on an individual's specific physiological data. By integrating knowledge from textile engineering, sensor technology, and AI, this study presents a fatigue monitoring solution that is tailored to the unique needs of each athlete. The testing and validation of the system in a realistic cycling scenario demonstrate its potential to support athletes in understanding their

individual fatigue patterns and making informed decisions about their training and recovery. While the system's primary focus is on personalized fatigue prediction, this research aims to lay the foundation for future advancements in fatigue monitoring technology. By developing a customizable approach to fatigue assessment, this study takes a step towards more effective and accessible tools that cater to the diverse needs of athletes across various sports and performance levels. Further research and refinement may be necessary to expand the system's capabilities and explore its potential applications in different sports contexts. Nonetheless, this study contributes to the ongoing efforts to harness technology for enhancing our understanding and management of fatigue in sports, ultimately empowering athletes to optimize their performance while minimizing the risks associated with excessive fatigue.

CHAPTER 3 Design, Fabrication, and Evaluation of Intelligent Garment Systems

This chapter presents the development and assessment of an innovative Intelligent Garment System (IGS) for real-time bioelectric signal monitoring in sports applications. We begin by addressing the limitations of traditional electrode technologies and introduce a novel 3D knitted silver electrode design. The chapter details the systematic approach to electrode fabrication, optimization, and characterization, emphasizing the importance of parameters such as electrode geometry, applied pressure, and skin hydration levels on impedance performance.

We then describe the integration of these optimized electrodes into a functional intelligent garment, discussing the strategic placement of ECG and EMG sensors, innovative conductive pathways, and the incorporation of data acquisition hardware. The chapter also outlines the development of accompanying software for real-time signal visualization and analysis. Through rigorous experimental procedures and comprehensive data analysis, this chapter aims to demonstrate the potential of our IGS for accurate, comfortable, and continuous physiological monitoring in dynamic sporting environments.

IGS has revolutionized the field of bioelectrical signals monitoring. A critical aspect of IGS involves the development of electrodes for the monitoring of electrophysiological signals such as ECG, EMG, etc. to assess human physiological conditions[172-174]. Traditional clinical long-time monitoring practices have relied heavily on disposable adhesive silver/silver chloride (Ag/AgCl) electrodes for capturing these signals[175]. However, the practicality of these electrodes for long-term, continuous monitoring presents significant challenges. Despite the remarkable progress in wearable technology, the limitations of existing electrode technology remain a significant concern. The use of Ag/AgCl gel electrodes, while effective in the short term, is hindered by their inherent drawbacks. Skin irritation, caused by prolonged contact with the gel, poses discomfort and can lead to allergic reactions [176]. Moreover, the

gel's tendency to dehydrate over time results in the strong degradation of signal quality, rendering them unsuitable for long-term or daily use [177]. To address these issues, researchers have diligently sought alternatives, leading to the development of dry electrodes using conductive elastomeric materials [178-180]. Among these, conductive elastomeric materials have gained prominence, alongside innovative compositions such as Ag/G (silver-coated glass) composite materials [181], PDMS-CB (Polydimethylsiloxane-Carbon Black) conductive polymers [182, 183], and PEDOT:PSS (poly(3,4-ethylenedioxythiophene) polystyrene sulfonate) conductive composites [184-186]. The design of dry or semi-dry electrodes represents a significant enhancement to these developments, combining the hydration control of wet electrodes with the user-friendly attributes of dry types. These dry or semi-dry electrodes utilize super porous hydrogels to regulate electrolyte release through capillary action, effectively maintaining stable skin-electrode impedance and enhancing user comfort for extended wear [187, 188]. By incorporating materials like polyacrylamide and polyvinyl alcohol, these electrodes effectively reduce impedance and improve signal fidelity [189, 190]. This evolution illustrates a significant shift towards creating more adaptable electrodes that not only reduce skin irritation and improve wearer comfort but also maintain high conductivity and signal fidelity for ECG/EMG/EEG monitoring, offering substantial advantages over traditional Ag/AgCl electrodes [191]. Besides, in comparison to traditional Ag/AgCl electrodes, these electrodes offer significant advantages in terms of ease of use and non-invasiveness for electrocardiogram (ECG) monitoring. They, characterized by their lack of requirement for gel or other wetting agents, enable a quicker setup and are conducive to repeated long-term use without the risk of skin irritation common with their Ag/AgCl counterparts. However, despite their promise for revolutionizing ECG monitoring, they still encounter distinct challenges. Among them, the issues of breathability and comfort during extended periods of sporting activities are particularly notable. The integration of these electrodes into wearable technology for continuous health monitoring necessitates innovative solutions to enhance their adaptability and user experience, especially in dynamic and physically

demanding environments.

In recent years, the domain of textile electrodes has witnessed a notable surge in scholarly interest, particularly regarding electrodes fabricated from silver threads. This heightened focus is largely due to the distinctive attributes of textile materials, which include inherent softness and comfort, coupled with their facile integration into wearable devices. Silver yarn electrodes, characterized by their superior electrical conductivity, stand out as a promising avenue for advancement in wearable technologies. As for the realization of conducting flexible surface for electrode, such as compression garments, the most used technologies are screen-printing [192-195], dip-coating [196] and embroidery [197, 198]. However, they demonstrate some significant limitations. For instance, the durability of printed electronics on fabrics is a significant concern, particularly their ability to withstand the rigors of bending, stretching, abrasion, and repeated washing cycles [199]. Furthermore, dip-coating procedures exhibit inconsistencies in the surface texture and uniformity of conductive layers applied to textiles, which can result in fluctuations in electrical resistance. The control over the thickness of these layers is inherently limited, as it is contingent on the textile's surface morphology, tension within the substrate, and a range of processing parameters such as time, temperature, withdrawal speed, compound concentration, and the composition of the coating bath [200]. Embroidery technology, while adept at creating dense conductive surfaces, tends to produce structures that are excessively thick and rigid, consequently lacking in essential flexibility and stretchability [201].

In contrast, electrodes developed through knitting technology not only preserve the fabric's natural elasticity and comfort but also seamlessly integrate electronic functionalities, ensuring minimal impact on the textile's inherent stretchability and softness. This method proves especially advantageous for compression garments, where maintaining the original textile properties while incorporating electronic capabilities is crucial.

However, the contact issue between the electrodes and the human skin is crucial for the guarantee of the signal quality. The unstable physical contact introduces the

noise and distortions during the data acquisition because of the motion artifacts and varying contact pressures. Therefore, in this study, we propose a 3D format knitted textile electrode. The advancement in 3D knitted electrodes structure introduces a significant innovation in smart textile fabrication. This structure is inherently designed to accommodate complex shapes and functionalities, enabling a direct integration of electronic features into the textile's architecture and offering a one-step process that enhances the efficiency and feasibility of producing smart textiles. This methodology not only streamlines the manufacturing process but also opens new avenues for creating more sophisticated and integrated wearable technologies.

3.1 Design, Fabrication, and Evaluation of 3D Textile Biopotential Electrodes

3.1.1 Design and Fabrication of Textile Electrodes

Our research focuses on the innovative design and fabrication of 3D knitted silver electrodes, tailored for real-time biopotential signals monitoring during long-term physical activities. As shown in Figure 3-1, compared to gel electrodes (left side), dry electrodes (right side) are more concise in the skin contact model, and due to the abandonment of gel, sweat can be a better conductive medium, and the conductivity of dry electrodes does not decrease as much as that of gel electrodes along the increase of the exercise duration. It may be observed on the left side of Figure 3-1, two RC parallel cells, one of them illustrates the skin to electrode impedance and the other one for the gel impedance. When the gel dehydrates the corresponding impedance modulus in the RC cell increases strongly making very difficult for the bio-signal acquisition. On the right side of Figure 3-1, there is only one RC cell for the skin to textile dry electrode impedance. Besides, since of the 3D structure, the physical contact between the electrode and the skin is improved compared with traditional coating/embroidered textile electrodes. Therefore, 3D knitted silver electrodes can help to enable extended, real-time physiological signal monitoring while ensuring user comfort and ease of use.

To achieve this goal, we have leveraged advanced silver fiber materials, a leading-edge solution in the field. Through a systematic exploration of various electrode parameters, such as height, size, and pressure, we have conducted skin-electrode impedance experiments to determine the optimal electrode design. By addressing the existing limitations of dry electrodes, our work paves the way for practical, real-time, and continuous physiological monitoring. This development holds considerable promise for applications in healthcare, sports, and everyday life, with potential implications for early diagnosis and management of various conditions.

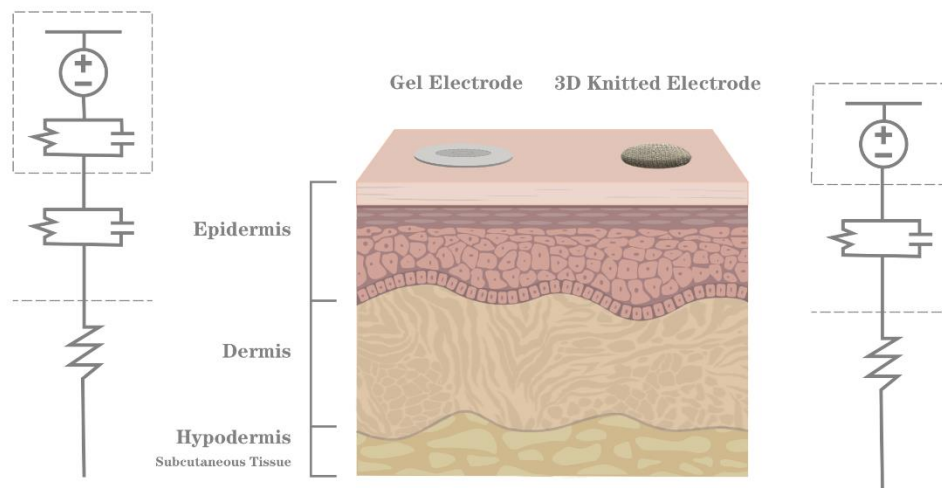


Figure 3-1. Skin contact model for gel and dry electrodes.

In this study, 3D knitted silver electrodes were fabricated using silver-plated nylon thread (DTY 140D/3 Silver Fiber Filamentn, Kazhtex Technology Co., Ltd, Suzhou, China). Figure 3-2 presents the SEM (Scanning Electron Microscope) images of the silver-plated nylon thread, highlighting its detailed microstructure. The thread exhibits a diameter of 0.45 mm and an electrical resistance of 200 Ω /m. It is constructed from a three-ply yarn incorporating 48 individual filaments, specifically utilized for knitting the 3D electrodes. This configuration is chosen to ensure optimal electrical conductivity and mechanical durability, which are critical for the functionality of the textile electrodes. This thread is called “electrode yarn” in the garment.

For the remaining components of the intelligent garment system, excluding the

electrodes, a high-elasticity nylon filament is employed. This filament (Yinrui Fiber Company, Shaoxing, China) is composed of a blend of 20D spandex and 40D nylon, with a spandex stretch ratio of 3.6. It is supplied by and is utilized for knitting the jersey stitch structures of the garment. The choice of this high-elasticity filament ensures that the garment maintains flexibility and comfort, essential for prolonged wear and practical usability in dynamic environments. This thread is called “structure yarn” in the garment.

Regarding the connection between the 3D knitted silver electrodes and the hardware (ECG/MG ADC chips), customized composite silver conductive yarns were selected. The core yarn of this conductive yarn consists of 18 strands of silver-plated nylon filament with a high silver content, demonstrating an electrical resistance of less than $2.7 \Omega/\text{m}$. This low resistance is crucial for reducing signal attenuation and ensuring accurate data transmission. An insulating layer encases the core to prevent unintentional conductivity issues with adjacent wires, thereby enhancing the reliability of the system. The outermost layer is a braided silver shield, designed to serve as an electromagnetic interference (EMI) shield. This design is aimed at minimizing the influence of power frequency interference on the collected ECG/EMG signals, thus ensuring the acquisition of clearer and more stable signals. This yarn is called “transmission yarn” in the garment.

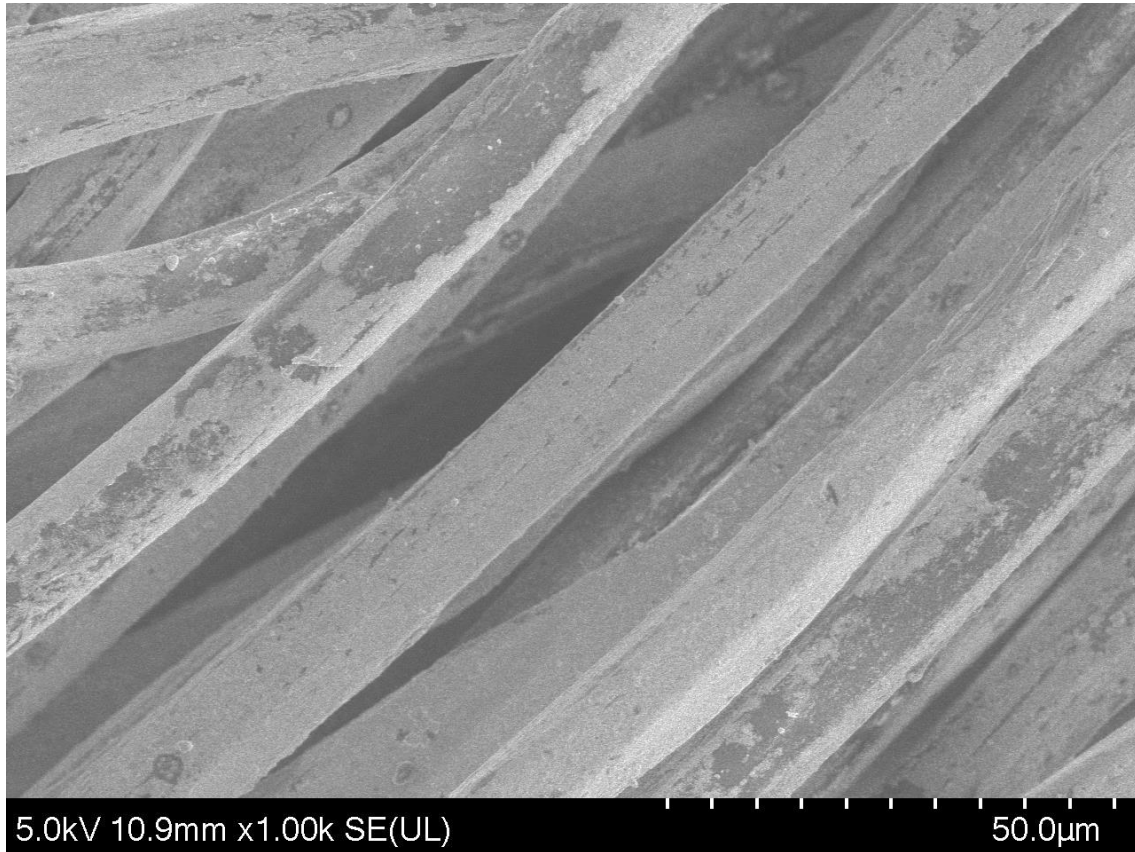


Figure 3-2. SEM of low silver-plated nylon thread.

The textile electrodes are fabricated using a STOLL 72G knitting machine (STOLL, Germany). The base knitted fabric utilizes a jersey stitch with high-elasticity nylon filament (structure yarn), a choice predominantly favored for manufacturing compression garments due to its superior stretchability and comfort. Figure 3-3 illustrates the structure of the 3D knitted silver electrode, which necessitates a harmonious combination of diverse knitting textures to achieve the envisioned complex 3D construct. The electrode component, highlighted in yellow, employs silver-plated nylon thread (electrode yarn) and is meticulously knitted in a round shape using the double tuck stitch. This specific knitting technique not only enhances the conductivity of the electrodes but also contributes to the creation of a localized three-dimensional effect, crucial for the accurate detection of biopotential signals.

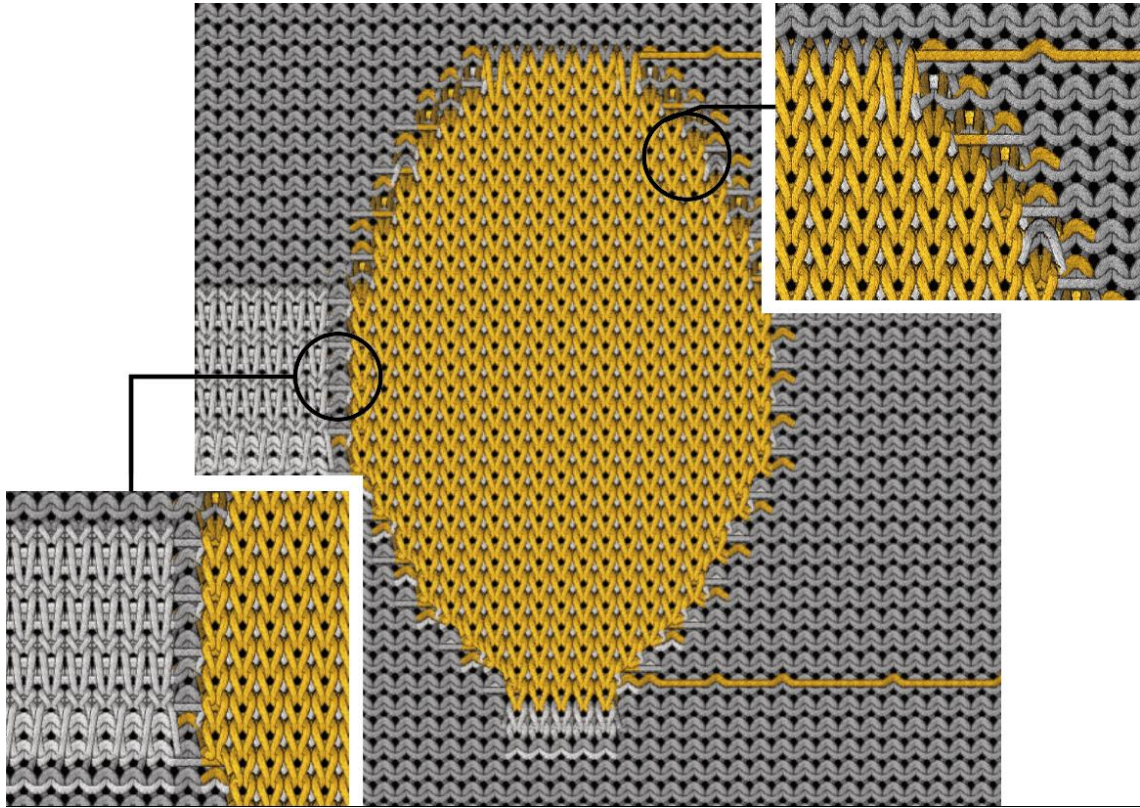


Figure 3-3. Structure of 3D knitted electrodes on the back side of fabric.

The detailed view of the knitted fabric structure reveals the incorporation of conductive yarn for transmission purposes. The silver-colored conductive yarn is placed on the back surface of the fabric using a specialized knitting technique called the "drop stitch" structure. In this method, the conductive yarn is introduced into the fabric during the knitting process of the 3D electrodes. It enters the fabric from above and exits below, essentially "floating" on the back surface without being fully integrated into the main jersey knit structure. To ensure a smooth knitting process and prevent potential issues such as excessive yarn length, thread breakage, or needle collisions in the knitting machine, a specific type of stitch called the "double tuck" stitch is used at regular intervals. These stitches help to secure the conductive yarn in place and provide additional mechanical stability and durability to the electrodes. By employing this combination of drop stitch structure and double tuck stitches, the conductive yarn can be effectively incorporated into the fabric without compromising the overall integrity of the knitted structure.

In the inset at the top right corner of Figure 3-3, the transition between the two

types of yarn (structure yarn and electrode yarn) is depicted, showcasing the application of localized intarsia techniques to seamlessly intertwine the differing yarns. The high elasticity of the nylon filament, contrasted with the non-elastic nature of the silver-plated nylon thread, along with the difference in knitting densities, collaboratively produce a significant 3D effect. By adjusting the yarn tension in the STOLL flat knitting process, we can precisely control the height of the electrode. Increased yarn tension results in a more pronounced electrode protrusion, thereby amplifying the three-dimensional effect and enabling meticulous control of the electrode's spatial attributes. This localized intarsia approach also aids in enclosing the edges of the electrodes, ensuring the stability of loop dimensions and preventing unraveling due to stretching or other external forces.

The lower left corner insert of Figure 3-3 demonstrates the knitted hollow channel, which is the knitted hollow channel through drop stitch techniques. This channel is specifically engineered to house low-resistance silver conductive wires (transmission yarn), which function as a medium for connecting the 3D silver electrodes to electronic components. The design of the channel is critical, as it ensures the robust and reliable connection necessary for effective biopotential signal transmission. This feature enhances the overall functionality of the intelligent garment system by maintaining the integrity of the electrical connections under various conditions of wear and use. A completed 3D knitted silver electrode is shown in Figure 3-4.



Figure 3-4. 3D knitted silver electrode. (Top) Back side of the knitted fabric. (Bottom) Front side of the knitted fabric.

Figure 3-5 presents the variations in electrode diameters and heights explored for impedance measurement. The diameter of the electrodes ranged from 1 cm to 3 cm, with increments of 0.5 cm. This range was chosen for its suitability in bioelectrical signal detection, as different electrode sizes can significantly influence the quality and specificity of the detected signals. Smaller electrodes can provide higher spatial

resolution, which is advantageous for detecting localized biopotential signals, whereas larger electrodes can capture broader signal areas, potentially improving signal stability and reducing noise.

The height of the electrodes varied from 0.5 mm to 3 mm, in increments of 0.5 mm. Adjusting the height allows for fine-tuning the contact interface between the electrode and the skin, which is essential for optimizing impedance and improving signal acquisition. Taller electrodes can penetrate deeper into the skin layers, potentially enhancing the contact quality and reducing contact impedance. This, in turn, can lead to a more accurate and stable signal acquisition, which is critical for applications such as ECG and EMG monitoring.

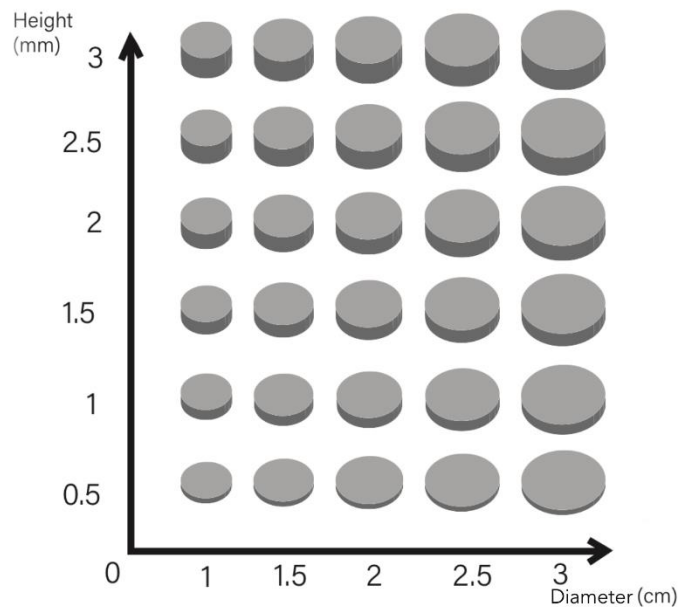


Figure 3-5. Parametric design of 3D knitted electrodes by height and diameter

These variations in electrode dimensions enable a comprehensive analysis of how different physical characteristics affect impedance and overall performance in biopotential signal detection. By systematically varying the diameter and height of the electrodes, we can identify the optimal dimensions that balance the need for precise signal detection with the practical considerations of electrode fabrication and user comfort. This detailed exploration helps in refining the electrode design, ensuring that

the final product provides reliable and high-quality biopotential signal detection for various biomedical applications.

3.1.2 Evaluation of Textile Electrodes

The circuit diagram (Figure 3-6) is purposefully designed to directly measure the impedance Z_{c2} of the skin-electrode contact in a three-lead configuration, drawing inspiration from the methodology presented by Emanuel Gunnarsson [202]. In this setup, segment Z_{b4} is effectively isolated from carrying any current, as it is connected in series with the high input impedance of the voltmeter. Consequently, the high-end potential of the voltmeter aligns precisely with the junction where impedances Z_{b3} , Z_{b4} , and Z_{c2} converge, specifically at one side of the skin-electrode contact Z_{c2} . This leads to the simplified measurement equation $V = Z_{c2} \times I$, enabling the direct measurement of the skin-electrode contact impedance Z_{c2} .

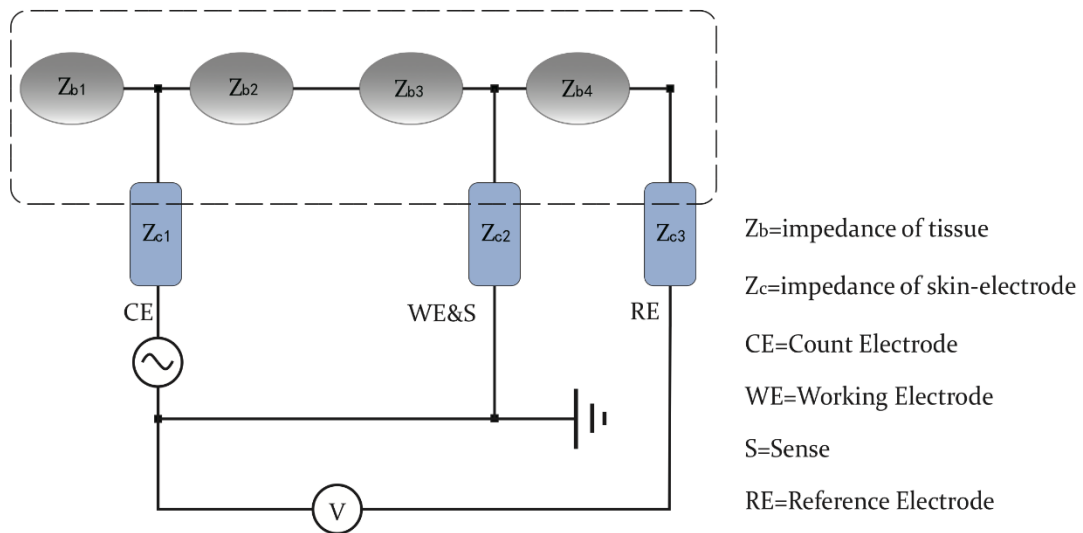


Figure 3-6. Circuit for impedance test

A key advantage of this methodological approach is that the impedance measurement does not rely on any assumptions about the symmetry or precise

knowledge of the surrounding tissue impedance, as these factors do not factor into the calculation. The only prerequisite is that the voltmeter's input impedance must be sufficiently high to prevent current leakage into that branch, a condition usually met by modern high-impedance voltmeters. Thus, this three-lead configuration is uniquely suited for directly measuring the skin-electrode contact impedance without resorting to estimations or indirect methods. Moreover, this three-lead approach overcomes limitations of traditional two-lead methods by not assuming uniformity of body and skin-electrode impedances across different anatomical locations. By focusing the measurement solely on the skin-electrode interface itself, it provides a direct and accurate characterization that is essential for the effective design and evaluation of textile electrodes used in wearable technologies. This method ensures precise measurement of the skin-electrode interface impedance, eliminating the need for assumptions about tissue impedance symmetry or comprehensive knowledge of surrounding tissue impedances, making it highly practical and suitable for real-world applications.

The Ivium-n-stat impedance analyzer (Ivium Technologies Inc., Eindhoven, Netherlands) was employed to perform the impedance measurements. The complete electrode-skin impedance test setup is depicted in Figure 3-7 (a). To simulate the effects of skin pressure, stainless steel blocks were fabricated with pressure settings of 10 mmHg, 20 mmHg, and 30 mmHg. These selected pressures are representative of those typically used in medical-grade compression garments and serve as meaningful reference points for evaluating the performance of compression textile electrodes [203, 204].

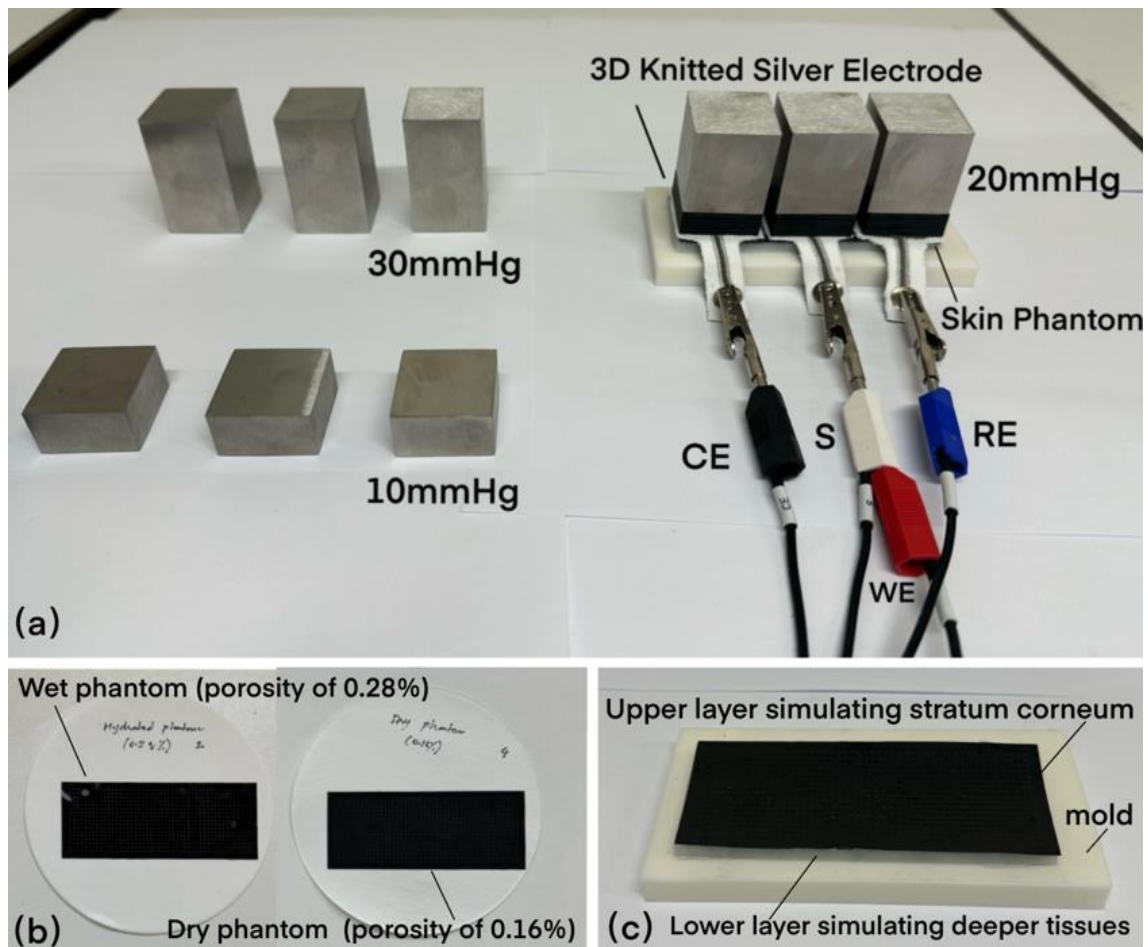


Figure 3-7. (a) Electrode-Skin impedance test setup. (b) Wet phantom and Dry phantom. (c) Upper and Lower layers of the skin phantom and mold.

Skin phantoms made from agar have been commonly reported in literature for evaluating the performance of biopotential electrode designs [205-207]. However, the existing agar-based phantoms have only been validated for simulating the electrical characteristics of deeper tissue layers, such as the dermis and hypodermis, and only in higher frequency ranges. Furthermore, the hydration state of the skin, which can significantly impact skin impedance, cannot be readily modeled using conventional agar-based phantoms.

To address these limitations and more accurately model skin behavior during physical activity, a novel two-layer skin phantom was adapted from the work of Goyal et al. [208]. This phantom can simulate the impedance of the skin in the frequency range of 1 Hz–1000 Hz, which encompasses the bandwidth of typical biopotential signals. Importantly, it also enables the modeling of different skin hydration levels in a

controlled manner by varying the porosity of the phantom's upper layer. The effects of varying porosity to represent distinct skin hydration states are visually apparent in the phantoms shown in Figure 3-7 (b). The "wet" phantom, with an upper layer porosity of 0.28%, mimics well-hydrated skin, while the "dry" phantom, with a porosity of 0.16%, simulates dehydrated skin conditions.

The layered structure of the skin phantom is illustrated in Figure 3-7 (c). The upper layer represents the stratum corneum, the outermost layer of the skin, while the lower layer corresponds to the deeper dermal and hypodermal tissue layers. To fabricate the upper layer, a mixture of polydimethylsiloxane (PDMS), carbon black (2.5% W/W) for increased conductance, and barium titanate (40% W/W) for enhanced dielectric properties was prepared and spin coated to a thickness of 100 μm , mimicking the thickness and electrical properties of the stratum corneum. As mentioned, the porosity of this upper layer was varied between 0.16% and 0.28% to simulate dry and wet skin conditions, respectively.

The lower layer of the phantom, representing the deeper tissue layers, was fabricated using a polyvinyl alcohol (PVA) cryogel solution and a cyclical freeze-thaw process. The PVA solution was prepared by mixing 8.8 g of PVA with a 0.9% W/W saline solution. This mixture was then poured into a mold to a thickness of 5 mm and subjected to repeated freeze-thaw cycles to crosslink the PVA, resulting in a flexible and electrically stable cryogel that mimics the bulk impedance characteristics of the dermis and hypodermis.

By combining a conductive, porosity controlled PDMS upper layer with a PVA cryogel lower layer, this novel skin phantom enables realistic modeling of both the stratum corneum and deeper tissues, while also allowing for controlled variation of skin hydration states. This makes it a valuable tool for evaluating the performance of textile electrodes under different skin conditions representative of real-world use scenarios.

Figure 3-8 presents the impedance-frequency and phase-frequency characterization results for the 3D knitted electrodes, obtained under a constant pressure of 30 mmHg on a skin phantom with a porosity of 0.28%, simulating well-hydrated

skin. The data reveals two distinct trends that highlight the influence of electrode geometry on impedance performance, a critical consideration in the design of biopotential monitoring devices.

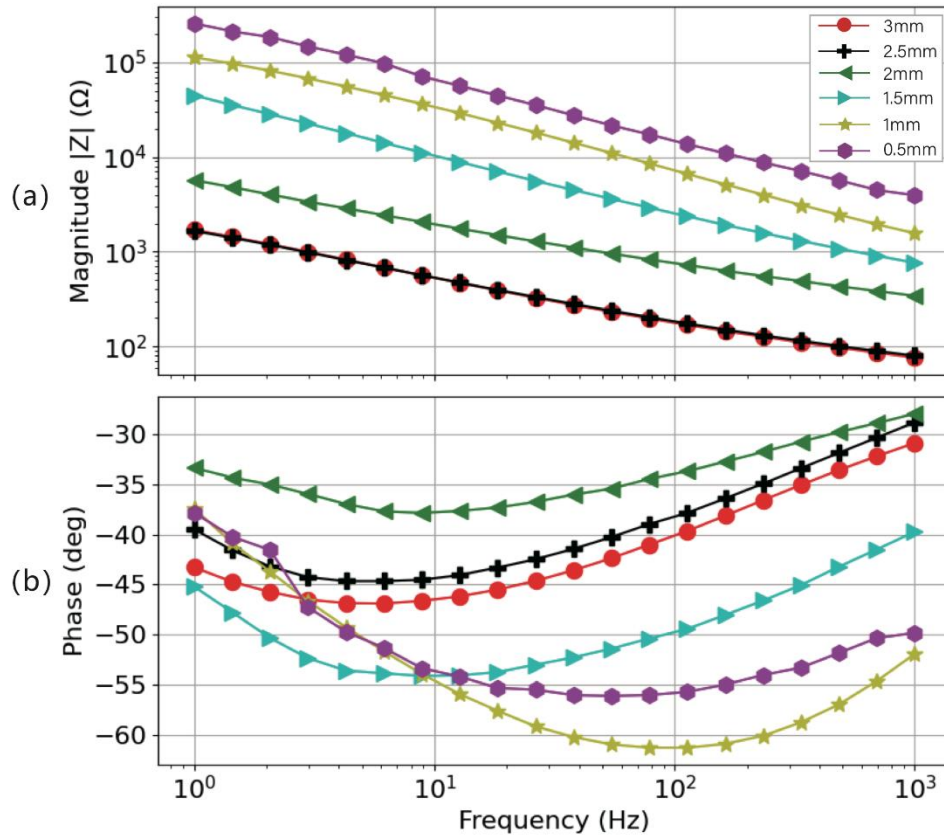


Figure 3-8. Impedance measurement result for the circle electrode with 3 cm as diameter and 0.5 to 3 mm as height under the pressure of 30 mmHg. (a) Impedance magnitude and (b) phase response.

Firstly, for a given electrode configuration, the impedance magnitude exhibits a clear decrease with increasing frequency across the measured range of 1 Hz to 1000 Hz. This behavior is consistent with the typical frequency response of skin-electrode interfaces, where capacitive effects dominate at lower frequencies, leading to higher impedance values, while at higher frequencies, the resistive component becomes more prominent, resulting in lower impedance magnitudes. Secondly, the impedance magnitude at a fixed measurement frequency shows a notable dependence on the electrode height. Electrodes with smaller heights consistently display higher impedance values compared to their taller counterparts. This trend suggests that the electrode height plays a significant role in determining the skin-electrode contact impedance. A

plausible explanation for this observed relationship between electrode height and impedance lies in the internal structure of the 3D knitted electrodes. As the electrode height increases, the number of silver-plated conductive fibers within the electrode also increases. Under the same applied pressure, taller electrodes likely experience greater compression, leading to increased contact area between the internal conductive yarns. This results in a denser and more interconnected internal structure, which facilitates improved electrical conductivity and, consequently, lower contact impedance.

It is particularly noteworthy that the electrodes with heights of 3 mm and 2.5 mm exhibit similar impedance profiles, consistently maintaining lower impedance values across the entire frequency range compared to the shorter electrodes. This observation hints at a potential threshold effect in the relationship between electrode height and impedance reduction. Beyond a certain electrode height, in this case, around 2.5 mm to 3 mm, further increases in height may yield diminishing returns in terms of impedance improvement.

The phase response data reveals the intricate electrical characteristics of the skin-electrode interface. As depicted in Figure 3-8(b), all electrode configurations exhibit negative phase angles across the entire measured frequency range, indicating that the reactive component of the impedance dominates. The magnitude of the negative phase angle reflects the strength of the capacitive effects, with -90 degrees corresponding to purely capacitive behavior and -45 degrees representing equal resistive and capacitive contributions.

At lower frequencies (1 Hz to 10 Hz), the phase angles for all electrode heights approach -50 degrees, suggesting a strong capacitive influence. This observation aligns with the expected behavior of the stratum corneum, the outermost layer of the skin, which acts as a dielectric material. The stratum corneum's high impedance and capacitive properties are particularly prominent at low frequencies, as the electrical current faces difficulty in penetrating this layer. As the frequency increases, the phase angles gradually become less negative, indicating a shift towards more resistive behavior. This trend can be attributed to the current's increased ability to penetrate the

stratum corneum and reach the more conductive deeper layers of the skin at higher frequencies, which aligns with the findings of several scholars' research [209, 210]. The phase angles for the 3 mm and 2.5 mm height electrodes converge to approximately -35 degrees at 1000 Hz, suggesting that the resistive component becomes more significant at higher frequencies.

Interestingly, the phase response curves for the 3 mm and 2.5 mm height electrodes remain remarkably close throughout the frequency range, with a maximum difference of only 4 degrees. This similarity implies that the electrical properties of the skin-electrode interface, particularly the balance between resistive and capacitive components, do not vary significantly once the electrode height exceeds a certain threshold. This finding corroborates the notion of a threshold effect in the relationship between electrode height and impedance characteristics. Furthermore, the phase response curves for the shorter electrodes (with a height of 1 mm and 0.5 mm) exhibit a more gradual transition from capacitive to resistive behavior as the frequency increases. This slower transition suggests that the shorter electrodes may face greater difficulty in overcoming the capacitive barrier posed by the stratum corneum, possibly due to reduced contact area and less effective penetration of the conductive fibers into the skin. The phase response analysis provides valuable insights into the frequency-dependent electrical behavior of the skin-electrode interface. The dominant capacitive effects at lower frequencies, attributed to the stratum corneum, gradually give way to more resistive behavior as the frequency increases and the current penetrates deeper into the skin. The similarity in phase response between the 3 mm and 2.5 mm height electrodes reinforces the presence of a threshold effect, beyond which further increases in electrode height have limited impact on the electrical properties of the interface.

After understanding the influence of electrode height on impedance, we focused our investigation on electrodes with a height of 3 mm, which exhibited favorable impedance characteristics. Figure 3-9 presents the impedance magnitude and phase response of a 3 cm diameter circular electrode with a height of 3 mm applied to a skin phantom with a porosity of 0.28%, simulating well-hydrated skin under various levels

of applied pressure.

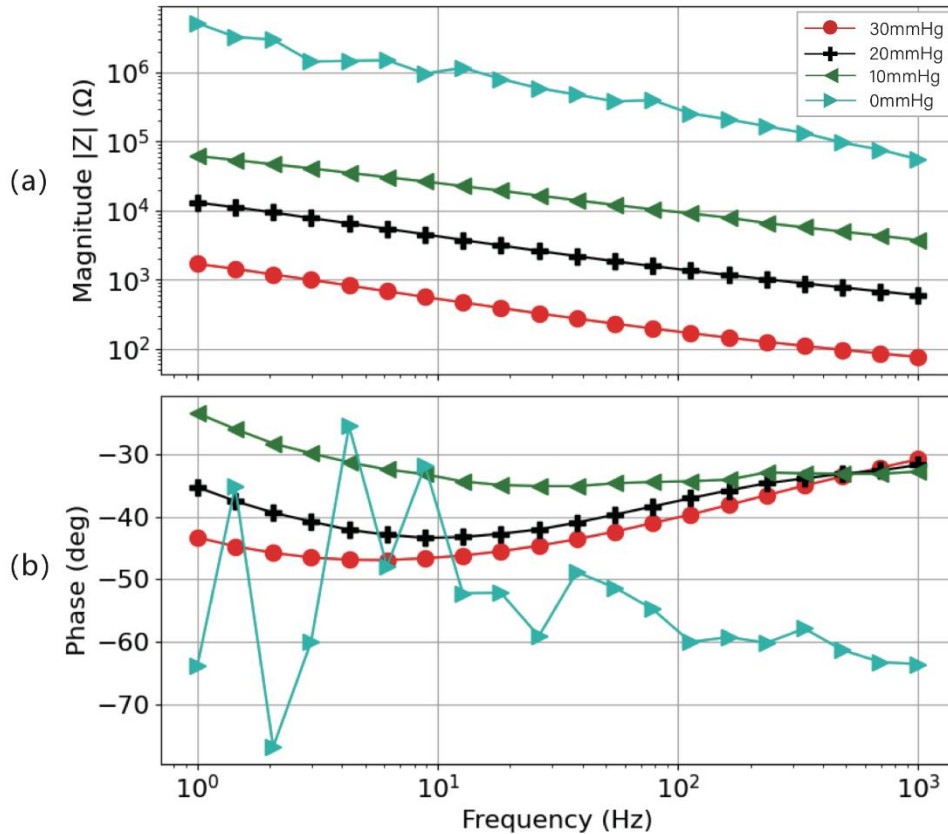


Figure 3-9. The impedance-frequency characterization and phase-frequency characterization, performed under controlled conditions featuring a 3 cm diameter circular electrode with a height of 3 mm and a skin model at 0.28% porosity. a) Impedance magnitude and b) phase response.

The impedance magnitude data (Figure 3-9(a)) reveals a clear inverse relationship between the applied pressure and the skin-electrode contact impedance. As the pressure exerted on the electrode decreases from 30 mmHg to 0 mmHg, the impedance magnitude exhibits a corresponding increase, highlighting the significant role of pressure in determining the quality of the skin-electrode interface. This pressure-dependent behavior is particularly pronounced at lower frequencies, where the impedance values show a more substantial variation with changing pressure. The plot effectively illustrates this trend, with the impedance magnitude progressively increasing as the applied pressure diminishes. This is in complete agreement with the previously reported work, as a higher-area electrode leads to lower impedance [211]. The relatively high skin-electrode impedance, on the order of mega ohms, obtained at

0 mmHg pressure suggests insufficient contact between the electrode and the skin phantom. This observation underscores the importance of maintaining adequate contact pressure to ensure reliable biopotential signal acquisition.

The phase response data (Figure 3-9(b)) provides further insights into the electrical characteristics of the skin-electrode interface under varying pressure conditions. At 0 mmHg pressure, the phase response indicates a dominant capacitive behavior, with phase angles approaching -90 degrees across the measured frequency range. This capacitive dominance can be attributed to the lack of effective contact between the electrode and the skin phantom, leading to a high impedance interface dominated by capacitive effects. As the applied pressure increases from 10 mmHg to 30 mmHg, the phase response curves exhibit a notable shift towards more resistive behavior, particularly in the higher frequency range (100 Hz - 1000 Hz). In this frequency range, the phase responses for pressures between 10 mmHg and 30 mmHg converge and remain within a narrow range, indicating that the electrical characteristics of the skin-electrode interface become less sensitive to pressure variations once a certain level of contact is established. In the lower frequency range (1 Hz - 100 Hz), the phase responses for pressures between 10 mmHg and 30 mmHg show a slightly larger variation, with a maximum difference of 15 degrees. This suggests that the capacitive effects of the skin-electrode interface are more sensitive to pressure changes at lower frequencies, where the stratum corneum's influence is more dominant.

The observed pressure-dependent behavior of the skin-electrode impedance has significant implications for biopotential signal monitoring in sports applications. Consistent and reliable signal capture is crucial in these scenarios, where motion artifacts and varying contact pressures can introduce noise and distortions in the recorded signals. The results highlight the importance of maintaining adequate and stable contact pressure between the electrode and the skin to minimize impedance variations and ensure high-quality signal acquisition. Furthermore, the convergence of the phase response curves at higher pressures (10 mmHg - 30 mmHg) in the 100 Hz - 1000 Hz frequency range suggests that once a sufficient level of skin-electrode contact

is achieved, further increases in pressure may have diminishing returns on the electrical characteristics of the interface. This finding can guide the design and application of biopotential monitoring systems, emphasizing the need to optimize contact pressure while considering factors such as user comfort and long-term wearability.

In conclusion, the impedance and phase characterization results presented in Figure 3-9 demonstrate the significant influence of applied pressure on the skin-electrode contact impedance and the electrical behavior of the interface. The inverse relationship between pressure and impedance magnitude, along with the pressure-dependent shifts in phase response, underscore the importance of maintaining adequate and stable contact pressure for reliable biopotential signal monitoring in sports applications.

It is important to stress that the ECG signal's main power lies in 5 Hz–15 Hz [212, 213], thus the signal quality evaluation may also be performed by calculating the power spectral density of the signal in the 5 Hz–15 Hz to that of the overall signal in 5 Hz–40 Hz [214]. Therefore, it is important to measure the skin-to-electrode impedance in this frequency range (5 Hz–40 Hz).

Figure 3-10 presents the impedance measurement results for electrodes with a fixed height of 3 mm and varying diameters, subjected to an applied pressure of 30 mmHg on a wet skin phantom. The impedance magnitude (Figure 3-10(a)) and phase response (Figure 3-10(b)) provide valuable insights into the impact of electrode diameter on the electrical characteristics of the skin-electrode interface.

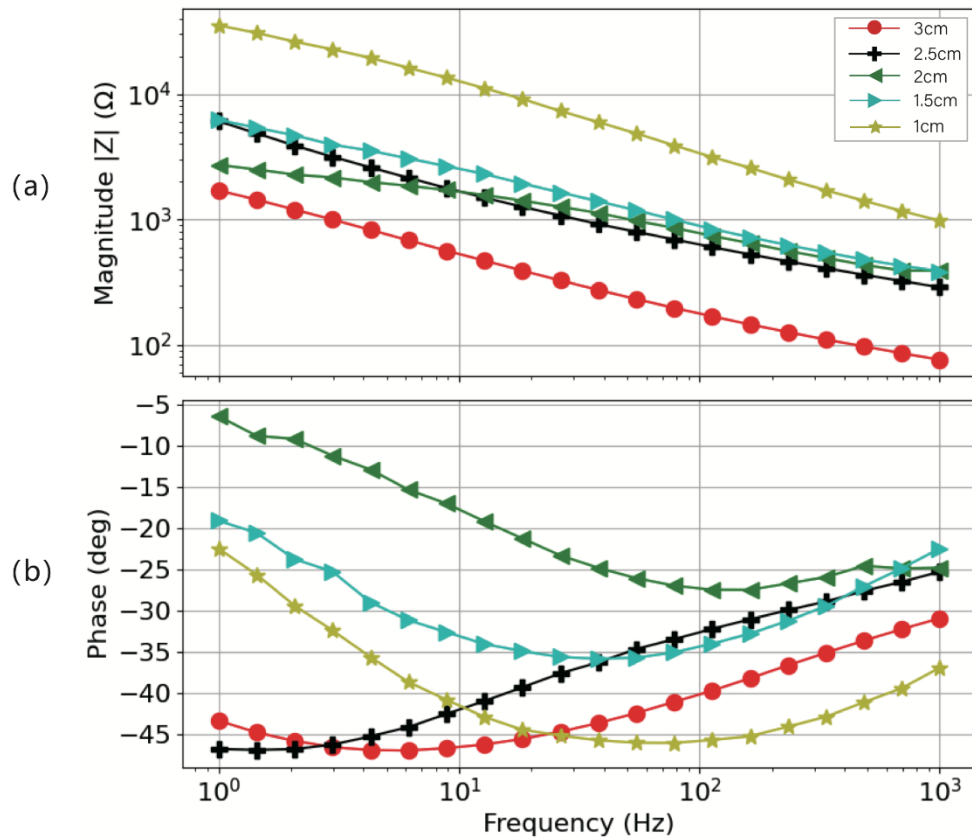


Figure 3-10. The impedance-frequency characterization and phase-frequency characterization, performed under controlled conditions featuring a height of 3 mm and a skin model at 0.28% porosity under the pressure of 30 mmHg. (a) Impedance magnitude and (b) phase response.

A clear trend emerges from the impedance magnitude data: as the electrode diameter increases, the impedance magnitude exhibits a corresponding decrease. This inverse relationship between electrode size and impedance can be attributed to several factors. Firstly, larger diameter electrodes have a greater surface area in contact with the skin phantom, facilitating improved electrical coupling and current distribution across the interface. Secondly, electrodes with larger diameters inherently contain a higher quantity of silver-plated conductive fibers, which enhances their overall electrical conductivity. The combination of increased contact area and superior conductivity results in lower impedance values for electrodes with larger diameters. Interestingly, the impedance magnitude curves for electrodes with diameters ranging from 1.5 cm to 2.5 cm exhibit remarkable similarity, particularly at frequencies below 10 Hz. In this low-frequency region, the differences in impedance between these

electrode sizes are minimal, suggesting the existence of a diameter range within which the impedance remains relatively stable. This observation hints at a potential optimal range for electrode diameter, where further increases in size may yield diminishing returns in terms of impedance reduction. The convergence of impedance curves for the 1.5 cm to 2.5 cm diameter electrodes at low frequencies is particularly noteworthy, as this frequency range is of great importance for biopotential signal acquisition. Many physiological signals, such as ECG and EEG, have significant spectral content in the low-frequency region. The diameter-related impedance stability observed in this range suggests that electrodes within this size range may provide consistent and reliable signal capture, minimizing the impact of electrode size variations on signal quality.

The phase response data (Figure 3-10(b)) provides further support for the diameter-related impedance stability phenomenon. The phase response curves for the 2.5 cm and 3 cm diameter electrodes exhibit a high degree of similarity across the entire frequency range, with a maximum difference of only 5 degrees between them. This close agreement in phase response indicates that the electrical characteristics of the skin-electrode interface, particularly the balance between resistive and capacitive components, remain relatively consistent for electrodes within this size range.

The findings presented in Figure 3-10 are in complete agreement with previously reported work, which has demonstrated that electrodes with higher surface areas generally exhibit lower impedance values. This consensus reinforces the validity of the observed trends and highlights the importance of electrode size considerations in the design of biopotential monitoring systems. From a practical standpoint, the diameter-related impedance stability phenomenon has significant implications for the development and application of wearable biopotential monitoring devices. It suggests that designers have some flexibility in selecting electrode sizes within the identified stability range without significantly compromising impedance performance.

The normalized magnitude, also known as normalized impedance, is a measure that allows for a comparative evaluation of electrode performance independent of their physical dimensions. This normalized magnitude is calculated as magnitude divided by

the surface area. By normalizing the impedance values with respect to the electrode area, the influence of electrode size is effectively eliminated, enabling a fair comparison between electrodes of different sizes or configurations [215]. This normalization technique is particularly valuable when assessing the intrinsic electrical properties and performance of electrodes, as it focuses on the inherent characteristics of the electrode-skin interface rather than the effects of varying electrode geometries.

Delving deeper into the normalized magnitude results presented in Figure 3-11 (a), it is evident that the 3D knitted silver textile electrodes exhibit lower normalized impedance than Ag/AgCl electrodes on wet skin across the frequency range of 10 Hz to 1000 Hz. This observation highlights the superior performance of textile electrodes in this frequency range under wet conditions, which can be attributed to several factors. Firstly, the inherent structural properties of the knitted textile electrodes, such as their high porosity and surface area, facilitate enhanced contact and conformability with the skin surface. This improved contact quality likely contributes to reduced impedance by minimizing the presence of air gaps or voids at the electrode-skin interface. Moreover, the hygroscopic nature of the textile material may promote the retention of moisture at the interface, further enhancing the conductive pathways and lowering the impedance in the wet state.

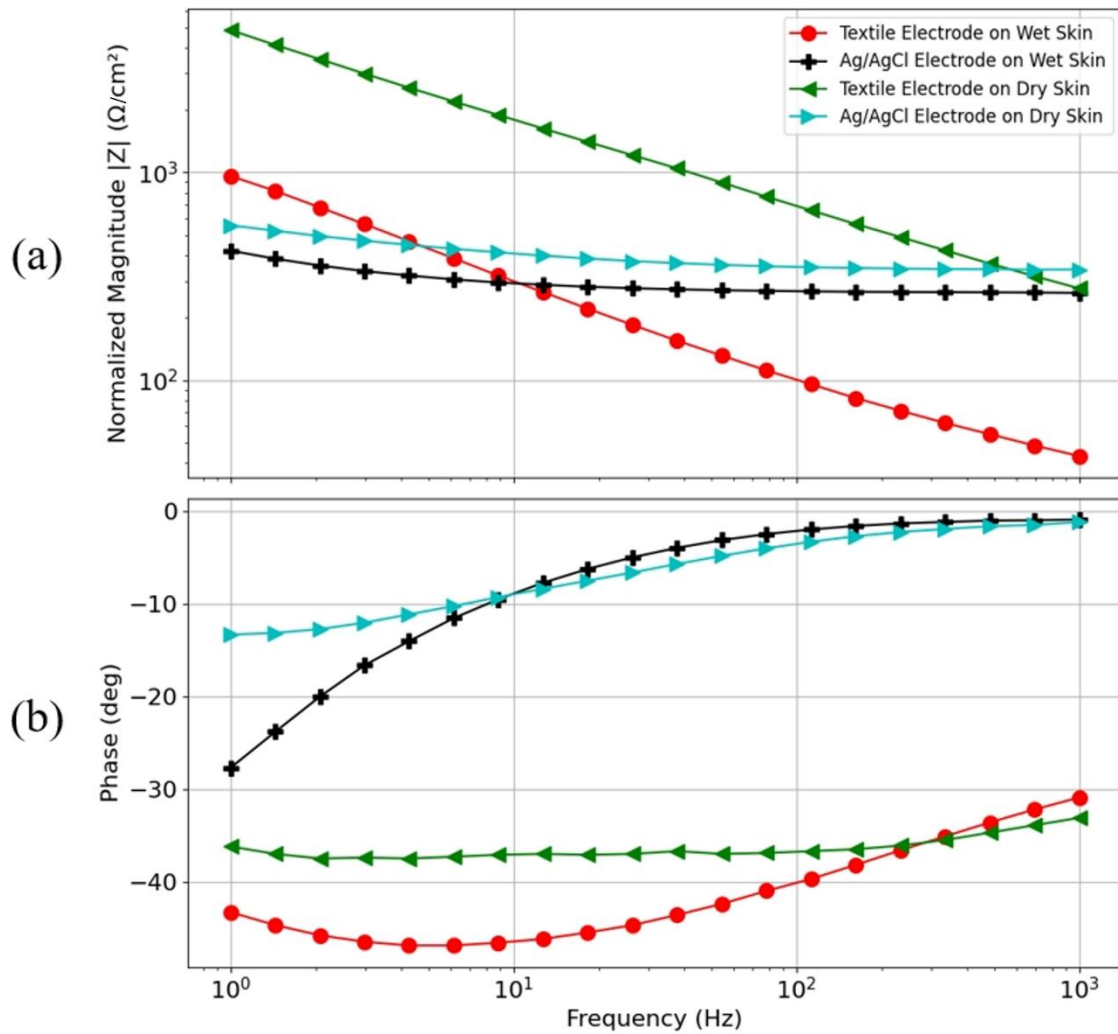


Figure 3-11. Impedance measurement results of 3D knitted silver electrodes and Ag/AgCl electrodes under dry and wet skin conditions. (a) Impedance magnitude and (b) phase response.

However, at frequencies below 10 Hz, the normalized impedance of textile electrodes on wet skin surpasses that of Ag/AgCl electrodes. This phenomenon can be explained by the fundamental differences in the charge transfer mechanisms between the two electrode types. Ag/AgCl electrodes primarily rely on resistive coupling, facilitated by the presence of an electrolytic gel that establishes a low-impedance conductive pathway. In contrast, dry textile electrodes exhibit a combination of capacitive and resistive coupling, with the capacitive component becoming more dominant at lower frequencies. The higher capacitive reactance at low frequencies contributes to the increased normalized impedance observed for textile electrodes in this regime.

Under dry skin conditions, Ag/AgCl electrodes maintain lower normalized impedance compared to textile electrodes across most of the frequency range, except for the region around 1000 Hz where the textile electrode impedance dips below that of Ag/AgCl. This observation suggests that the performance of textile electrodes is more susceptible to variations in skin hydration levels, whereas Ag/AgCl electrodes can maintain relatively stable impedance characteristics even in the absence of additional moisture. The steeper slope of the textile electrode impedance curve indicates a stronger frequency dependence, with the impedance increasing more rapidly as the frequency decreases. This behavior can be attributed to the increasing influence of the capacitive component of the electrode-skin interface at lower frequencies, leading to higher impedance values.

The phase response, depicted in Figure 3-11(b), provides complementary information regarding the frequency-dependent resistive and capacitive characteristics of the electrodes. For wet skin conditions, Ag/AgCl electrodes exhibit a phase close to 0° in the frequency range of 100 Hz to 1000 Hz, indicating a predominantly resistive behavior. This observation aligns with the expectation of resistive coupling being the primary mechanism for Ag/AgCl electrodes, facilitated by the presence of the electrolytic gel. In contrast, the textile electrodes display a phase of approximately 40° across the entire frequency range, suggesting a significant contribution from capacitive coupling. The higher phase values for textile electrodes highlight the presence of a more complex electrode-skin interface, with both resistive and capacitive components playing a role in the overall impedance characteristics.

The phase response under dry skin conditions further emphasizes the distinct behaviors of the two electrode types. Ag/AgCl electrodes maintain a relatively low phase, close to 0° , across the entire frequency range, confirming their primarily resistive nature even in the absence of additional moisture. On the other hand, textile electrodes exhibit higher phase values, reaching up to 40° , indicating a notable capacitive contribution to the impedance. This analysis confirms the dominant resistive behavior for the Ag/AgCl electrodes compared to the dry textile electrodes, echoing the distinct mechanistic principles that guide the behavior of Ag/AgCl and dry electrodes [216]. This observation underscores the challenges associated with dry electrode-skin

interfaces, where the lack of a conductive gel or moisture can lead to increased capacitive coupling and higher impedance values.

In summary, the normalized impedance and phase response analysis presented in Figure 3-11 provides valuable insights into the performance and underlying mechanisms of 3D knitted silver textile electrodes compared to conventional Ag/AgCl electrodes. The textile electrodes demonstrate lower normalized impedance on wet skin in the 10 Hz to 1000 Hz range, suggesting their potential for superior performance in this frequency range under moist conditions. However, the textile electrodes exhibit higher impedance and phase values at lower frequencies and under dry skin conditions, highlighting the challenges associated with capacitive coupling and the absence of a conductive gel. These findings underscore the importance of further optimization efforts to enhance the low-frequency performance and moisture retention capabilities of textile electrodes, with the ultimate goal of achieving stable and reliable biopotential measurements across a wide range of skin conditions and frequency ranges.

The comprehensive parametric design and impedance characterization of 3D knitted silver electrodes have culminated in the identification of the optimal electrode configuration for integration into intelligent garment systems. The meticulous impedance testing, conducted over a wide frequency range and under both dry and wet skin conditions, has provided compelling evidence for the superior performance of these electrodes compared to conventional Ag/AgCl electrodes. The unique material composition of the 3D knitted silver electrodes, coupled with their optimized geometric design, contributes to their excellent impedance characteristics. The inherent properties of the knitted structure, such as high porosity and surface area, facilitate improved conformability and contact with the skin surface, thereby reducing the impedance at the electrode-skin interface. Moreover, the hygroscopic nature of the textile material promotes moisture retention, further enhancing the conductive pathways and minimizing the impact of varying skin hydration levels on electrode performance. The ability of these 3D knitted silver electrodes to maintain lower impedance values across a wide frequency range, particularly in the 10 Hz to 1000 Hz band, highlights their suitability for capturing high-quality biopotential signals. This frequency range

encompasses many physiologically relevant signals, such as electrocardiography (ECG) and electromyography (EMG), making these electrodes well-suited for a variety of wearable health monitoring applications. Furthermore, the consistent performance of these electrodes under both dry and wet skin conditions underscores their adaptability and robustness. The capacity to maintain stable impedance characteristics, even in the absence of additional moisture or conductive gels, positions these electrodes as ideal candidates for long-term, continuous monitoring scenarios. This adaptability is particularly valuable in intelligent garment systems, where the electrodes may be subjected to varying environmental conditions and prolonged wear periods.

The comprehensive parametric design and impedance characterization process has provided a solid experimental foundation for the integration of these 3D knitted silver electrodes into intelligent garment systems. By systematically evaluating the impact of electrode geometry and skin pressure on impedance characteristics, this study has established a robust framework for electrode selection and optimization. The insights gained from this research will guide the design and development of advanced wearable health technologies, ensuring the seamless integration of high-performance electrodes into intelligent garments.

In conclusion, the rigorous experimental approach employed in this study has identified the optimal 3D knitted silver electrode configuration, with a diameter of 3 cm, a height of 3 mm, and a skin pressure of 30 mmHg, as the most suitable for integration into intelligent garment systems. The lower impedance values, consistent performance across various environmental conditions, and adaptability to different skin hydration levels exhibited by these electrodes underscore their potential for reliable, long-term biopotential monitoring.

3.2 Fabrication of the Intelligent Garment

3.2.1 Garment Design and Fabrication

The design of the intelligent garment, as depicted in Figure 3-12, incorporates a

sophisticated configuration to monitor both ECG and EMG signals. For ECG monitoring, two electrodes are strategically positioned at the chest area, with an additional electrode at the left side of abdomen, utilizing a single-lead approach. Given the susceptibility of the deltoid muscle on the arm and the erector spinae on the back to fatigue during sports activities, three electrodes are placed at each location to effectively capture EMG signals. In adherence to the guidelines established by the Consensus for Experimental Design in Electromyography (CEDE) project [217], the selection of EMG electrode for these muscles was conducted with meticulous consideration. The integration of electrodes not only enhances the accuracy of EMG signal measurements but also maintains the comfort of the athlete, which is paramount.

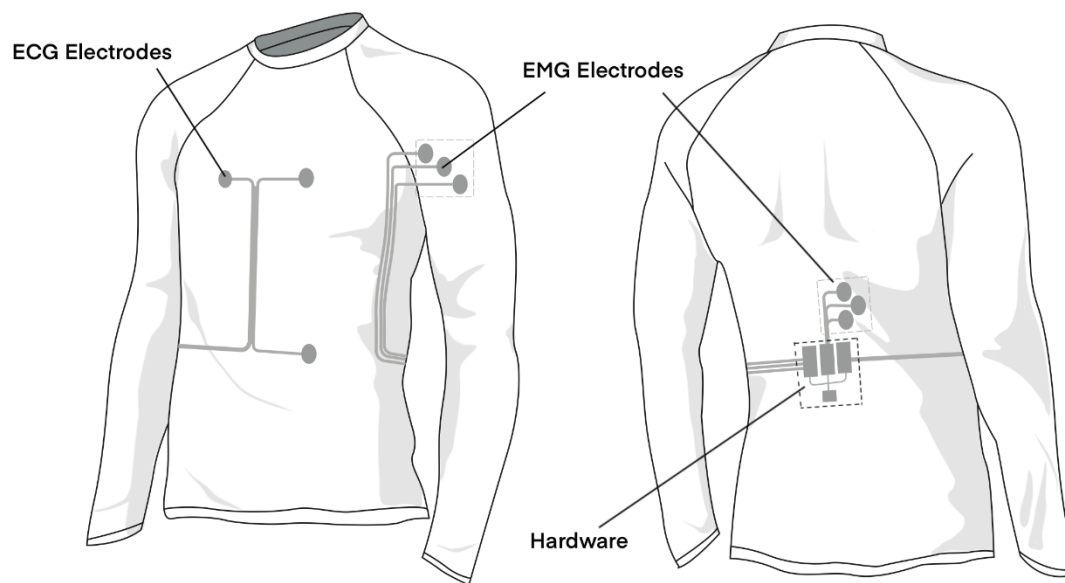


Figure 3-12. Design of Intelligent garment system

To further enhance the functionality of the intelligent garment system, ADC (analog-to-digital converter) chips of ECG and EMG, along with the Arduino Nano 33 IoT, are positioned on the lower part of the back. This specific location was determined to be the most stable during sports activities, thereby minimizing displacement due to

motion and reducing any potential impact on the wearer's bodily perception. This strategic placement ensures that comfort is not compromised during activities such as riding.

For the connection between sensors and electrodes, a previously mentioned channel design was employed. Low-resistance silver conductive wires (transmission yarn) are placed within these channels, providing a flexible connection that is barely noticeable to the wearer. In order to connect the ADC chips, the conductive wires are soldered in to 3.5 jack plug, as shown in Figure 3-13. This design represents an innovative attempt to balance comfort with functionality, allowing for seamless integration of the conductive pathways within the garment.



Figure3-13 3.5 mm jack plug with conductive wires

The Intelligent Garment System's front and back photos, as illustrated in Figure 3-14. This assembly is adeptly integrated into the overall design of the system. Notably, the three-dimensional effect of the electrodes, which creates a concave surface on one side, can produce a convex bulge under skin pressure, potentially detracting from contact quality. To address this issue, laser-cut sponges matching the electrodes in size and thickness are used. These sponges are affixed with an insulating adhesive layer to ensure dimensional stability and maintain a close skin-electrode fit during use.

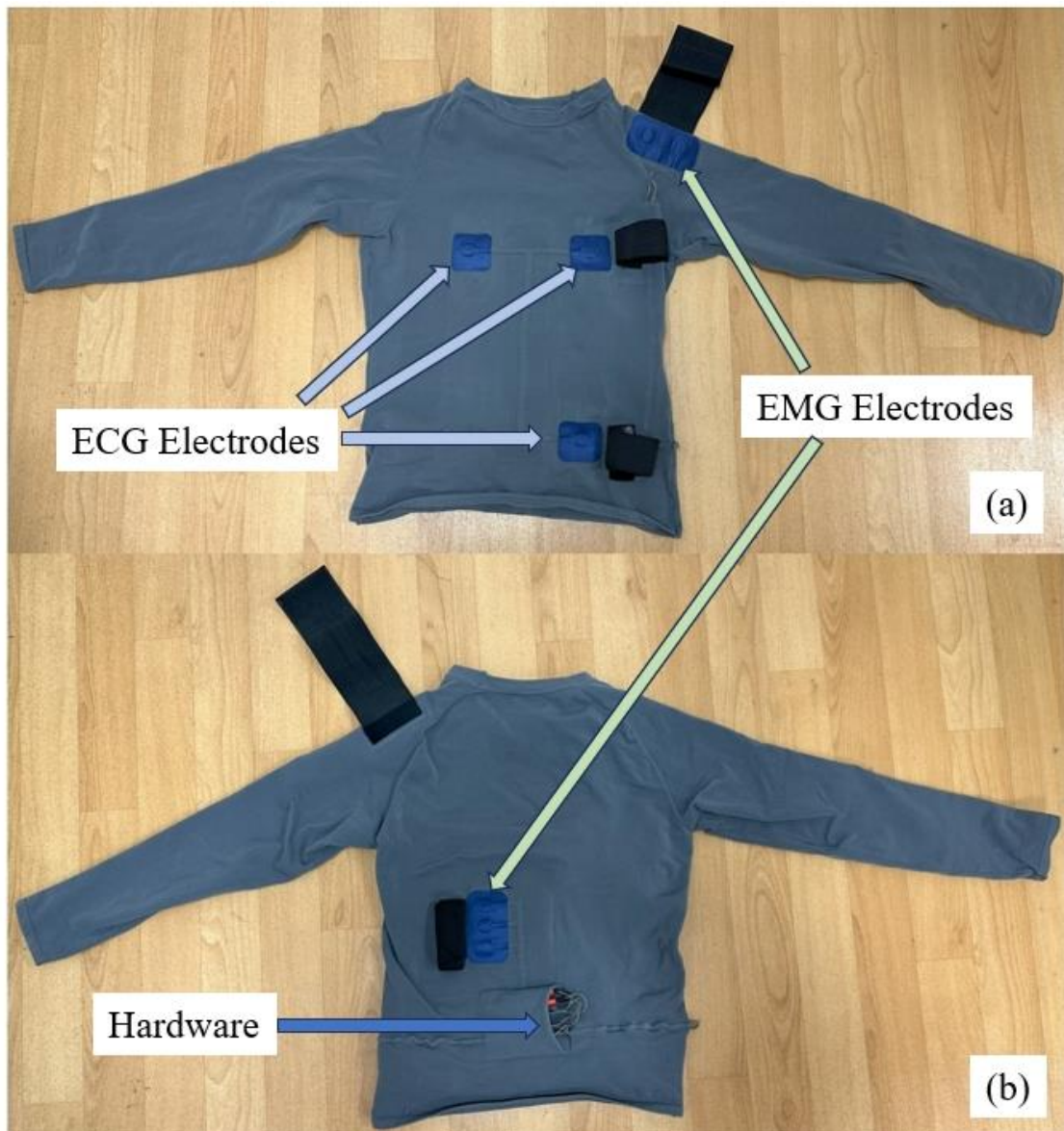


Figure 3-14. Front and back views of Intelligent garment system. (a) Front side of the garment. (b) Back side of the garment.

The Consensus for Experimental Design in Electromyography (CEDE) project is an initiative aimed at establishing standardized guidelines for EMG recording and analysis[217]. According to the CEDE project's recommendations, maintaining a stable and secure electrode-to-skin interface is crucial for ensuring high-quality signal acquisition, particularly under the dynamic conditions typical of sports activities. The Intelligent Garment System addresses this requirement by incorporating adjustable Velcro straps strategically placed around the perimeter of each electrode. These straps enable precise regulation of pressure, ensuring that the electrodes remain firmly and

comfortably attached to the skin.

The adjustable Velcro straps are designed to follow the CEDE project's advice on optimizing electrode performance through a customizable fit. By allowing wearers to adjust the tightness of the straps, the system ensures that the electrodes maintain consistent contact with the skin, reducing the risk of signal degradation due to movement or sweat. This adaptability is essential in sports, where athletes engage in a wide range of movements that could otherwise disrupt the electrode-skin interface. This adjustable feature significantly enhances the overall functionality of the intelligent garment, facilitating the accurate recording of EMG signals. A tighter fit, achieved through the precise adjustment of the Velcro straps, results in improved electrode performance by minimizing the movement and ensuring a stable contact area. This stability is crucial for capturing high-fidelity EMG signals, as any displacement can lead to signal artifacts and reduced data quality. Furthermore, the design of the Velcro straps takes into consideration the athlete's comfort and the need for ease of use. The straps are easily adjustable, allowing athletes to quickly modify the fit before, during, or after activities without requiring assistance. This user-friendly aspect ensures that athletes can maintain optimal electrode performance throughout their activities, contributing to more reliable and consistent data collection. The incorporation of adjustable Velcro straps around each electrode on the Intelligent Garment System is a thoughtful and practical solution to the challenge of maintaining a stable electrode-to-skin interface. By allowing for customizable pressure regulation, the system adheres to the CEDE project's guidelines, enhancing the reliability and accuracy of EMG signal acquisition. This design not only improves electrode performance but also ensures athlete comfort and ease of use, making it a robust and effective tool for monitoring muscle activity during sports.

The intelligent garment design incorporates several innovative elements to ensure high-quality signal acquisition for both ECG and EMG monitoring while maintaining the wearer's comfort during sports activities. The strategic placement of electrodes, the use of 3D knitted silver electrodes, the innovative channel design for conductive wires,

and the adjustable Velcro straps all contribute to the garment's enhanced functionality and reliability.

3.2.2 Hardware Integration

In terms of hardware, the architecture is shown in Figure 3-15. The intelligent garment system employs a sophisticated array of components to facilitate accurate and efficient physiological monitoring. Central to the ECG monitoring capability is the ADS1292R chip, a highly integrated analog front-end specifically designed for biopotential measurements. This chip offers high-resolution data acquisition, low noise, and low power consumption, making it an ideal choice for wearable applications where power efficiency and signal fidelity are paramount. For the detection of EMG signals, two SEN0240 ADC provided by OYMotion are utilized. These ADC are renowned for their sensitivity and reliability in capturing muscle activity, ensuring precise and real-time monitoring of muscle fatigue and performance. The sensors are interfaced with a development board that features the Arduino Nano 33 IoT, a versatile microcontroller that integrates seamlessly with various sensors and components. The real photo of hardware for intelligent garment system is shown in Figure 3-16

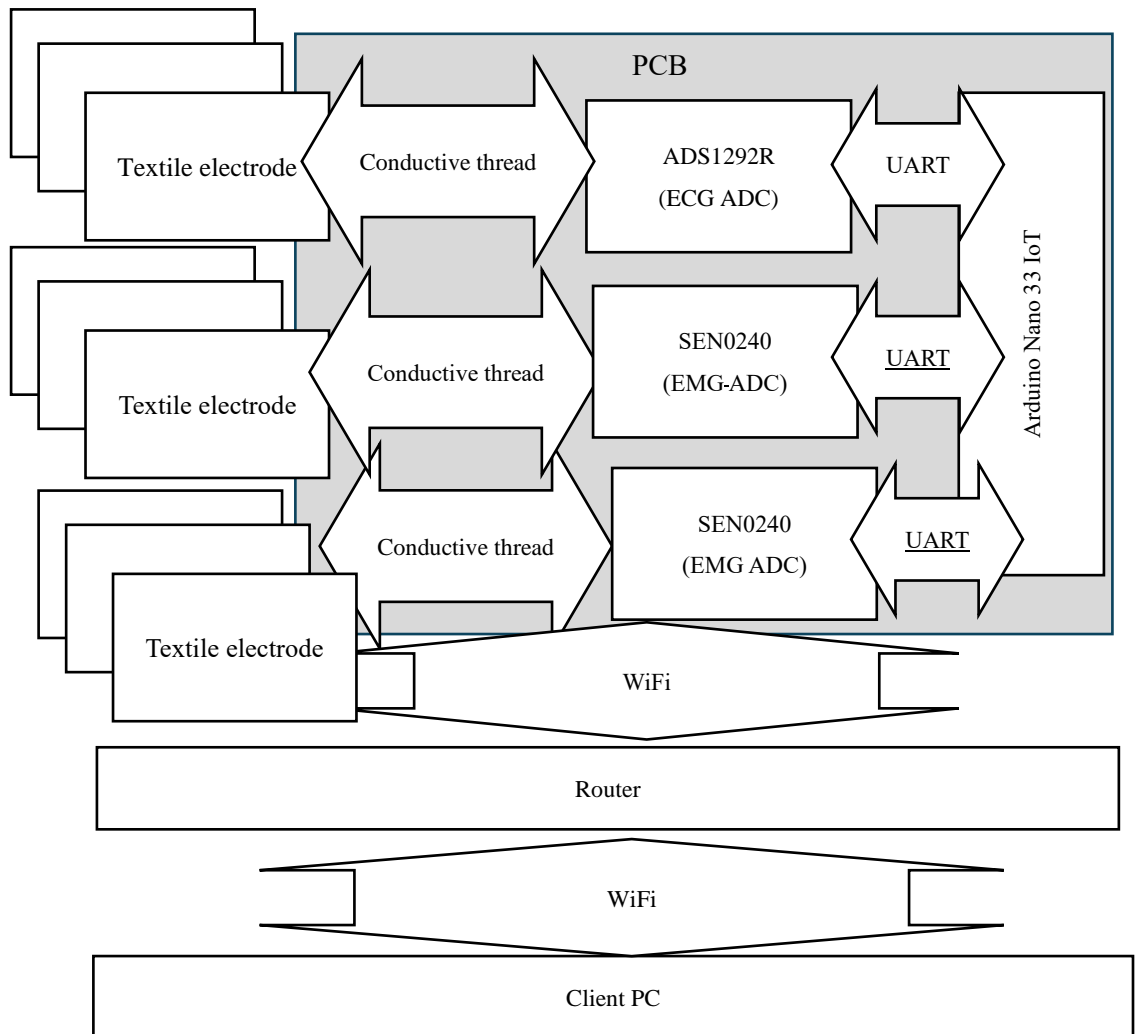


Figure 3-15: Architecture of hardware design.

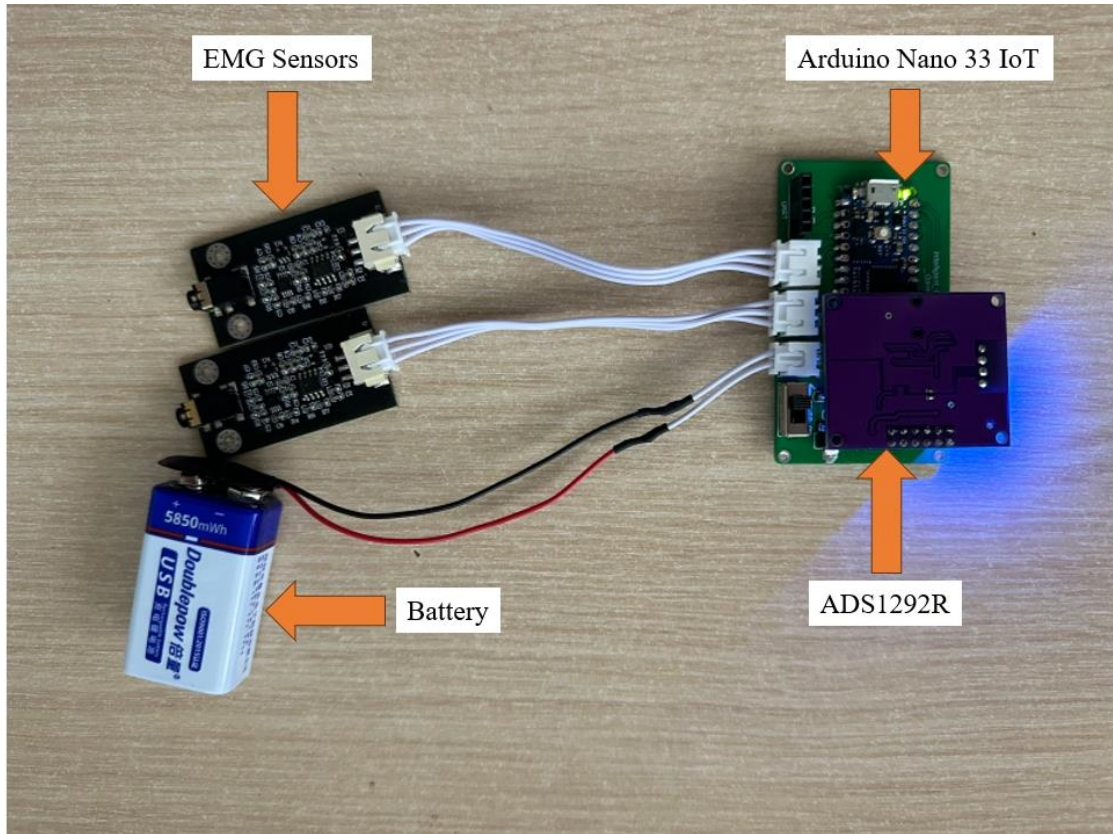


Figure 3-16. Photo of hardware for intelligent garment system

The Arduino Nano 33 IoT plays a microcontroller role in this setup due to its advanced features, including built-in Wi-Fi connectivity. This connectivity enables the remote acquisition and transmission of real-time ECG and EMG data, facilitating continuous monitoring without the constraints of physical connections. The capability to transmit data wirelessly is crucial for applications involving dynamic and mobile subjects, such as athletes, where tethered solutions could hinder movement and performance.

Powering the entire system is a 9V battery, chosen for its ability to provide a stable and sufficient power supply to all components. The battery ensures that the system can operate continuously over extended periods, which is essential for long-duration sports activities or monitoring sessions.

This hardware configuration underscores the intelligent garment system's capability to provide robust, real-time monitoring of critical physiological parameters. By leveraging advanced components like the ADS1292R chip and the Arduino Nano

33 IoT, coupled with high-quality SEN0240 EMG chips, the system ensures high accuracy, reliability, and user comfort. This setup not only enhances the performance monitoring of athletes but also represents a significant advancement in wearable health technology, offering insights that can be used to optimize training regimens, prevent injuries, and improve overall athletic performance.

3.2.2 Software Development

At the beginning of this section, it is important to discuss the sampling frequencies employed in the Intelligent Garment System. For the acquisition of EMG signals from the erector spinae and anterior deltoid muscles, a sampling frequency of 1000 Hz was chosen, as it is commonly used in EMG studies. This high sampling rate ensures that the system captures the full spectrum of EMG signals, which typically contain frequencies up to 500 Hz. By adhering to the Nyquist-Shannon sampling theorem, which states that the sampling frequency should be at least twice the highest frequency component of the signal, the 1000 Hz sampling rate guarantees that the EMG signals are accurately represented without aliasing.

In contrast, a sampling frequency of 125 Hz was selected for the acquisition of ECG signals. This sampling rate is widely accepted as a standard in ECG monitoring systems, as it provides a balance between data resolution and system efficiency. Most of the relevant information in an ECG signal is contained within a frequency range of 0.5 to 50 Hz. By sampling at 125 Hz, the system comfortably satisfies the Nyquist-Shannon criterion for this frequency range, ensuring that the ECG signal is faithfully captured without significant loss of information. Moreover, using a lower sampling rate for ECG compared to EMG reduces the overall data throughput and storage requirements, optimizing system resources without compromising the quality of the acquired signals.

The software of the Intelligent Garment System for Client PC enables the processing, visualization, and storage of the bioelectric signals acquired by the hardware. As illustrated in Figure 3-17, software of the Intelligent Garment System was

developed using the Qt framework to receive, display, and record the real-time ECG and EMG data transmitted wirelessly from the Arduino Nano 33 IoT.

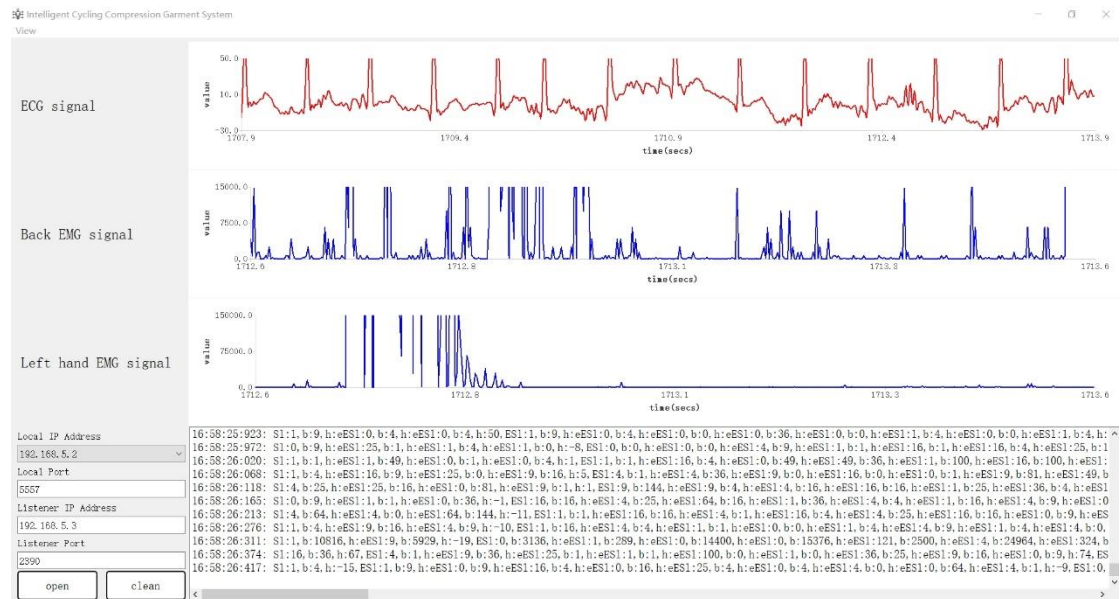


Figure 3-17 Software of the Intelligent Garment System

The main window of the application features three dedicated charts that provide a visual representation of the athlete's physiological data. These charts, implemented using the powerful Qt Charts module, render the ECG signal, EMG of the erector spinae muscle, and EMG of the left anterior deltoid muscle respectively. The Qt Charts module features a wide range of customization options for axes, series, and legends, enabling the creation of visually appealing and informative charts. Users can interact with the charts by zooming and scrolling, facilitating detailed examination of specific data segments and allowing for a more in-depth analysis of the athlete's performance.

In addition to the graphical display, the application incorporates a text browser that serves as a log for the raw data packets received from the hardware. This feature proves invaluable for debugging purposes and data validation, as it allows developers and researchers to inspect the incoming data in its original format. The inclusion of a menu bar with options to reset the zoom level of each chart independently further enhances the user's ability to navigate and analyze the data, providing a more flexible and user-friendly experience.

To facilitate seamless wireless communication between the hardware and the

software, the application leverages the Qt Network module. By binding to a specified local IP address and port, the application can listen for incoming UDP packets from the Arduino Nano 33 IoT. Upon receiving a packet, the application employs robust parsing algorithms to extract the ECG and EMG values, ensuring data integrity and reliability. The extracted values are then used to update the corresponding charts and text browser in real-time, providing a live feed of the athlete's physiological state.

Recognizing the importance of data persistence and post-session analysis, the application implements a comprehensive data logging functionality. When the "open" button is toggled, the application automatically creates a CSV file with a timestamp-based filename in a designated directory. The CSV file is structured with well-defined headers for each signal type, allowing for easy interpretation and analysis of the logged data. As the application receives and parses the bioelectric signals, it appends the data to the CSV file along with a sequence number, ensuring a chronological record of the athlete's performance. This data logging feature empowers researchers and coaches to conduct in-depth post-session analysis, track the athlete's progress over time, and make informed decisions regarding training regimens and performance optimization strategies.

The software development for the Intelligent Cycling Compression Garment System showcases the seamless integration of real-time data visualization, wireless communication, and data logging capabilities. By leveraging the robustness and efficiency of the Qt framework, the desktop application provides a reliable and high-performance platform for monitoring and analyzing the athlete's physiological data. The modular design of the software allows for future enhancements and extensions, ensuring the system can adapt to evolving research needs and technological advancements. The intuitive user interface and interactive charting features enable users to easily interpret and explore the bioelectric signals.

CHAPTER 4 Testing and Analysis of Intelligent Garment System in Cycling Sport

This chapter evaluates the performance of the intelligent garment system in cycling. We present a cycling fatigue test that mimics the varying intensity levels athletes experience during training or competition. The study combines conventional analysis methods with deep learning techniques to assess the system's ability to predict fatigue levels in real-time. We begin by describing the experimental setup, including the cycling protocol and subjective fatigue assessment using the Borg Rating of Perceived Exertion (RPE) scale. The chapter then analyzes electrocardiogram (ECG) and electromyography (EMG) data using statistical methods to examine heart rate variability and muscle fatigue patterns.

To address limitations in conventional analysis, we explore artificial intelligence approaches. The chapter investigates several time-series deep learning models, including Temporal Convolutional Networks (TCN), Gated Recurrent Units (GRU), Transformers, and Long Short-Term Memory (LSTM) networks. These models are evaluated for their effectiveness in processing the ECG and EMG data from the intelligent garment system.

4.1 Test Setup and Methodology

As shown in Figure 4-1, the experimental setup used the Essential Exercise Bike EB 140 (Decathlon, France) to carry out a structured cycling plan designed to assess gradual levels of fatigue while allowing for optimal signal collection.



Figure 4-1 Cycling Test

Table 4-1 Protocol of cycling plan

Low pace (5 km/h)	High pace (30 km/h)	Low pace (5 km/h)	High pace (30 km/h)	Low pace (30 km/h)	High pace (30 km/h)
Low-intensity	High-intensity	Low-intensity	High-intensity	Low-intensity	High-intensity
7 min	3 min	7 min	3 min	7 min	3 min
Sequence 1		Sequence 2		Sequence 3	

The protocol of cycling plan is illustrated in Table 4-1. The cycling test included three repeated sequences, each with two distinct phases: a 7-minute ride at a low pace phase of 5 km/h, followed right away by a 3-minute high-intensity sprint phase at 30 km/h. This two-phase approach was carefully designed to bring out a wide range of physical responses, going from a resting state to one of increased physical stress and fatigue. Each cycling fatigue assessment session lasted a total of 30 minutes. One important part of this method was purposely leaving out rest periods between the two phases in each sequence. This unbroken change from low to high intensity cycling aimed to closely copy real-world athletic situations, where athletes often go through dynamic changes in effort levels without significant recovery breaks. By keeping the cycling fatigue assessment continuous, we wanted to capture the subtle interaction between varying levels of physical exertion and their impact on the quality and reliability of the ECG and EMG signals. This protocol choice was driven by the necessity to rigorously evaluate the robustness and signal quality of the 3D knitted

silver electrode in IGS under conditions that accurately simulate the demands of real sports activities. Factors like perspiration, rapid body movements, and variations in pressure at the electrode-skin interface can significantly affect signal quality during intense physical exertion. By putting the IGS through these realistic stressors without interruption, we aimed to comprehensively assess its performance and suitability for continuous, real-time monitoring of athletes' physiological parameters.

To measure the subjective perception of fatigue during the cycling test, we used the well-known Borg Rating of Perceived Exertion (RPE) scale. This scale, which goes from 6 to 20, lets subjects self-report their level of perceived effort at any given moment during the exercise. For our study, we further combined several different evaluation grades in the Borg scale into four distinct fatigue levels: 0 (No fatigue), 1 (Slightly fatigued), 2 (Fatigued), and 3 (Extremely fatigued), as shown in Table 4-2. Throughout the cycling session, the subjects were instructed to verbally express their current level of fatigue whenever they felt a change in their fatigue state. This self-reported fatigue level, which we refer to as the "Fatigued Labeled State," was based entirely on the subjects' own perception and assessment of their fatigue at any given moment. By encouraging the subjects to report their fatigue levels as they experienced changes, rather than at predetermined intervals, the researchers were able to collect real-time data on the subjects' subjective fatigue states at different points during the exercise. This approach ensures that the subjective fatigue ratings are promptly and accurately reflect the real-time fatigue state during the cycling exercise.

Table 4-2 Subjective scale

Evaluation Grade	Subjective Feelings	Fatigued labeled State
6	No exertion at all	0. No fatigue
7	Extremely light	
8	Very light	
9		
10	Light	1. Slightly fatigued
11		
12		
13	Somewhat hard	
14	Hard	
15		

16		
17	Very hard	
18		
19	Extremely hard	
20	Maximal exertion	3. Extremely fatigued

The subjects selected for this study were regular cycling enthusiasts who were well-acquainted with the physical exertion and fatigue associated with the sport. This familiarity made them better equipped to accurately perceive and report their own fatigue levels during the experiment. To further enhance the reliability of their subjective assessments, each subject received a detailed introduction to the Borg Rating of Perceived Exertion (RPE) scale prior to the tests. This introduction ensured that the participants had a clear understanding of the fatigue classification method and could provide more consistent and reliable feedback on their perceived fatigue states throughout the cycling session. To ensure the repeatability and reliability of the findings, each subject completed three identical trials of the cycling experiment, with each trial conducted at 10 o'clock in the morning on separate days to minimize any potential variations caused by circadian rhythms or daily fluctuations in physical condition. These repeated measures design let us account for potential differences within individuals and assess the consistency of the intelligent garment system's performance across multiple sessions.

Table 4-3 Basic information of subjects

Number	Age	Height(cm)	Weight(kg)	BMI
1	29	175	75	24.4
2	23	178	77	24.3
3	26	176	74	23.8

4.2 Data Processing and Analysis

In the previous section, we introduced the experimental protocol for the 30-minute cycling fatigue assessment. In this section, several traditional statistical methods were employed to analyze the data, focusing on the heart rate (HR) patterns and their relationship to fatigue. To facilitate the analysis, the calculation of Heart Rate (HR) was based on the formula defined as Formula (1). Specifically, HR was determined by the

frequency of R-R intervals, calculated as follows:

$$\text{Heart Rate (BPM)} = \frac{60}{\text{R-R Interval (seconds)}} \quad (1)$$

This formula provides a direct measure of heart rate in beats per minute (BPM) by calculating the reciprocal of the time elapsed between two consecutive R-waves on the ECG, normalized to a minute. Utilizing the heart rate calculation method showed in Formula (1), we obtained heart rate variability curves for the entire 30-minute cycling test. This enabled us to track changes in heart rate over time and under different exercise intensities.

Figure 4-2 presents the heart rate plots for each of the three subjects (4-2(a), 4-2(b), and 4-2(c)) throughout the cycling test. Upon examination of these plots, a consistent trend emerges in the HR patterns for all three subjects. In the first low-intensity cycling phases (blue regions), the HR values remain relatively stable, indicating a steady-state of cardiovascular and autonomic function. In contrast, during the high-intensity sprint phases (red regions), there is a rapid increase in HR, followed by a swift decrease in the subsequent low-intensity phases.

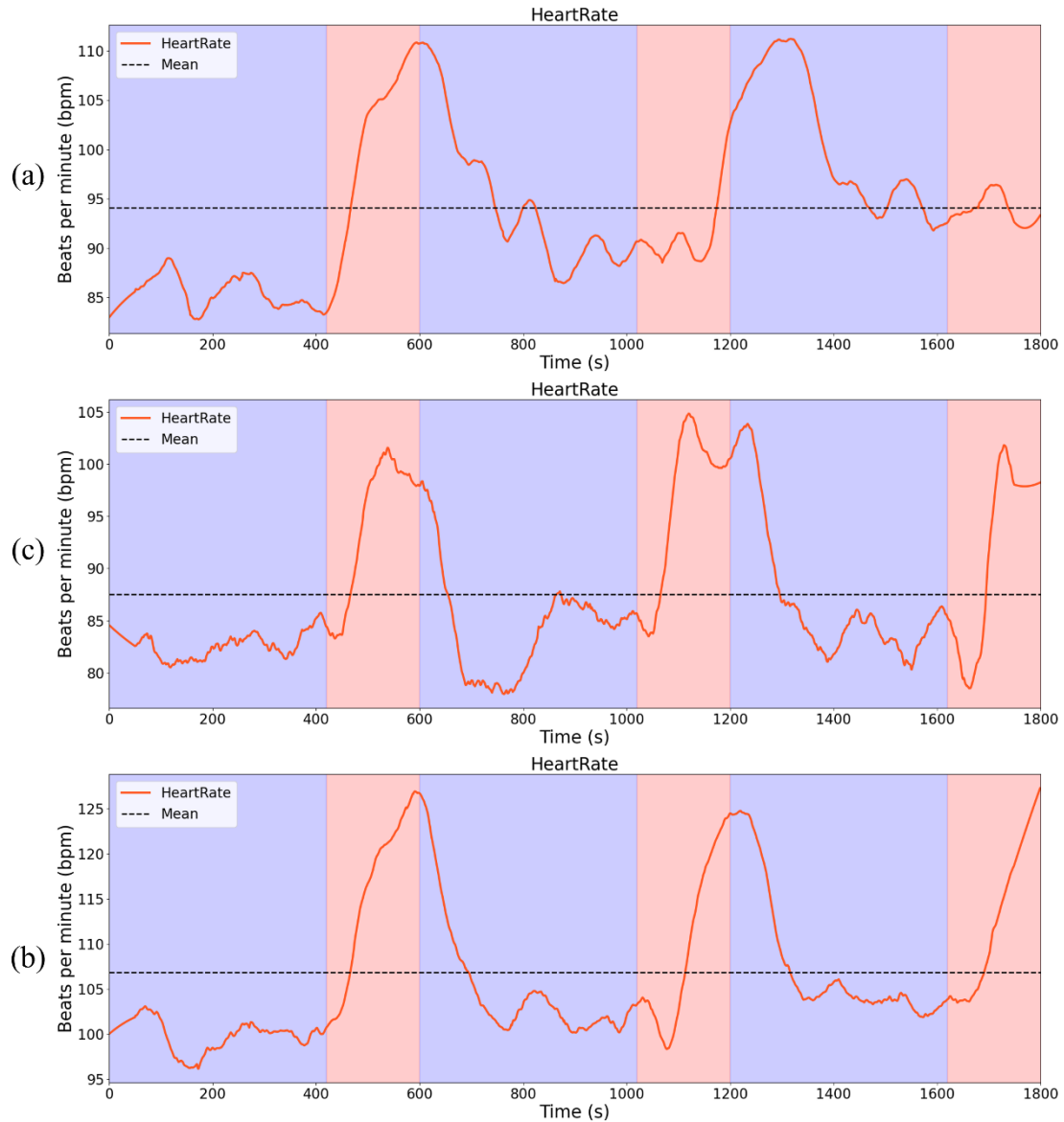


Figure 4-2 Plots of Heart Rate evolution in 3 subjects over a 30-minute Cycling Test: (a) Subject 1; (b) Subject 2; (c) Subject 3.

The sharp increase in HR during the high-intensity sprints phase can be attributed to several physiological factors. Firstly, the sudden increase in exercise intensity leads to a rapid elevation in heart rate, which may result in greater beat-to-beat variability, thus increasing HR. Secondly, high-intensity exercise is associated with significant changes in breathing patterns, such as increased respiratory rate and depth, which can directly influence heart rate variability. Lastly, the abrupt onset of high-intensity exercise may trigger a swift response from the autonomic nervous system, leading to a temporary dominance of sympathetic activity and a corresponding increase in HR.

The rapid decrease of HR to a stable level during the low-intensity phases following each sprint suggests efficient autonomic regulation and a well-functioning cardiovascular system in all three subjects. This ability to quickly restore homeostasis after acute stress is crucial for maintaining performance and preventing excessive fatigue accumulation. Despite the consistent overall HR pattern, there are notable individual differences among the subjects. Subject 1 (Figure 4-2(a)) exhibits the most stable HR values during the low-intensity phases, with relatively uniform increases during the sprints, indicating a well-balanced autonomic response and a good capacity for recovery. Subject 2 (Figure 4-2(b)) shows slightly more variability in HR during the low-intensity phases, with more pronounced HR spikes during the sprints, suggesting a stronger autonomic response to high-intensity exercise. Subject 3 (Figure 4-1(c)) demonstrates the highest overall HR variability, both during the low-intensity phases and the high-intensity sprints, indicating a more intense autonomic response to exercise stress. These individual differences in HR variability may reflect varying levels of cardiovascular fitness, autonomic function, and adaptability to exercise. Subjects with higher cardiovascular fitness and more efficient autonomic regulation may exhibit more stable HR patterns and faster recovery after high-intensity bouts. In contrast, individuals with lower fitness levels or less efficient autonomic function may show greater heart rate variability and slower recovery.

In terms of fatigue, the consistent HR patterns throughout the cycling test suggest that all three subjects were able to cope with the demands of the exercise protocol without showing signs of excessive fatigue accumulation. The stable HR during low-intensity phases and the rapid recovery after high-intensity sprints indicate efficient cardiovascular and autonomic regulation, which are essential for maintaining performance and preventing fatigue. However, it is important to note that the 30-minute cycling test represents a relatively short duration of exercise, and the HR patterns observed may not fully reflect the potential for fatigue accumulation over longer periods or more intense exercise protocols. Future research should investigate HR responses during prolonged or more strenuous exercise to better understand the

relationship between HR variability and fatigue.

Furthermore, the individual differences in HR patterns highlight the importance of personalized monitoring and training strategies. By assessing each athlete's unique HR response to exercise, coaches and sports scientists can tailor training plans to optimize performance, minimize fatigue, and reduce the risk of overtraining. Individualized HR monitoring can also help detect early signs of fatigue accumulation or autonomic imbalances, allowing for timely interventions and recovery strategies. In conclusion, the analysis of HR patterns during the 30-minute cycling test reveals a consistent trend of stable HR during low-intensity phases, rapid increases during high-intensity sprints, and swift recovery in all three subjects. While individual differences in HR variability exist, the overall pattern suggests efficient cardiovascular and autonomic regulation, with no clear signs of excessive fatigue accumulation within the context of this relatively short exercise protocol.

In the study of muscle fatigue during the 30-minute cycling test, we focused on the electromyography (EMG) signals from the anterior deltoid and erector spinae muscles to assess changes indicative of muscle fatigue, particularly alterations in muscle fiber conduction velocity. To achieve this, we calculated the Median Frequency (MF) of the EMG signals. The following describes the detailed signal processing methodology employed:

Firstly, to ensure the integrity of the EMG data for analysis, any DC offset present in the raw EMG recordings was removed using the mean subtraction method. This was achieved by calculating the mean value of the entire EMG signal and subtracting it from each data point. The purpose of removing the DC offset is to eliminate the constant component of the signal, centering the signal around zero, and laying the foundation for subsequent processing.

Subsequently, the signal was subjected to a bandpass filtering process using a 2nd order Butterworth filter with a frequency range of 20-450 Hz. The lower cutoff frequency of 20 Hz was chosen to remove low-frequency noise, such as motion artifacts, while the upper cutoff frequency of 450 Hz was selected to preserve the relevant high-

frequency components of the EMG signal. These cutoff frequencies are commonly used in EMG studies, as they effectively capture the primary frequency range of muscle activity while minimizing the influence of external noise and other non-relevant frequency components. The 2nd order Butterworth filter was chosen for its flat passband response and minimal ripple. This step was critical for focusing the analysis on the frequencies most relevant to muscle activity.

Following bandpass filtering, the EMG signal was rectified by taking the absolute value of each point. This rectification is crucial as it transforms the signal into a purely positive form, simplifying the analysis of signal amplitude and power. Rectification is essential for subsequent processing steps, such as smoothing and amplitude analysis, as it ensures that all signal values are non-negative.

To further process the rectified signal, a low-pass filter with a cutoff frequency of 10 Hz was applied. The choice of a 10 Hz cutoff frequency was based on the desired level of smoothing, as it effectively removes high-frequency fluctuations while preserving the overall shape of the EMG envelope. This cutoff frequency is widely used in EMG studies to obtain a clear representation of muscle activation patterns over time. A 2nd order Butterworth filter was used for the low-pass filtering step to maintain consistency with the bandpass filter. This step produced a linear envelope of the EMG signal, which smooths out the rapid fluctuations and provides a clear representation of muscle activation patterns over time.

Having processed the data through these steps, we focused on analyzing the frequency content of the EMG signals to identify patterns related to muscle fatigue. The power spectral density $P(f)$ of the EMG signal was calculated using the Fourier transform (Formula (2)). The total power of the EMG signal was then computed by summing the power spectral density across all frequencies (Formula 3).

To determine the Median Frequency (MF), we first calculated the cumulative power distribution by summing the power spectral density from the lowest frequency up to each successive frequency (Formula 4). The MF was then defined as the frequency at which the cumulative power distribution reached 50% of the total power (Formula

5). This calculation provides insight into the shift of frequency components, which is typically observed as a decrease in MF with increasing muscle fatigue due to reduced muscle fiber conduction velocities.

$$P(f) = |X(f)|^2 \quad (2)$$

$$\text{Total Power} = \sum_{i=1}^N P(i) \quad (3)$$

$$C(f) = \sum_{i=1}^f P(i) \quad (4)$$

$$\text{Find } f_{\text{MF}} \text{ such that } C(f_{\text{MF}}) \geq \frac{1}{2} \text{Total Power} \quad (5)$$

Figure 4-3 presents the MF plots for the anterior deltoid and erector spinae muscles of the three subjects throughout the cycling test. A consistent pattern emerges in the MF dynamics, particularly for subjects 2 and 3. During the low-intensity cycling phases, the MF values for both muscles gradually increase, indicating a recovery from muscle fatigue. In contrast, during the high-intensity sprint phases, the MF values exhibit a marked decrease, suggesting the onset of muscle fatigue and a reduction in muscle fiber conduction velocity.

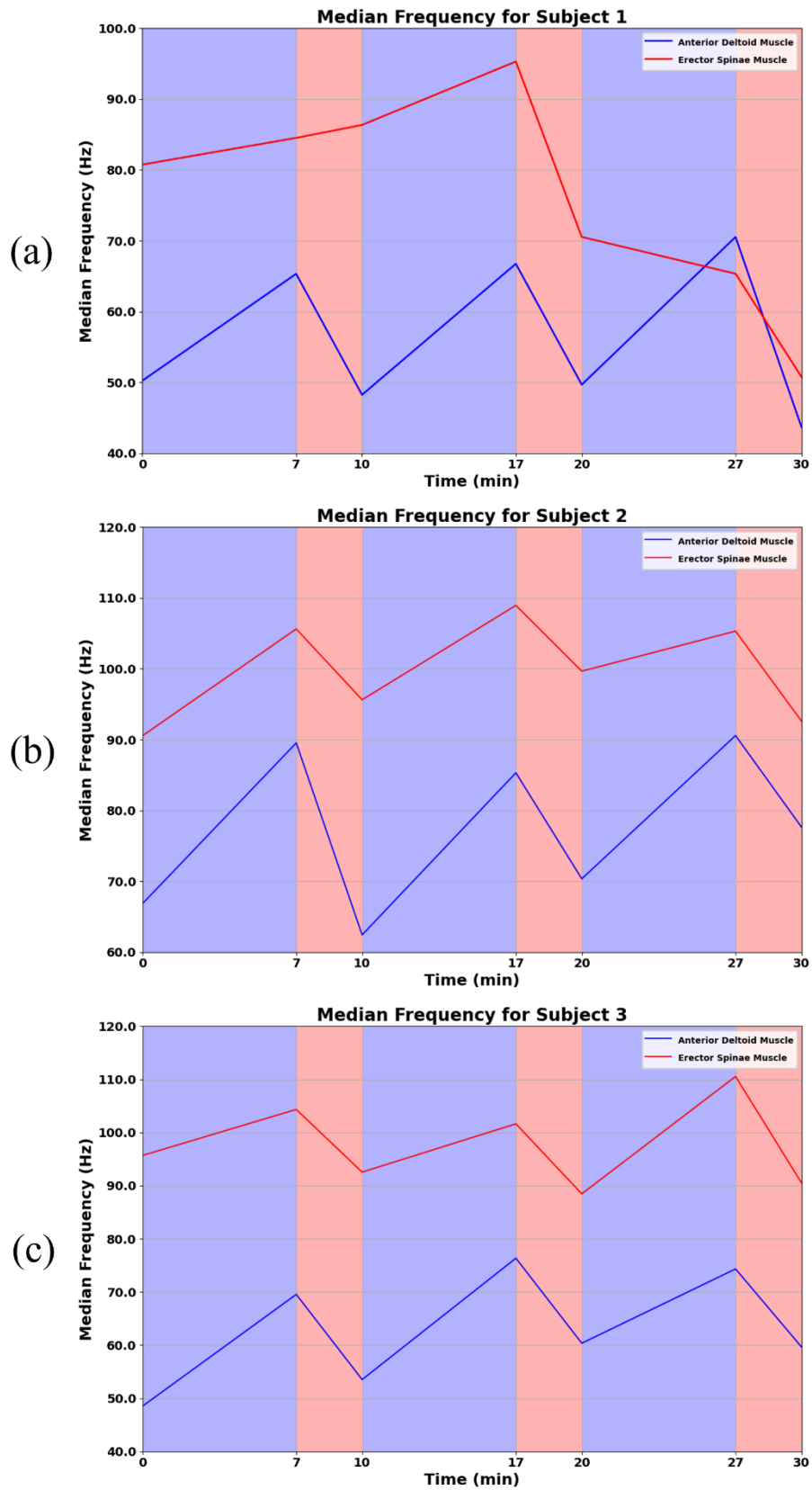


Figure 4-3 Plots of median frequency variability in 3 subjects over a 30-minute cycling test: (a) Subject 1; (b) Subject 2; (c) Subject 3.

This fatigue pattern is evident in both the anterior deltoid and erector spinae muscles of subjects 2 and 3, with the MF values consistently declining during sprints and recovering during low-intensity phases. The pronounced decrease in MF during sprints suggests that the high-intensity exercise induces significant muscle fatigue, leading to a slowing of muscle fiber conduction velocity. The subsequent recovery of MF during low-intensity phases indicates a gradual restoration of muscle function and a reduction in fatigue. Interestingly, subject 1 exhibits a slightly different fatigue pattern in the erector spinae muscle compared to the other subjects. While the anterior deltoid muscle shows a similar trend of fatigue and recovery, the erector spinae muscle does not demonstrate fatigue during the first sprint phase. However, fatigue is evident in the erector spinae muscle during the second sprint phase, and notably, the muscle does not fully recover during the third low-intensity phase. This sustained fatigue leads to an accelerated fatigue rate during the final sprint phase, as reflected by a steeper decline in MF values.

The individual differences in muscle fatigue patterns, particularly in the erector spinae muscle of subject 1, highlight the importance of personalized fatigue assessment and training strategies. The sustained fatigue in the erector spinae muscle of subject 1 may indicate a slower recovery rate compared to the other subjects. This information can be valuable for coaches and athletes in designing targeted training programs to improve muscle endurance and optimize performance. The EMG analysis complements the findings from the HR analysis, providing a more comprehensive understanding of the physiological responses to the cycling test. While the HR patterns suggest efficient cardiovascular and autonomic regulation, the EMG results reveal the specific muscle fatigue dynamics during the test. The combination of these analyses offers valuable insights into the overall fatigue profile of the subjects and can guide the development of personalized training and recovery strategies. In conclusion, the analysis of EMG median frequency during the 30-minute cycling test reveals distinct patterns of muscle fatigue in the anterior deltoid and erector spinae muscles. The consistent decrease in median frequency during high-intensity sprints and the subsequent recovery during

low-intensity phases suggest a dynamic interplay between fatigue accumulation and recovery.

Figure 4-4 presents the subjective fatigue ratings reported by three subjects during a 30-minute cycling session using the Borg scale. The Borg scale is a widely used tool for assessing perceived exertion and overall fatigue.

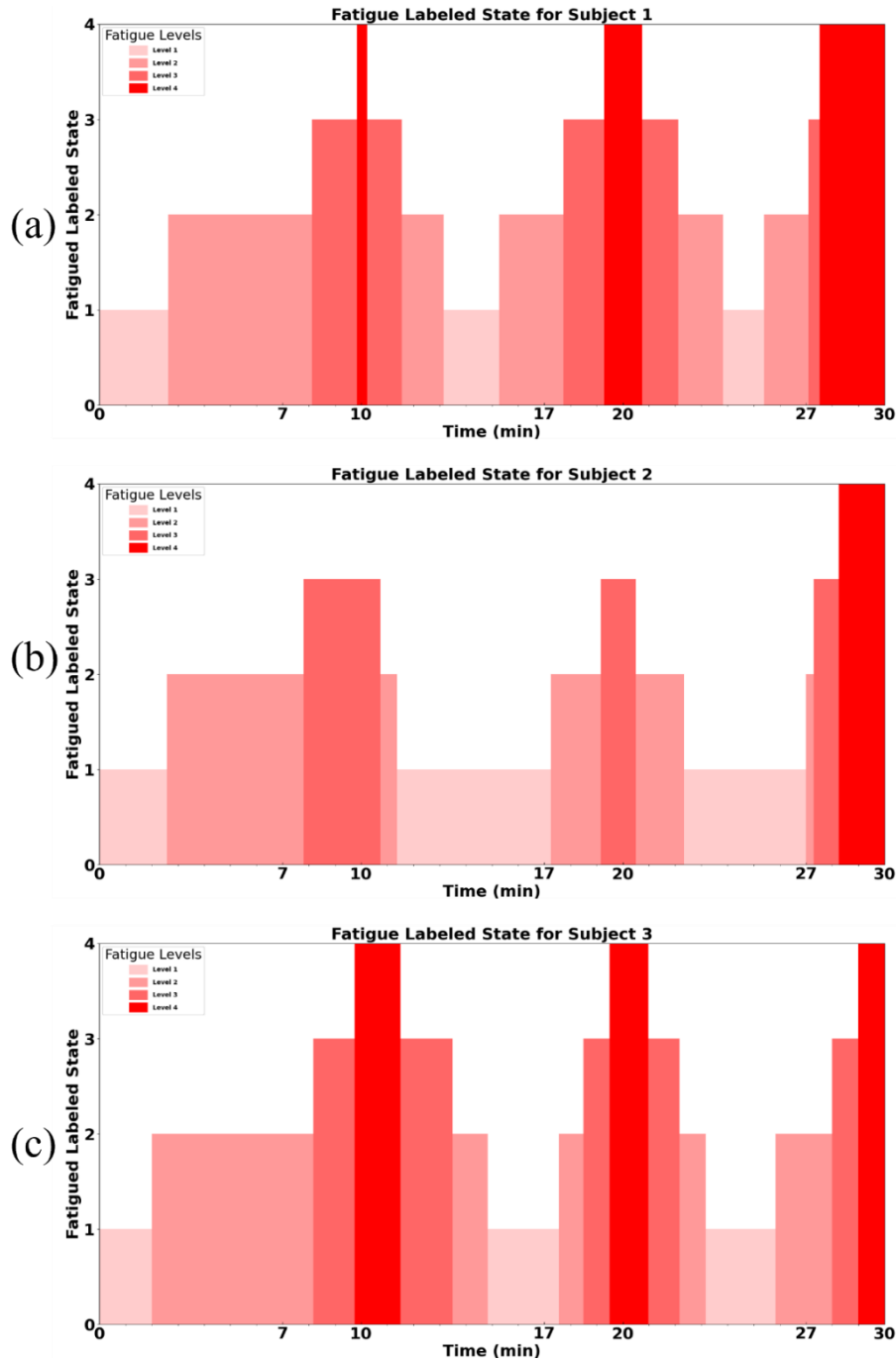


Figure 4-4 Fatigue labeled state for 3 subjects for 30 minutes cycling: (a) Subject 1; (b) Subject 2; (c) Subject 3.

From the Figure 4-4, we can observe that all three subjects exhibit an increasing trend in their fatigue levels over time, with individual variations in the rate and magnitude of fatigue development. Subject 1 shows a steep increase in fatigue during the first 10 minutes, followed by a more gradual increase until the end of the session. Subject 2 demonstrates a relatively steady increase in fatigue throughout the 30-minute period. Subject 3 exhibits a more pronounced stepwise increase in fatigue, with notable jumps at around 7, 17, and 27 minutes.

Interestingly, when comparing these subjective fatigue trends with the median frequency (MF) analysis of muscle fatigue discussed earlier, we can observe that the overall patterns are similar. However, the subjective fatigue ratings and MF-based fatigue indicators are not perfectly synchronized in real-time, suggesting that additional factors may contribute to the overall perceived fatigue experienced by the subjects.

While these conventional methods provide valuable insights into fatigue through statistical trends and intuitive physiological data, they may overlook certain characteristic indicators that could contribute to a more comprehensive understanding of fatigue. The relationship between these potentially relevant features and fatigue may not be readily apparent or fully understood, leading to their potential omission from the analysis.

However, it is important to understand that while these conventional methods provide valuable insights into fatigue through statistical trends and intuitive physiological data, they may overlook certain characteristic indicators that could contribute to a more comprehensive understanding of fatigue. The relationship between these potentially relevant features and fatigue may not be readily apparent or fully understood, leading to their potential omission from the analysis.

To address this limitation and maximize the utility of the real-time ECG and EMG data acquired by the Intelligent Garment System, we propose an innovative approach in the following sections of this work. By leveraging the power of artificial intelligence (AI) and employing state-of-the-art time-series deep learning models, we aim to process and analyze the data in a more sophisticated manner. This AI-driven approach seeks to

uncover hidden patterns, correlations, and fatigue-related features that may be overlooked by conventional methods. Deep learning algorithms can be trained on large datasets containing both physiological measurements (such as MF, heart rate, and oxygen consumption) and subjective fatigue ratings. These models can learn to recognize complex, non-linear relationships between various physiological parameters and fatigue perception. By incorporating multiple physiological indicators and considering their temporal dynamics, deep learning models have the potential to provide a more comprehensive understanding of the fatigue process. Moreover, deep learning techniques can be used to develop personalized fatigue prediction models. By training models on individual-specific data, we can capture the unique fatigue patterns and responses of each subject. This could lead to the development of tailored interventions and training strategies that optimize performance and minimize the risk of fatigue-related injuries.

4.3 Data Preparation for Deep Learning Model

4.3.1 ECG Data

To ensure consistency in data quantity between the ECG and EMG signals for input into the deep learning model, a spline interpolation method was applied to the ECG data. As our system acquires ECG signals at a sampling frequency of 125 Hz, which is lower than that of the EMG, the interpolation technique was employed to upsample the ECG data to match the 1000 Hz sampling rate of the EMG. This upsampling process preserves the original ECG waveform while increasing the number of data points, enabling seamless integration with the EMG data for subsequent analysis and modeling.

The electrocardiogram (ECG) signals acquired from each subject across multiple experiments were processed and analyzed using the NeuroKit2 Python toolbox[218]. The raw ECG data underwent cleaning procedures to remove noise, baseline wander, and artifacts, ensuring signal quality for subsequent analysis.

To extract relevant features, the cleaned ECG signal was segmented using a sliding window approach with a window size of 2 seconds and a step of 1 second. This allowed for the capture of important ECG patterns while maintaining temporal information. Within each window, NeuroKit2 was employed to perform R-peak detection, heart rate calculation, and feature extraction.

A comprehensive set of 72 ECG features was extracted, as shown in Table 4-4. These features encompass various aspects of the ECG signal, including time-domain, frequency-domain, and non-linear measures. Notable features include heart rate variability (HRV) parameters such as SDNN, RMSSD, and pNN50, which provide insights into the autonomic nervous system's influence on cardiac activity. Frequency-domain features like HF, VHF, and LF offer information about the power distribution across different frequency bands. Non-linear features, including entropy measures (ApEn, SampEn, ShanEn) and fractal dimensions (HFD, KFD), capture the complexity and self-similarity of the ECG signal.

Table 4-4 ECG features

Number	ECG Feature	Number	ECG Feature	Number	ECG Feature
1	ECG Rate Mean	25	HRV LnHF	49	HRV Cd
2	HRV MeanNN	26	HRV SD1	50	HRV Ca
3	HRV SDNN	27	HRV SD2	51	HRV SDNNd
4	HRV RMSSD	28	HRV SD1SD2	52	HRV SDNNa
5	HRV SDDSD	29	HRV S	53	HRV DFA alpha1
6	HRV CVNN	30	HRV CSI	54	HRV MFDFA alpha1 Width
7	HRV CVSD	31	HRV CVI	55	HRV MFDFA alpha1 Peak
8	HRV MedianNN	32	HRV CSI Modified	56	HRV MFDFA alpha1 Mean
9	HRV MadNN	33	HRV PIP	57	HRV MFDFA alpha1 Max
10	HRV MCVNN	34	HRV IALS	58	HRV MFDFA alpha1 Delta
11	HRV IQRNN	35	HRV PSS	59	HRV MFDFA alpha1 Asymmetry
12	HRV SDRMSSD	36	HRV PAS	60	HRV MFDFA alpha1 Fluctuation

13	HRV Prc20NN	37	HRV GI	61	HRV MFDFA alpha1 Increment
14	HRV Prc80NN	38	HRV SI	62	HRV ApEn
15	HRV pNN50	39	HRV AI	63	HRV SampEn
16	HRV pNN20	40	HRV PI	64	HRV ShanEn
17	HRV MinNN	41	HRV C1d	65	HRV FuzzyEn
18	HRV MaxNN	42	HRV C1a	66	HRV MSEn
19	HRV HTI	43	HRV SD1d	67	HRV CMSEn
20	HRV TINN	44	HRV SD1a	68	HRV RCMSEn
21	HRV HF	45	HRV C2d	69	HRV CD
22	HRV VHF	46	HRV C2a	70	HRV HFD
23	HRV TP	47	HRV SD2d	71	HRV KFD
24	HRV HF _n	48	HRV SD2a	72	HRV LZC

To ensure consistent data dimensions and facilitate further processing, the extracted ECG features were resampled to a fixed length of 1800 using cubic spline interpolation. This step preserves the overall shape and trends of the features while standardizing the data representation. The resampled features were organized into a structured data frame, and irrelevant or redundant columns were removed to optimize the dataset.

Lastly, a time series was generated to represent the start time of each 2-second window, allowing for the alignment of feature values with their respective time points. This temporal information is crucial for understanding the dynamics and trends of the ECG features over time. The ECG data has a scale of $(30 \times 60 - 1) \times 2000$, where $(30 \times 60 - 1)$ represents the total number of 2-second windows in a 30-minute recording (1799), and 2000 denotes the number of data points within each 2-second window. On the other hand, the ECG features exhibit a scale of $(30 \times 60 - 1) \times 72$, where $(30 \times 60 - 1)$ signifies the total number of 2-second windows (1799), and 72 denotes the number of extracted features for each window.

4.3.2 EMG Data

The electromyogram (EMG) data, collected from the anterior deltoid and erector spinae muscles, underwent feature extraction to quantify muscle activation patterns. The raw EMG signals were processed using a sliding window approach, with a window

size of 2 seconds and a step of 1 second, consistent with the ECG data processing.

Within each window, the EMG envelope was calculated, providing a smooth representation of the muscle activation levels. From the EMG envelope, several time-domain features were extracted, as listed in Table 4-5. These features include the root mean square (RMS), integrated EMG (iEMG), mean frequency (MF), and median power frequency (MPF).

Table 4-5 EMG features

Number	EMG Feature
1	RMS
2	iEMG
3	MF
4	MPF

The RMS feature quantifies the average amplitude of the EMG signal, reflecting the overall muscle activation level. The iEMG feature represents the area under the EMG envelope curve, providing a measure of the total muscle activity within the window. The MF and MPF features, derived from the frequency-domain analysis of the EMG signal, offer insights into the frequency content and power distribution of the muscle activation. In addition to these frequency-domain features, time-domain measures such as mean, minimum, and maximum values of the EMG envelope were calculated. These features capture various aspects of muscle activation, including the average activation level, the lowest and highest activation points within the window.

The extracted EMG features for each muscle were appended to separate lists, maintaining the distinction between the anterior deltoid and erector spinae. This approach allows for the independent analysis and comparison of muscle-specific activation patterns. The feature lists were then converted to data frames, providing a structured format for further analysis and integration with other data sources. By extracting a comprehensive set of EMG features, including both time-domain and frequency-domain measures, the study aims to characterize muscle activation patterns and investigate their associations with ECG features and other physiological variables. These EMG features serve as valuable inputs for statistical analysis, pattern recognition, and machine learning techniques, facilitating the identification of meaningful patterns

and potential biomarkers related to muscle function and fatigue.

The raw EMG data acquired from the erector spinae muscle (EMG1) and the anterior deltoid muscle (EMG2) exhibits a scale of $(30*60-1) * 2000$ for each respective muscle. This scale is derived from the total number of 2-second windows in a 30-minute recording, which is calculated as $(30*60-1)$, resulting in 1799 windows. Each window comprises 2000 data points, capturing the fine-grained temporal dynamics and activation patterns of the muscles under investigation. In parallel, the extracted EMG features for both the erector spinae muscle (EMG1) and the anterior deltoid muscle (EMG2) demonstrate a scale of $(30*60-1) * 4$. This scale is a product of the total number of 2-second windows (1799) and the number of features extracted from each window (4).

4.3.3 Input data for machine learning

In this study, we propose a novel approach to integrate and analyze ECG and EMG data using a combination of deep learning and traditional machine learning techniques. As illustrated in Figure 4-5, the input to our model consists of three distinct datasets: ECG data, EMG data from the anterior deltoid muscle (EMG1), and EMG data from the erector spinae muscle (EMG2). To leverage the complementary information provided by these modalities, we concatenate these three datasets along the feature dimension, creating a unified input representation.

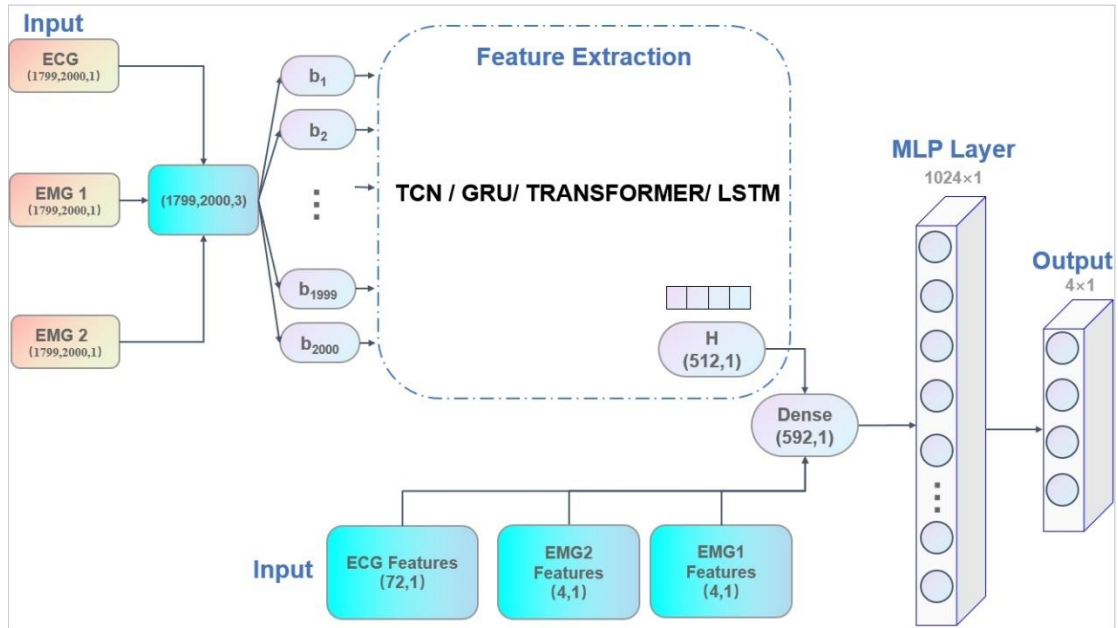


Figure 4-5 Neural Network Architecture Diagram

The concatenated input is then fed into a deep learning model, which serves as a feature extractor. This model is designed to capture the intricate patterns and relationships present in the combined ECG and EMG data. Through multiple layers of nonlinear transformations, the deep learning model learns a compact and informative representation of the input. The output of this feature extraction process is a 512-dimensional feature vector, denoted as H in Figure 4-5.

To further enhance the representational power of our approach, we incorporate hand-crafted features derived from the individual ECG, EMG1, and EMG2 datasets. These features, referred to as ECG features, EMG1 features, and EMG2 features, are concatenated with the 512-dimensional feature vector H obtained from the deep learning model. This concatenation step allows us to combine the automatically learned features with domain-specific knowledge captured by the hand-crafted features.

The resulting concatenated feature vector, which now encompasses both the deep learning-based representation and the hand-crafted features, is passed through a Multilayer Perceptron (MLP) for further processing. The MLP is a type of feedforward artificial neural network that consists of an input layer, one or more hidden layers, and an output layer. Each neuron in the hidden and output layers applies a nonlinear activation function to the weighted sum of its inputs, enabling the network to learn

complex decision boundaries and capture high-level abstractions.

In our proposed framework, the MLP takes the concatenated feature vector as input and processes it through its fully connected layers. The hidden layers of the MLP learn to extract higher-order relationships and interactions among the features, allowing for a more comprehensive understanding of the ECG and EMG dynamics. The output layer of the MLP produces the final predictions or classifications based on the learned representations.

4.4 Application of Deep Learning Model for Predicting

4.4.1 Temporal Convolutional Network (TCN)

The Temporal Convolutional Network (TCN) model was implemented and evaluated for its effectiveness in predicting fatigue levels based on ECG and EMG signals. The architecture of the TCN model, as illustrated in Figure 4-6, consists of multiple convolutional layers with increasing dilation factors, followed by a global average pooling layer and a fully connected layer for classification. This structure allows the model to efficiently learn temporal patterns and dependencies in the input data. The model parameters, such as the number of channels (64, 128, 256), number of classes (4), number of epochs (100), learning rate (0.0005), batch size (32), kernel size (3), dropout rate (0.2), were carefully selected to optimize the model's performance and generalization ability. The loss function is Cross-Entropy. The optimizer is ADAM.

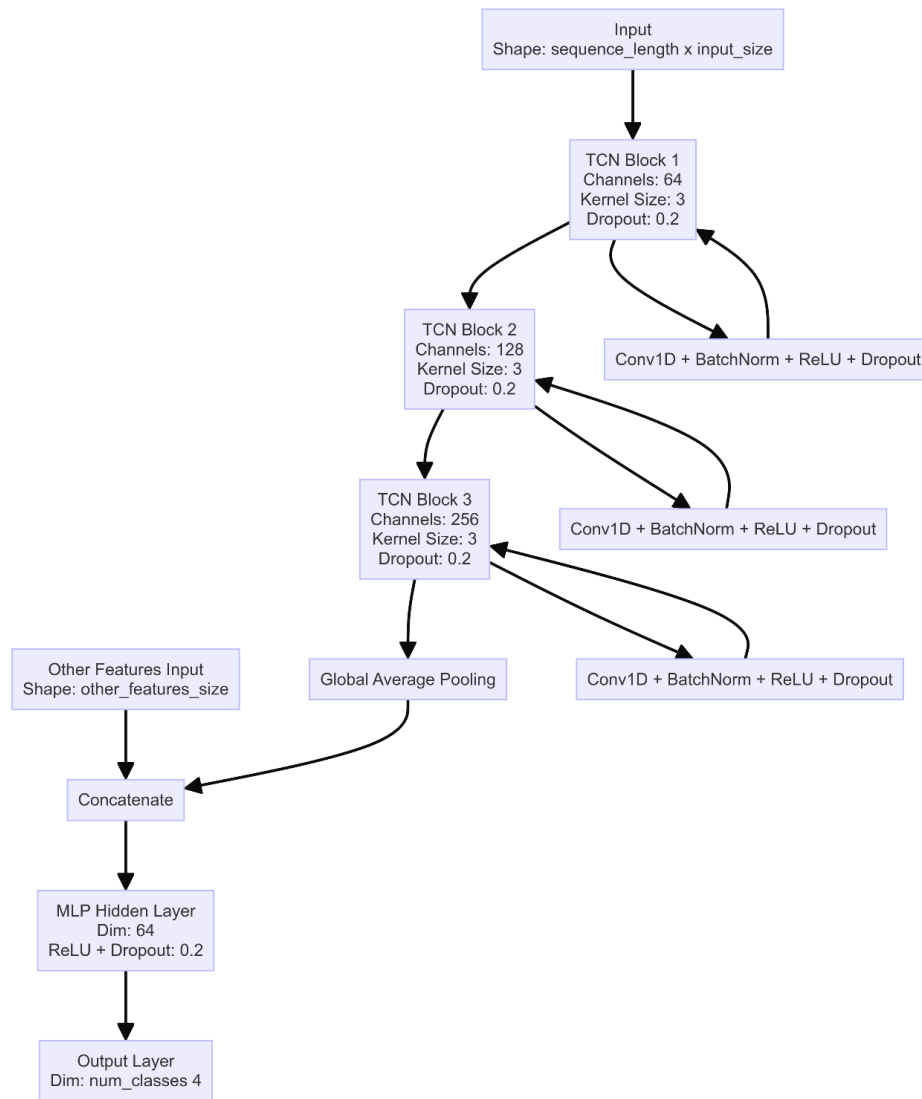


Figure 4-6 TCN model structure

Table 4-6 presents the accuracy metrics across the five folds for each of the three subjects, demonstrating that the TCN model achieves reasonable accuracy in predicting fatigue levels, with some variability across subjects and folds.

Table 4-6 Accuracy metrics across five folds for three subjects in TCN

Subjects	Flod 1	Flod 2	Flod 3	Flod 4	Flod 5
1	78.66%	73.70%	75.12%	65.92%	69.65%
2	80.27%	70.79%	71.57%	73.50%	74.61%
3	82.50%	79.00%	76.33%	71.50%	75.33%

Figure 4-7 displays the confusion matrices obtained from TCN model for each subject. These matrices provide a detailed breakdown of the model's performance, showing the percentage of correctly classified samples for each fatigue level. The confusion matrices indicate that TCN model achieves reasonable accuracy in predicting

fatigue levels across all subjects, although there is room for improvement.

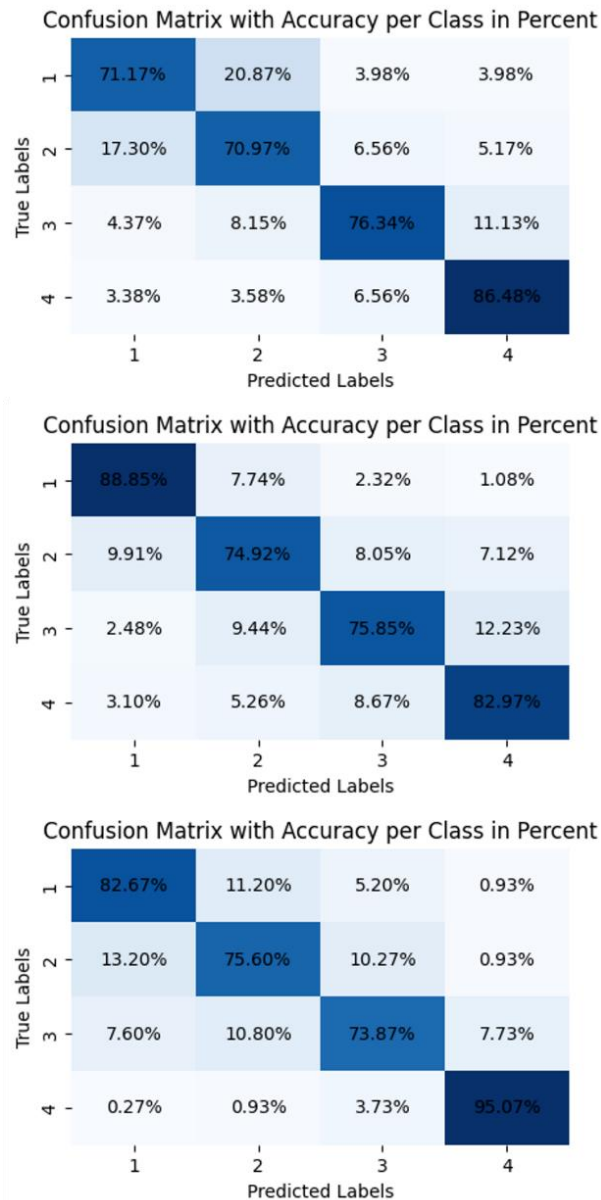


Figure 4-7 Confusion matrix of three subjects in TCN model

The performance metrics of TCN model are summarized in Table 4-7, including accuracy, precision, recall, F1 score, and area under the receiver operating characteristic curve (AUC). These metrics provide a comprehensive evaluation of the model's predictive capabilities. Notably, the AUC values range from 84.16% to 87.87%, indicating the model's strong discriminatory power in distinguishing between different fatigue levels.

Table 4-7 Recognition performance of three subjects in TCN model.

Number	Accuracy	Precision	Recall	F1	AUC
1#	76.24%	76.38%	76.24%	76.18%	84.16%
2#	80.65%	80.77%	80.65%	80.59%	87.10%
3#	81.80%	81.79%	81.80%	81.68%	87.87%

Figures 4-8 illustrates the training and test loss, as well as the training and test accuracy, respectively, across the three subjects. These graphs provide insights into the model's learning behavior and generalization ability. The convergence of the model during training and its reasonable performance on the test data are evident from these figures.

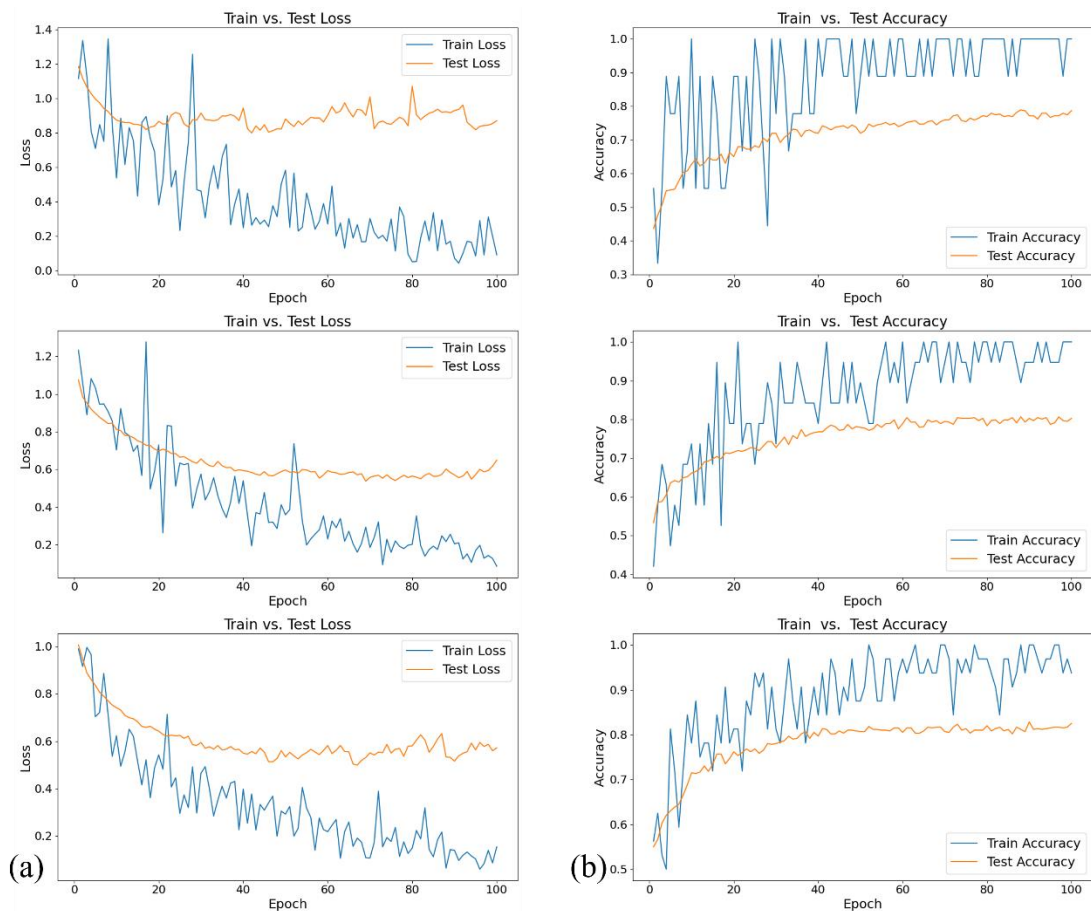


Figure 4-8 (a) Training and test loss comparison across three subjects in TCN model (b) Training and test accuracy comparison across three subjects in TCN model

However, the varying performance across subjects highlights the individual differences in physiological responses to fatigue and the challenges in developing a one-size-fits-all fatigue prediction model. The results suggest that personalized approaches and further refinement of the model architecture and hyperparameters may be necessary to improve the predictive performance for everyone. Despite these

challenges, the TCN model demonstrates promise in capturing temporal dependencies and learning discriminative features for fatigue prediction. Its ability to handle sequential data, such as ECG and EMG signals, makes it a suitable candidate for integration into the intelligent garment system. The TCN model's architecture, with its dilated causal convolutions, allows for efficient learning of long-term dependencies while maintaining a manageable number of parameters. This is particularly advantageous for real-time fatigue monitoring in wearable devices, where computational efficiency is crucial. The application of the TCN model to predict fatigue levels based on ECG and EMG signals shows promising results, with room for improvement. The model's performance varies among the three subjects, emphasizing the need for personalized fatigue monitoring and the development of adaptive models. Nevertheless, the TCN model's ability to capture temporal dependencies and its computational efficiency make it a suitable choice for integration into the intelligent garment system for real-time fatigue monitoring.

4.4.2 Gated Recurrent Unit (GRU)

Gated Recurrent Unit (GRU) model, a variant of the recurrent neural network (RNN), was implemented and evaluated for its effectiveness in predicting fatigue levels based on ECG and EMG signals. The GRU architecture addresses the vanishing gradient problem and captures long-term dependencies more effectively than traditional RNNs. The model architecture, as illustrated in Figure 4-8, consists of multiple GRU layers followed by a multilayer perceptron (MLP) classifier. The key hyperparameters of the model were tuned to optimize performance, with a hidden size of 512 for the GRU layers, 4 GRU layers, 100 training epochs, a learning rate of 0.0001, a batch size of 64, and an MLP hidden dimension of 1024.

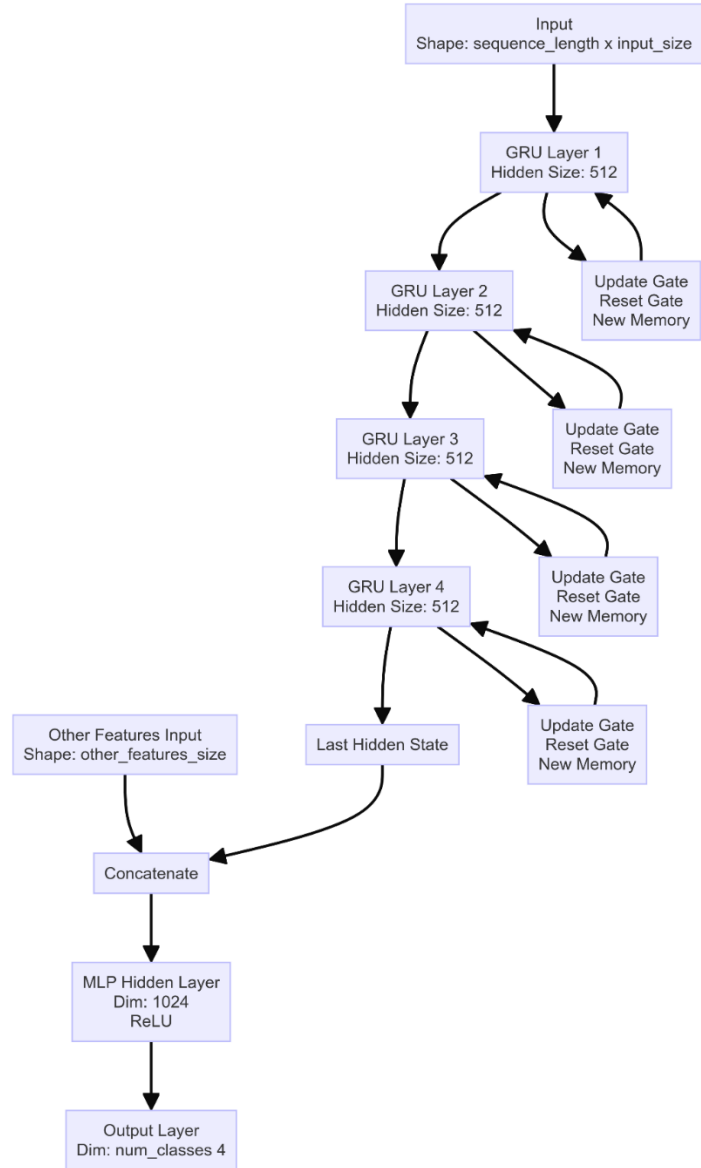


Figure 4-9 GRU model structure

Table 4-8 presents the accuracy metrics across the five folds for each of the three subjects, indicating that the GRU model achieves relatively lower accuracy compared to the TCN model.

Table 4-8 Accuracy metrics across five folds for three subjects in GRU

Subjects	Flo d 1	Flo d 2	Flo d 3	Flo d 4	Flo d 5
1	68.24%	51.36%	67.16%	78.11%	88.31%
2	70.79%	45.65%	68.09%	83.75%	93.99%
3	74.00%	68.50%	72.67%	59.17%	73.50%

Figure 4-10 displays the confusion matrices obtained from the GRU model for each of the three subjects, providing insights into the model's performance in predicting

fatigue levels. The results suggest that the GRU model may not be as well-suited as the TCN model for capturing the temporal dependencies in the ECG and EMG signals for fatigue prediction.

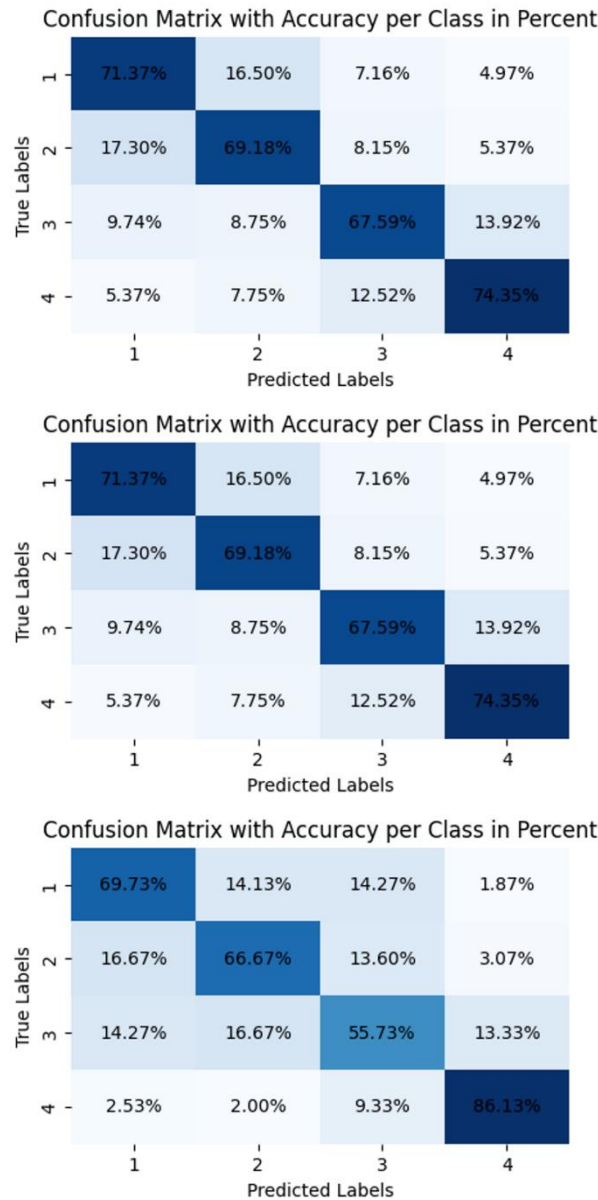


Figure 4-10 Confusion matrix of three subjects in GRU model

Table 4-9 summarizes the performance metrics obtained from the GRU model, including accuracy, precision, recall, F1 score, and area under the receiver operating characteristic curve (AUC) for each subject. The accuracy of the GRU model ranges from 69.57% to 72.45%, indicating that it correctly predicts the fatigue level for a moderate portion of the samples. The precision and recall values are also relatively

lower compared to the TCN model, suggesting a higher occurrence of false positives and false negatives. The F1 scores, which provide a balanced measure of precision and recall, range from 69.39% to 72.34%. The AUC values, ranging from 79.71% to 81.64%, indicate that the GRU model's ability to discriminate between different fatigue levels is somewhat limited compared to the TCN model.

Comparing the performance metrics across the three subjects, we observe that Subject 2 achieves the highest accuracy of 72.45%, followed by Subject 1 with an accuracy of 70.64% and Subject 3 with an accuracy of 69.57%. The precision, recall, and F1 score follow a similar trend, with Subject 2 exhibiting slightly better performance compared to the other two subjects. The AUC values are also highest for Subject 2 at 81.64%, while Subject 1 and Subject 3 have AUC values of 80.42% and 79.71%, respectively.

Table 4-9 Recognition performance of three subjects in GRU model.

Number	Accuracy	Precision	Recall	F1	AUC
1#	70.64%	70.83%	70.64%	70.64%	80.42%
2#	72.45%	72.40%	72.45%	72.34%	81.64%
3#	69.57%	69.36%	69.57%	69.39%	79.71%

Figures 4-11 illustrates the training and test loss, as well as the training and test accuracy, respectively, across the three subjects for the GRU model. These graphs provide insights into the model's learning behavior and generalization ability. The convergence of the model during training and its reasonable performance on the test data are evident from these figures.

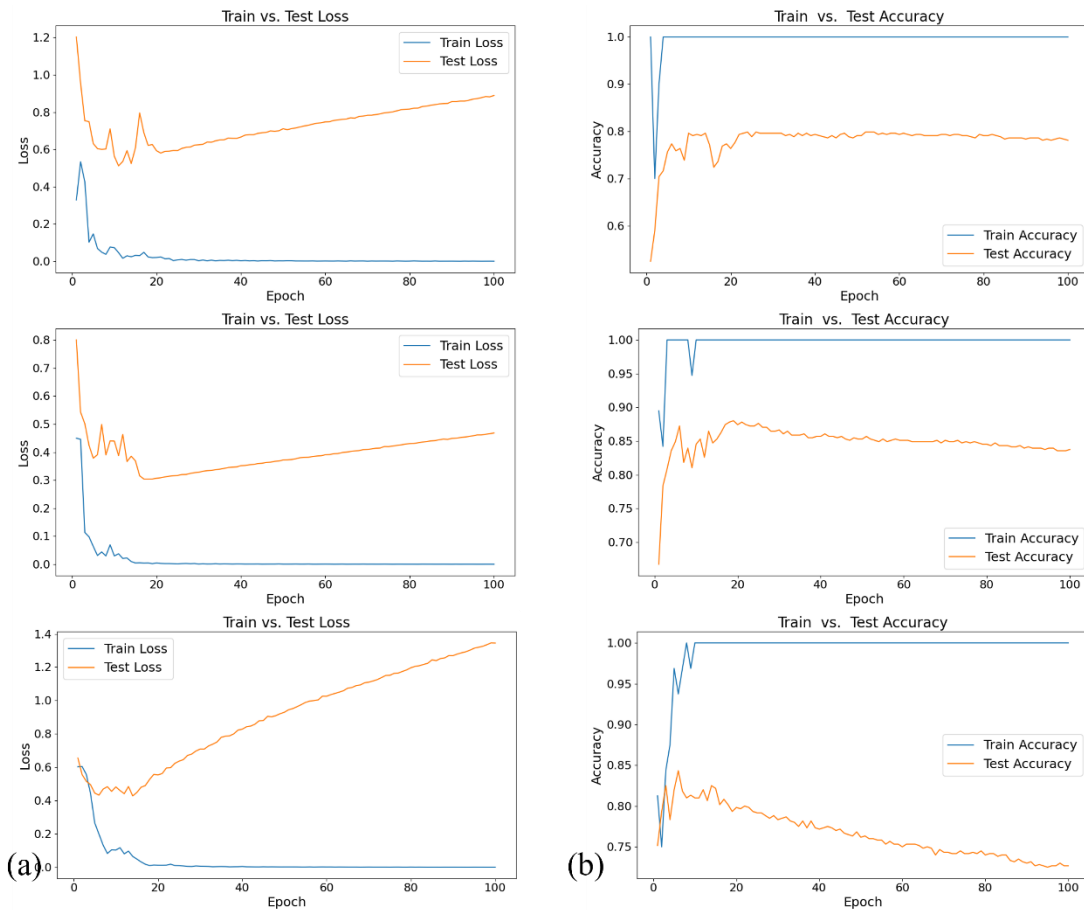


Figure 4-11 (a) Training and test loss comparison across three subjects in GRU model (b) Training and test accuracy comparison across three subjects in GRU model

The lower performance of the GRU model compared to the TCN model suggests that the GRU architecture may not be the most suitable choice for predicting fatigue levels based on the given ECG and EMG signals. The GRU model's ability to capture long-term dependencies and temporal patterns in the data may be limited, leading to suboptimal performance.

Several factors could contribute to the GRU model's lower performance. First, the temporal dependencies and patterns in the ECG and EMG signals related to fatigue may be more complex and require a more sophisticated architecture to capture effectively. The GRU model's simpler structure compared to the TCN model may not be sufficient to learn these intricate patterns. Second, the GRU model's ability to handle long-term dependencies may be limited, as it relies on a single gating mechanism to control the flow of information. In contrast, the TCN model's dilated causal convolutions allow for a larger receptive field and more efficient capture of long-term dependencies.

Furthermore, the GRU model's performance may be affected by the limited amount of training data available for each subject. With a smaller dataset, the model may struggle to generalize well and capture the full range of fatigue-related patterns in the ECG and EMG signals. The TCN model's convolutional architecture and ability to share weights across time steps may be more resilient to limited data scenarios. GRU model's lower performance compared to the TCN model indicates that it may not be the most suitable choice for predicting fatigue levels based on the ECG and EMG signals in the context of the intelligent garment system. The GRU model's limitations in capturing complex temporal dependencies and its potential sensitivity to limited training data make it less desirable for this specific application.

4.4.3 Transformer

Transformer model, a deep learning architecture that has gained significant attention in natural language processing, was explored to investigate its applicability in predicting fatigue levels based on ECG and EMG signals. The Transformer model leverages attention mechanisms and self-attention to capture long-term dependencies in sequential data. The model architecture, as illustrated in Figure 4-12, consists of multiple encoder layers, each incorporating multi-head self-attention mechanisms and feed-forward neural networks. Key hyperparameters were tuned to optimize performance, with 2 encoder layers, a hidden size of 64, 4 attention heads, a feed-forward network dimension of 256, and a dropout rate of 0.1.

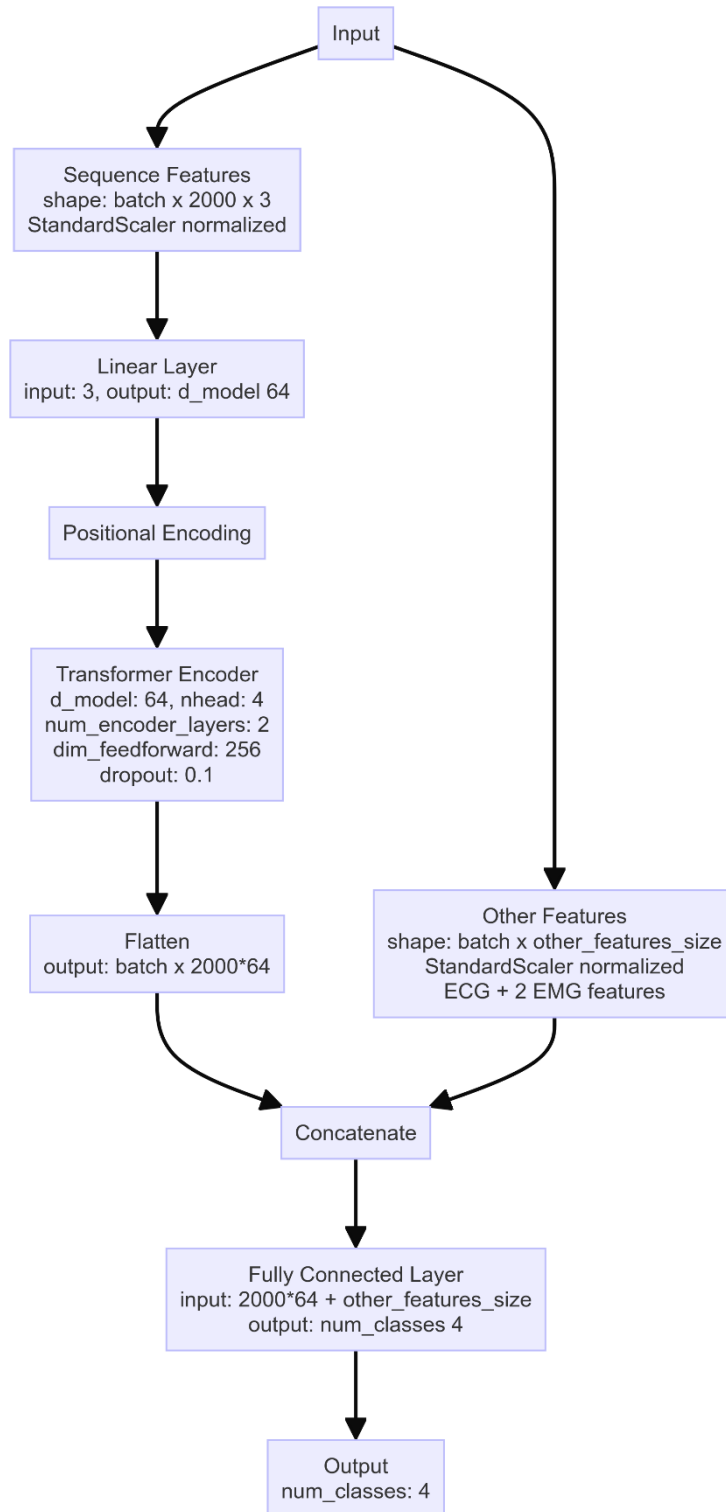


Figure 4-12 Transformer model structure

Transformer model was trained and evaluated using a 5-fold cross-validation approach, consistent with the methodology employed for TCN and GRU models. The input features encompassed both the sequence data (ECG and EMG signals) and

additional static features, and the model was trained to classify the input data into one of the four fatigue levels. Table 4-10 presents the accuracy metrics across the five folds for each of the three subjects, indicating that the Transformer model exhibits the lowest accuracy among the three models investigated.

Table 4-10 Accuracy metrics across five folds for three subjects in Transformer

Subjects	Flod 1	Flod 2	Flod 3	Flod 4	Flod 5
1	47.39%	48.39%	45.27%	47.76%	51.00%
2	50.10%	54.35%	54.93%	51.84%	58.14%
3	59.00%	58.17%	62.00%	59.17%	59.83%

Figure 4-13 presents the confusion matrices obtained from the Transformer model for each of the three subjects. The results indicate that the Transformer model exhibits the lowest accuracy among the three models investigated, suggesting that it may not be well-suited for capturing the temporal dependencies and nuances in the ECG and EMG signals for accurate fatigue prediction.

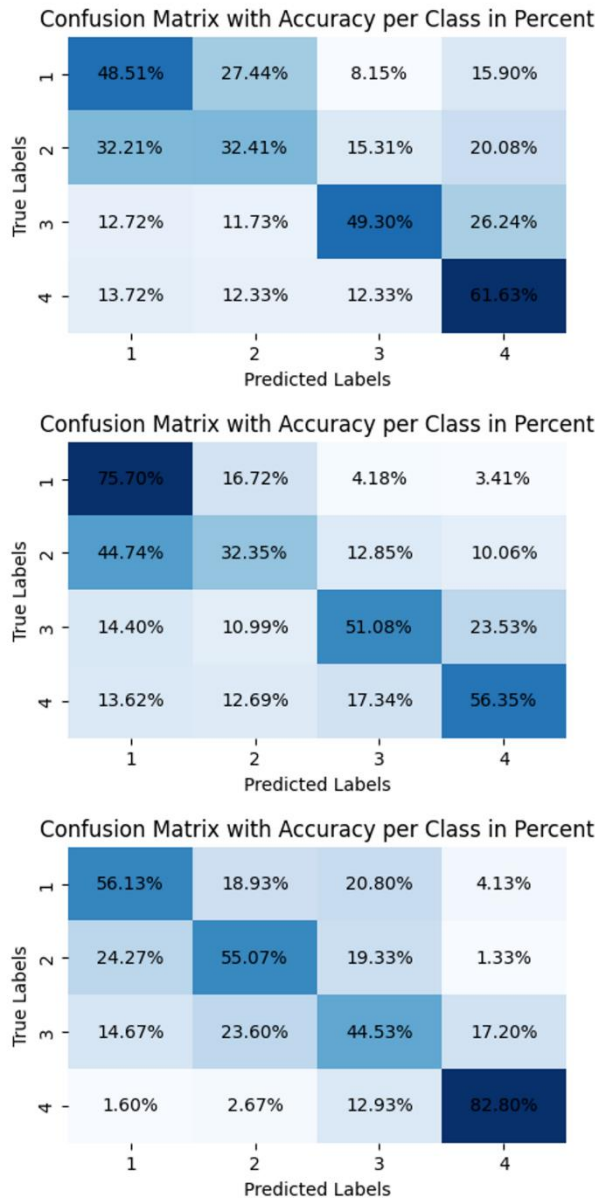


Figure 4-13 Confusion matrix of three subjects in transformer model

Table 4-11 summarizes the performance metrics achieved by the Transformer model, including accuracy, precision, recall, F1 score, and area under the receiver operating characteristic curve (AUC) for each subject. Across all subjects, the Transformer model demonstrates lower performance compared to TCN and GRU models. The accuracy ranges from 46.52% to 56.83%, precision and recall values are relatively low, F1 scores range from 46.30% to 56.46%, and AUC values span from 64.34% to 71.22%.

Table 4-11 Recognition performance of three subjects in Transformer model.

Number	Accuracy	Precision	Recall	F1	AUC
1#	46.52%	47.05%	46.52%	46.30%	64.34%
2#	53.99%	54.94%	53.99%	52.01%	69.32%
3#	56.83%	56.84%	56.83%	56.46%	71.22%

Figures 4-14 illustrates the training and test loss, as well as the training and test accuracy, respectively, across the three subjects in Transformer model. These graphs provide insights into the model's learning behavior and generalization ability. The convergence of the model during training and its reasonable performance on the test data are evident from these figures.

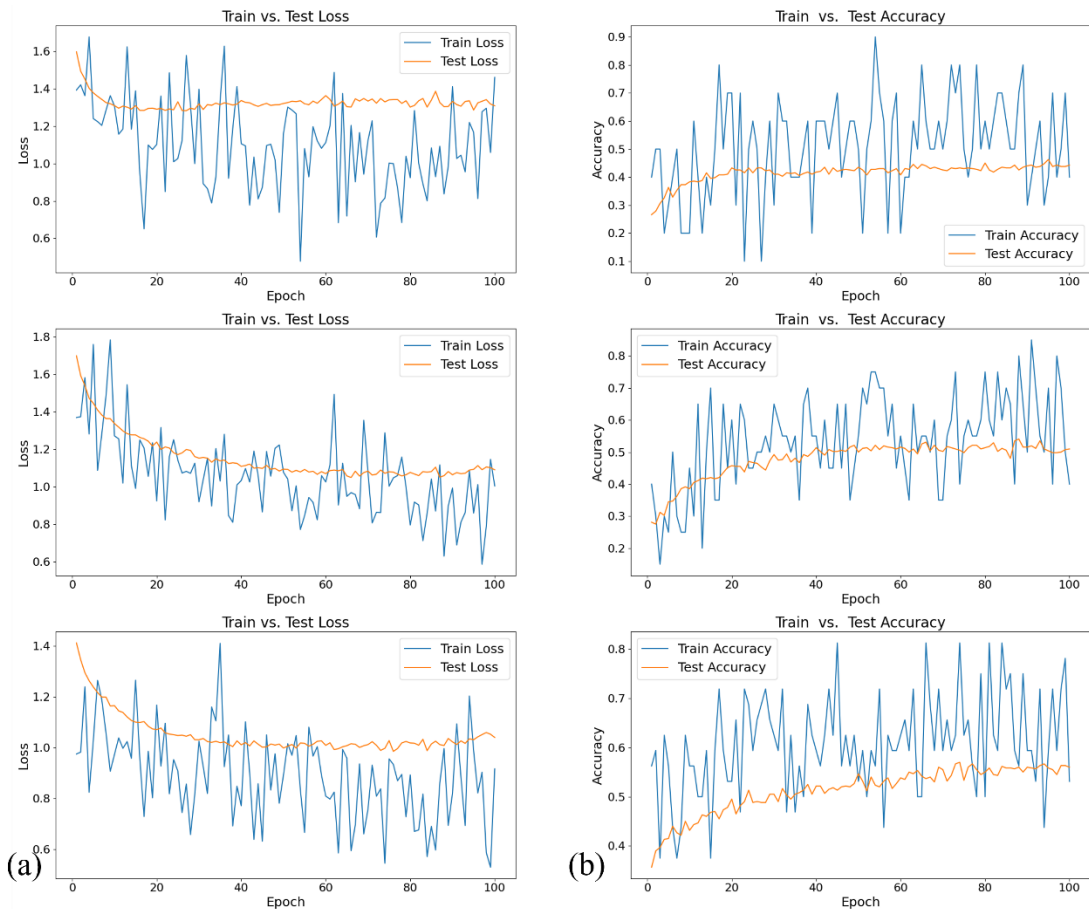


Figure 4-14 (a) Training and test loss comparison across three subjects in Transformer model (b)

Training and test accuracy comparison across three subjects in Transformer model

The suboptimal performance of the Transformer model in this study suggests that its architecture, despite its remarkable success in natural language processing tasks, may not be directly transferable to the domain of fatigue prediction using physiological signals. Several factors could contribute to the Transformer model's ineffectiveness in capturing the relevant patterns and dependencies in the ECG and EMG signals.

First, the inherent differences between text data and time series signals, such as ECG and EMG, could pose challenges for the Transformer model. The self-attention mechanism, which is highly effective in capturing long-range dependencies in text, may not be as well-suited for the specific temporal patterns and characteristics of physiological signals related to fatigue.

Second, the limited amount of training data available for each subject may hinder the Transformer model's ability to learn and generalize effectively. Transformer models typically require large amounts of data to achieve optimal performance, and the relatively small dataset in this study could be insufficient for the model to capture the complex patterns associated with fatigue.

Furthermore, the Transformer model's architecture, with its multiple encoder layers and self-attention mechanisms, may introduce additional complexity that is not necessarily beneficial for the task at hand. The increased complexity could lead to overfitting, especially when dealing with limited training data, resulting in poor generalization and lower performance on unseen data. Transformer model, despite its prominence in other domains, does not appear to be well-suited for predicting fatigue levels based on the ECG and EMG signals collected by our intelligent garment system. The model's performance falls short of TCN and GRU models, with lower accuracy, precision, recall, F1 score, and AUC values across all subjects. The inherent differences between text data and physiological signals, limited training data, and the model's complexity are likely factors contributing to its suboptimal performance in this specific application.

4.4.4 Long Short-Term Memory (LSTM)

Long Short-Term Memory (LSTM) model, a variant of recurrent neural networks (RNNs), was employed to predict fatigue levels based on the ECG and EMG signals collected by the Intelligent Garment System. The architecture of the LSTM model, as illustrated in Figure 4-15, consists of several components that work in harmony to extract meaningful features and make accurate predictions.

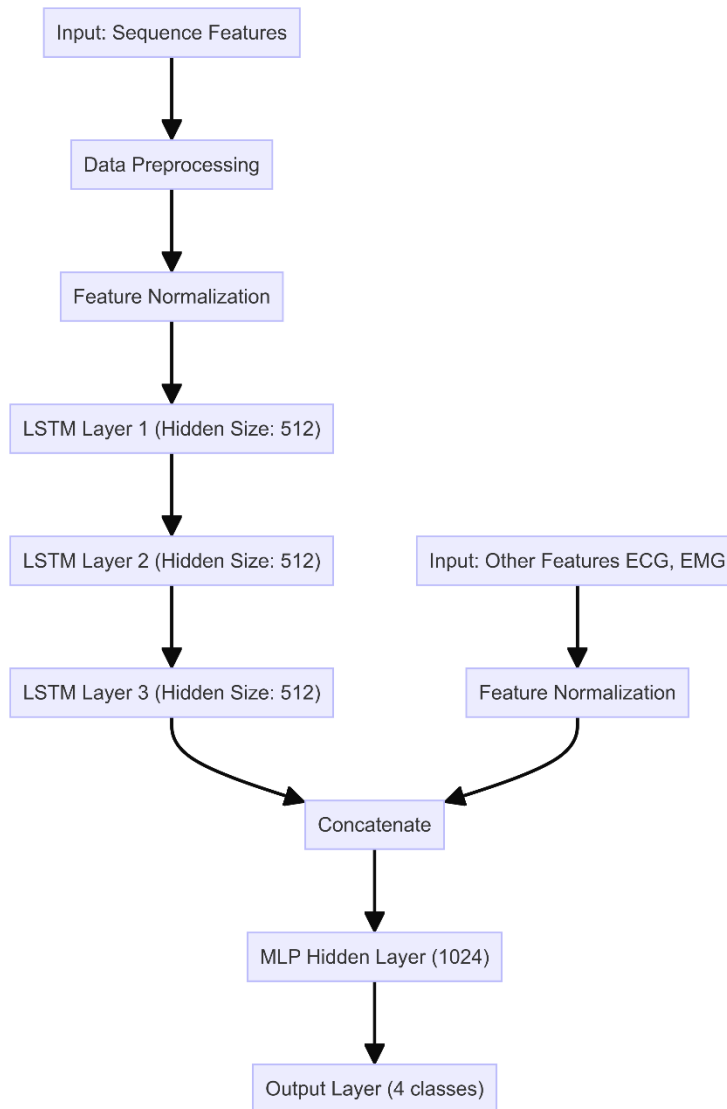


Figure 4-15 LSTM model structure

LSTM model's architecture is characterized by four stacked LSTM layers, each containing 512 hidden units. This stacked architecture allows the model to learn hierarchical representations of the data, with each layer capturing increasingly abstract and complex patterns. The choice of 512 hidden units per layer strikes an optimal balance between the model's expressive capacity and computational efficiency. The output from the LSTM layers undergoes further processing through a dense layer with 1024 hidden units, serving as a critical feature transformation and dimensionality reduction step. The transformed features are then fed into a final output layer with four units, corresponding to the four fatigue levels.

The LSTM model's training process is carefully designed to optimize its performance and generalization ability. The model is trained for 100 epochs using the Adam optimizer with a learning rate of 0.001 and a batch size of 64. These hyperparameters were determined through extensive experimentation and fine-tuning. To mitigate overfitting, a dropout regularization technique with a rate of 0.2 is applied to the LSTM layers.

Table 4-12 presents the accuracy metrics across five folds for each of the three subjects, demonstrating the LSTM model's exceptional performance. The model achieves high accuracy values consistently across all folds and subjects, ranging from 81.84% to 90.50%. These results highlight the LSTM model's ability to effectively learn and generalize from the training data, capturing the intricate patterns and dependencies associated with different fatigue levels.

Table 4-12 Accuracy metrics across five folds for three subjects in LSTM

Subjects	Fold 1	Fold 2	Fold 3	Fold 4	Fold 5
1	82.63	84.12	83.83	84.08	81.84
2	89.17	87.62	87.43	87.43	88.76
3	87.00	90.50	89.33	87.50	90.33

Table 4-13 summarizes the overall performance metrics for each subject, further emphasizing the LSTM model's exceptional predictive capabilities. The model achieves accuracies ranging from 83.30% to 88.60%, precision and recall values consistently above 83%, and F1 scores exceeding 83% for all subjects. These high values indicate the model's ability to correctly identify and classify fatigue levels with great precision and sensitivity. Moreover, the AUC values, ranging from 88.87% to 92.40%, demonstrate the model's outstanding discriminative power in distinguishing between different fatigue levels.

Table 4-13 Recognition performance of three subjects in LSTM model.

Number	Accuracy	Precision	Recall	F1	AUC
1#	83.30%	83.34%	83.30%	83.23%	88.87%
2#	87.73%	87.71%	87.73%	87.67%	91.82%
3#	88.60%	88.60%	88.60%	88.56%	92.40%

Figure 4-16 presents the confusion matrices for each subject, offering a detailed breakdown of the LSTM model's performance across the four fatigue levels. The

confusion matrices reveal that the model accurately predicts a significant proportion of samples in each fatigue category, with a high concentration of correct predictions along the main diagonal. This fine-grained analysis highlights the LSTM model's capacity to capture the subtle nuances and patterns associated with different fatigue states, enabling precise and reliable predictions.

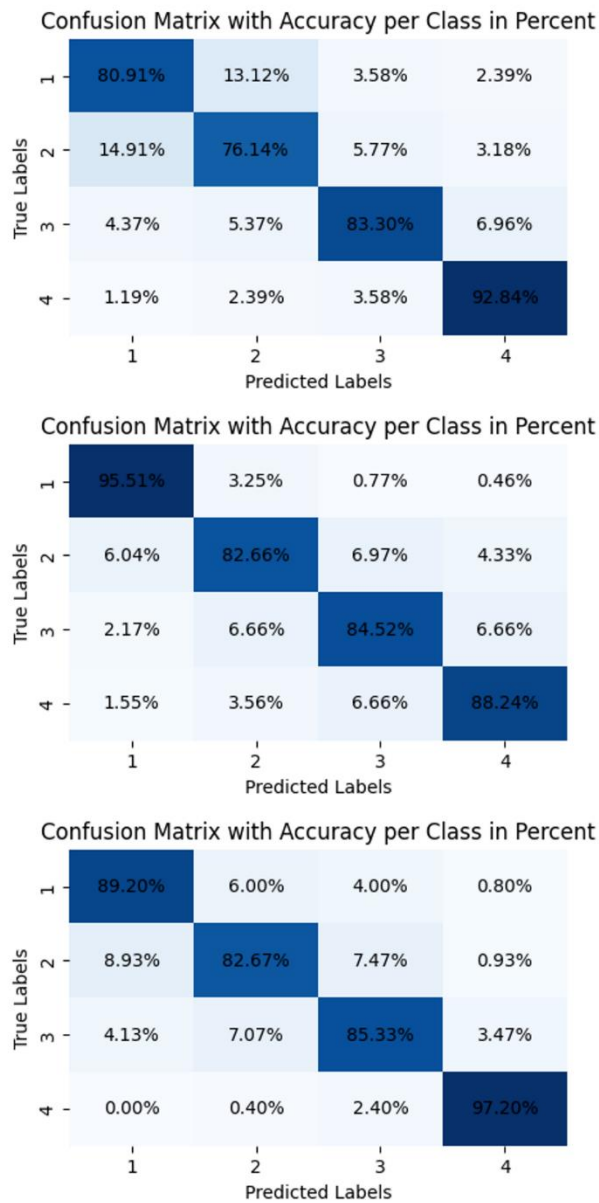


Figure 4-16 Confusion matrix of three subjects in LSTM model

Figures 4-17 illustrates the training and test loss, as well as the training and test accuracy, respectively, across the three subjects in LSTM model. The graphs demonstrate the model's stable and consistent learning process, with the loss decreasing

steadily and the accuracy increasing over the epochs. The convergence of the training and test curves indicates that the model generalizes well to unseen data, minimizing overfitting and achieving robust performance.

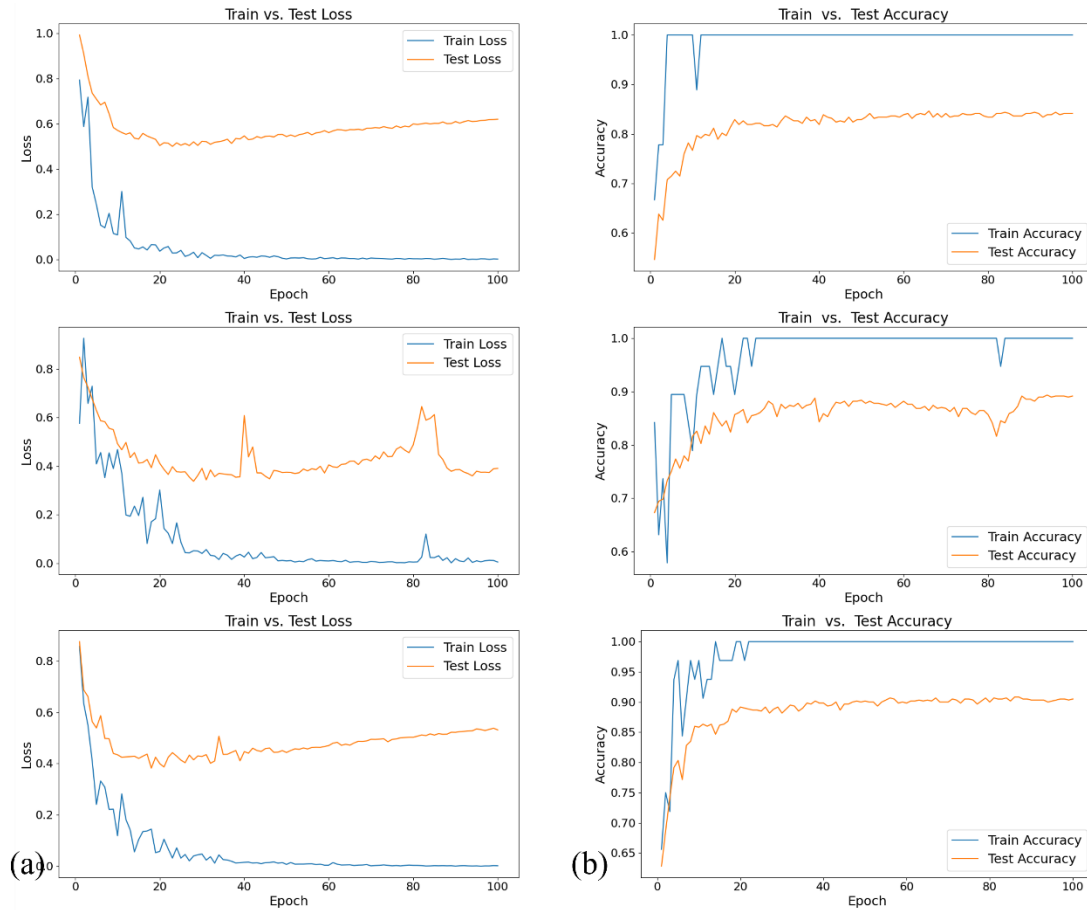


Figure 4-17 (a) Training and test loss comparison across three subjects in LSTM model (b) Training and test accuracy comparison across three subjects in LSTM model

The superior performance of the LSTM model compared to the other models (TCN, GRU, and Transformer) can be attributed to several factors. First, the LSTM architecture's ability to capture long-term dependencies and retain relevant information over time makes it particularly well-suited for analyzing time series data such as ECG and EMG signals. The LSTM's gating mechanism allows it to selectively remember or forget information, enabling it to capture the complex temporal patterns associated with fatigue.

Second, the LSTM model's architecture, with its stacked layers and carefully chosen hyperparameters, demonstrates a well-designed approach to fatigue level prediction. The multiple LSTM layers enable the model to learn hierarchical

representations, capturing both low-level and high-level patterns in the data. The dense layer provides additional discriminative power, enhancing the model's ability to differentiate between fatigue levels.

LSTM model's superior performance in predicting fatigue levels based on ECG and EMG signals makes it the most suitable choice for integration into the Intelligent Garment System. Its ability to capture long-term dependencies and learn hierarchical representations enables it to accurately assess fatigue levels in real-time.

4.5 Results and Discussion

The cycling test, which simulated different intensity levels typical of a training or competition session, allowed us to evaluate the intelligent garment system's performance in a realistic setting. We collected and analyzed ECG and EMG data from three subjects to assess the system's fatigue prediction capabilities using both traditional methods and advanced deep learning techniques.

The conventional ECG analysis showed consistent HR across all subjects. HR was stable during low-intensity phases, indicating steady cardiovascular and autonomic function, while high-intensity sprints caused rapid HR increases followed by quick decreases. These findings suggest that the garment system can effectively capture HR changes related to different levels of physical effort.

EMG analysis of the anterior deltoid and erector spinae muscles revealed muscle fatigue dynamics. The EMG signal's median frequency (MF), a known fatigue indicator, gradually increased during low-intensity phases and markedly decreased during high-intensity sprints, especially in Subjects 2 and 3. Subject 1 showed a slightly different erector spinae fatigue profile. These results demonstrate the system's ability to detect and measure muscle fatigue in real-time, showing its potential for personalized monitoring.

To improve the system's predictive capabilities, we used advanced deep learning techniques, including TCN, GRU, Transformers, and LSTM models. The models were trained and evaluated using 5-fold cross-validation after data preprocessing. TCN

model showed reasonable accuracy in predicting fatigue levels, with slight performance variations among subjects. The GRU and Transformer models performed lower than expected, suggesting they may not be the best choice for this application.

The LSTM model emerged as the most promising approach, with its architecture combining stacked LSTM layers for temporal feature extraction and an MLP for static feature integration and classification. It achieved impressive results across all evaluation metrics, consistently demonstrating high accuracy, precision, recall, F1 score, and AUC values for all subjects. The confusion matrices further confirmed its superior performance.

These findings have important implications for developing intelligent garment systems in sports and fitness. They highlight the importance of combining multiple physiological signals for comprehensive fatigue assessment and the potential of deep learning techniques, particularly LSTM, for enhancing wearable monitoring systems. The results also emphasize the need for personalized fatigue monitoring strategies and lay the foundation for further exploration of intelligent garment systems in various physical activities.

In conclusion, the intelligent garment system effectively predicted fatigue levels during cycling, with the LSTM model significantly enhancing its predictive capabilities. However, more research is needed to address individual variability, explore the system's applicability to other activities, and refine the models for improved accuracy and personalization. Continuing advancements in wearable technology and artificial intelligence can optimize athletic performance, prevent injuries, and promote overall well-being.

CHAPTER 5 Conclusion

5.1 Summary of Finding

This doctoral thesis presents a comprehensive study on the development and evaluation of a novel fatigue assessment system for athletes using smart clothing and artificial intelligence techniques. The research encompasses several key aspects, including the design and fabrication of 3D knitted silver electrodes, their integration into compression garments, and the application of advanced AI models for real-time fatigue prediction based on ECG and EMG signals.

One of the main focuses of this thesis was the optimization of electrode design through a parametric approach. By systematically exploring various electrode parameters, such as diameter, height, and applied pressure, the research aimed to identify the optimal configuration for achieving high-quality signal acquisition while ensuring user comfort. The findings suggest that electrodes with a diameter of 3 cm, a height of 3 mm, and an applied pressure of 30 mmHg provide the best balance between signal quality and user experience. These insights contribute to the advancement of smart clothing design and highlight the importance of considering both technical and ergonomic factors in the development of wearable health monitoring systems.

Another significant aspect of this research was the seamless integration of the optimized 3D knitted silver electrodes into compression garments. The resulting intelligent garment system features strategically placed electrodes, conductive channels for signal transmission, and adjustable fasteners to maintain a stable electrode-skin interface during dynamic movements. This innovative design approach not only ensures reliable signal acquisition but also enhances user comfort and ease of use, making it suitable for real-world applications in sports and athletic performance monitoring.

To evaluate the effectiveness of the developed system, rigorous testing was conducted in the context of cycling sports. A comprehensive experimental setup was designed to simulate real-world cycling conditions, and a data preparation process was

established to ensure the quality and consistency of the collected ECG and EMG signals. The study employed a range of state-of-the-art AI models, including Temporal Convolutional Networks (TCN), Gated Recurrent Units (GRU), Long Short-Term Memory (LSTM), and Transformer architectures, to predict fatigue levels based on the acquired physiological data.

Among the tested AI models, the LSTM architecture demonstrated the most promising results, accurately assessing fatigue levels in real-time based on the ECG and EMG signals. The LSTM model's ability to capture long-term dependencies and temporal patterns in the data proved crucial for reliable fatigue prediction. This finding highlights the potential of AI techniques, particularly deep learning approaches, in enhancing the capabilities of wearable health monitoring systems and enabling personalized training and recovery strategies for athletes.

Furthermore, the study showcases the successful integration of knowledge from multiple disciplines, including textile engineering, sensor technology, biomedical signal processing, and artificial intelligence. This interdisciplinary approach has led to the development of a comprehensive and innovative solution for fatigue assessment in sports, demonstrating the potential for collaboration across different fields to drive advancements in wearable technology and athletic performance monitoring.

In addition to the technical aspects, the research also emphasizes the practical implications of the developed system. The ability to provide real-time, accurate insights into an athlete's fatigue state opens new possibilities for optimizing training plans, preventing injuries, and ultimately improving athletic performance. The findings suggest that the intelligent garment system can serve as a valuable tool for coaches, trainers, and athletes, enabling data-driven decision-making and personalized interventions.

5.2 Contributions of the Study

This research has made several significant contributions to the field of wearable technology for sports monitoring, specifically in developing an AI-based fatigue

assessment system using smart textile wearables. The key contributions are as follows:

(1) Development of Advanced 3D Knitted Silver Electrodes:

The study introduced a novel design and fabrication process for 3D knitted silver electrodes. These electrodes demonstrated superior performance in terms of signal quality and stability compared to conventional Ag/AgCl electrodes, especially in wet skin conditions. The optimized electrode configuration, with a diameter of 3 cm and a height of 3 mm, represents a significant advancement in textile-based biosensing technology.

(2) Integration of Electrodes into an Intelligent Garment System:

The research successfully integrated the developed 3D knitted silver electrodes into a comprehensive intelligent garment system. This system incorporated strategically placed ECG and EMG sensors, along with innovative conductive pathways and adjustable fastening mechanisms. The design ensured both effective signal acquisition and user comfort, addressing a critical challenge in wearable sports monitoring technology.

(3) Comprehensive Evaluation in Real-Time Cycling:

The intelligent garment system was rigorously tested in realistic cycling, providing valuable insights into its performance and reliability in dynamic sports environments. This practical evaluation adds credibility to the system's potential applications in real-time sports monitoring.

(4) Integration of Multiple Physiological Signals:

By combining ECG and EMG data in the fatigue prediction model, the study demonstrated the value of a multi-modal approach to physiological monitoring. This integrated approach provides a more comprehensive assessment of an athlete's fatigue state than single-signal methods.

(5) Implementation of Advanced AI Algorithms for Fatigue Prediction:

The study explored and compared various deep learning models for fatigue prediction, including TCN, GRU, Transformer, and LSTM architectures. The LSTM model, in particular, demonstrated superior performance in accurately predicting

fatigue levels based on ECG and EMG signals. This represents a significant step forward in real-time, personalized fatigue monitoring for athletes.

(6) Advancement in Personalized Sports Monitoring:

The research highlighted individual differences in fatigue patterns and physiological responses, emphasizing the importance of personalized monitoring approaches. This contribution aligns with the growing trend towards individualized training and performance optimization in sports science.

These contributions collectively advance the field of wearable technology for sports monitoring, offering new possibilities for real-time, accurate, and non-invasive fatigue assessment. The developed system and methodologies provide a foundation for future research in sports science, wearable technology, and personalized health monitoring.

5.3 Limitations and Future Work

While this study has made significant contributions to the field of wearable technology for sports monitoring, it is important to acknowledge its limitations and identify areas for future research:

(1) Sample Size and Diversity:

The current study was conducted with a limited number of subjects, all of whom were male. Future work should expand the sample size and include a more diverse group of subjects, considering factors such as gender, age, and fitness levels. This expansion would enhance the generalizability of the findings and potentially reveal additional insights into individual variations in fatigue patterns.

(2) Long-term Durability of Textile Electrodes:

Although the 3D knitted silver electrodes showed promising performance, their long-term durability under repeated use and washing cycles was not extensively tested. Future research should focus on assessing and improving the longevity of these electrodes to ensure their reliability in real-world, long-term applications.

(3) Environmental Factors:

The cycling tests were conducted in a controlled indoor environment. Future studies should investigate the system's performance under various environmental conditions, such as different temperatures, humidity levels, and outdoor settings, to ensure its reliability across diverse sporting scenarios.

(4) Range of Sports Activities:

While the current study focused on cycling, future work should extend the application of the intelligent garment system to a broader range of sports activities. This expansion would help validate the system's versatility and potentially lead to sport-specific adaptations of the fatigue prediction models.

(5) Real-time Processing Capabilities:

The current system relies on post-hoc data analysis. Future developments should focus on implementing real-time processing capabilities, allowing for immediate feedback to athletes and coaches during training or competition.

(6) Integration with Other Physiological Markers:

While the study combined ECG and EMG data, future research could explore the integration of additional physiological markers, such as skin temperature or respiratory rate, to further enhance the accuracy of fatigue prediction.

(7) Customization of AI Models:

The AI models developed in this study, while effective, were not personalized to individual athletes. Future work could explore adaptive learning techniques that allow the models to fine-tune their predictions based on an individual's unique physiological responses over time.

(8) User Experience and Comfort:

Although efforts were made to ensure user comfort, more comprehensive studies on the long-term wearability and user acceptance of the intelligent garment system are needed. This could include extended wear trials and user feedback studies.

(9) Power Management and Battery Life:

Future research should focus on optimizing the power consumption of the system to extend battery life, potentially exploring energy harvesting technologies to enhance

the system's autonomy during prolonged use.

(10) Data Privacy and Security:

As the system collects sensitive physiological data, future work should address robust data encryption and secure transmission protocols to ensure user privacy and compliance with data protection regulations.

Addressing these limitations and pursuing these future research directions will further advance the field of wearable technology for sports monitoring, potentially leading to more accurate, versatile, and user-friendly systems for fatigue assessment and performance optimization in sports.

References

1. Hasan, M.M. and M.M. Hossain, *Nanomaterials-patterned flexible electrodes for wearable health monitoring: a review*. Journal of Materials Science, 2021. **56**(27): p. 14900-14942.
2. Nigusse, A.B., et al., *Wearable smart textiles for long-term electrocardiography monitoring—A review*. Sensors, 2021. **21**(12): p. 4174.
3. La Spada, L., *Metasurfaces for advanced sensing and diagnostics*. Sensors, 2019. **19**(2): p. 355.
4. Pacheco-Peña, V., et al., *On the performance of an ENZ-based sensor using transmission line theory and effective medium approach*. New Journal of Physics, 2019. **21**(4): p. 043056.
5. La Spada, L. and L. Vegni, *Electromagnetic nanoparticles for sensing and medical diagnostic applications*. Materials, 2018. **11**(4): p. 603.
6. Lincoln, R.L., et al., *Multifunctional composites: A metamaterial perspective*. Multifunctional Materials, 2019. **2**(4): p. 043001.
7. La Spada, L., et al., *Curvilinear metasurfaces for surface wave manipulation*. Scientific reports, 2019. **9**(1): p. 3107.
8. Greybush, N.J., et al., *Plasmonic optical and chiroptical response of self-assembled Au nanorod equilateral trimers*. ACS nano, 2019. **13**(2): p. 1617-1624.
9. Akbari, M., et al., *The graphene field effect transistor modeling based on an optimized ambipolar virtual source model for DNA detection*. Applied Sciences, 2021. **11**(17): p. 8114.
10. Acar, G., et al., *Wearable and flexible textile electrodes for biopotential signal monitoring: A review*. Electronics, 2019. **8**(5): p. 479.
11. Islam, M.M., et al., *Wearable technology to assist the patients infected with novel coronavirus (COVID-19)*. SN computer science, 2020. **1**: p. 1-9.
12. Burki, T., *Wearable technology and COVID-19*. The Lancet Respiratory Medicine, 2022. **10**(10): p. 934-935.
13. Yu, H., et al., *Research on the construction of intelligent sports health management system based on Internet of Things and cloud computing technology*. Wireless Communications and Mobile Computing, 2022. **2022**(1): p. 7133810.
14. Enderle, J. and J. Bronzino, *Introduction to biomedical engineering*. 2011: Academic press.
15. Wang, Z. and Z. Gao, *Analysis of real-time heartbeat monitoring using wearable device Internet of Things system in sports environment*. Computational Intelligence, 2021. **37**(3): p. 1080-1097.
16. Alberdi, A., A. Aztiria, and A. Basarab, *Towards an automatic early stress recognition system for office environments based on multimodal measurements: A review*. Journal of biomedical informatics, 2016. **59**: p. 49-75.
17. Nemati, E., M.J. Deen, and T. Mondal, *A wireless wearable ECG sensor for long-term applications*. IEEE Communications Magazine, 2012. **50**(1): p. 36-43.
18. Berkaya, S.K., et al., *A survey on ECG analysis*. Biomedical Signal Processing and Control, 2018. **43**: p. 216-235.
19. Priya, K.J., K.H. Yadav, and K. Jyothsna, *A portable wearable tele ECG monitoring system*. International Journal Of Engineering Applied Sciences And Technology, 2020. **4**(12): p. 683-690.

20. Piuzei, E., et al., *Wearable belt with built-in textile electrodes for cardio—Respiratory monitoring*. Sensors, 2020. **20**(16): p. 4500.
21. Guan, X., et al. *Sports fatigue detection based on deep learning*. in *2021 14th International Congress on Image and Signal Processing, BioMedical Engineering and Informatics (CISP-BMEI)*. 2021. IEEE.
22. Soroudi, A., et al., *Surface modification of textile electrodes to improve electrocardiography signals in wearable smart garment*. Journal of Materials Science: Materials in Electronics, 2019. **30**: p. 16666-16675.
23. Saadatnejad, S., M. Oveisi, and M. Hashemi, *LSTM-based ECG classification for continuous monitoring on personal wearable devices*. IEEE journal of biomedical and health informatics, 2019. **24**(2): p. 515-523.
24. Shu, Y.-S., et al. *26.1 A 4.5 mm² multimodal biosensing SoC for PPG, ECG, BIOZ and GSR acquisition in consumer wearable devices*. in *2020 IEEE International Solid-State Circuits Conference-(ISSCC)*. 2020. IEEE.
25. Marutani, Y., et al., *An experimental feasibility study evaluating the adequacy of a sportswear-type wearable for recording exercise intensity*. Sensors, 2022. **22**(7): p. 2577.
26. Harpe, P., et al., *A 0.20mm² 3 nW Signal Acquisition IC for Miniature Sensor Nodes in 65 nm CMOS*. IEEE Journal of Solid-State Circuits, 2015. **51**(1): p. 240-248.
27. Ding, J., et al., *Reduction in the motion artifacts in noncontact ECG measurements using a novel designed electrode structure*. Sensors, 2023. **23**(2): p. 956.
28. Qian, L., et al. *Unselfish Cooperative Game-Based Communication Optimization of ECG Monitoring Network*. in *Proceedings of the 2022 International Conference on Computational Infrastructure and Urban Planning*. 2022.
29. Wang, J., et al. *Motion-Resilient ECG Signal Reconstruction from a Wearable IMU through Attention Mechanism and Contrastive Learning*. in *Proceedings of the Ninth International Conference on Animal-Computer Interaction*. 2022.
30. Pingitore, A., et al., *An overview of the electrocardiographic monitoring devices in sports cardiology: Between present and future*. Clinical Cardiology, 2023. **46**(9): p. 1028-1037.
31. Gohel, V. and N. Mehendale, *Review on electromyography signal acquisition and processing*. Biophysical reviews, 2020. **12**(6): p. 1361-1367.
32. Zhang, T. and C. Fu, *Application of improved VMD-LSTM model in sports artificial intelligence*. Computational Intelligence and Neuroscience, 2022. **2022**(1): p. 3410153.
33. Ahmed, R., et al. *Prosthetic arm control using electromyography (EMG) signal*. in *2018 International Conference on Advancement in Electrical and Electronic Engineering (ICAEEE)*. 2018. IEEE.
34. Sattar, N.Y., et al. *Real-time EMG signal processing with implementation of PID control for upper-limb prosthesis*. in *2019 IEEE/ASME International Conference on Advanced Intelligent Mechatronics (AIM)*. 2019. IEEE.
35. Ke, A., et al., *Improving the robustness of human-machine interactive control for myoelectric prosthetic hand during arm position changing*. Frontiers in Neurorobotics, 2022. **16**: p. 853773.
36. Asghar, A., et al., *Review on electromyography based intention for upper limb control using pattern recognition for human-machine interaction*. Proceedings of the Institution of Mechanical Engineers, Part H: Journal of Engineering in Medicine, 2022. **236**(5): p. 628-

- 645.
37. Biagetti, G., et al. *A portable wireless sEMG and inertial acquisition system for human activity monitoring*. in *Bioinformatics and Biomedical Engineering: 5th International Work-Conference, IWBBIO 2017, Granada, Spain, April 26–28, 2017, Proceedings, Part II* 5. 2017. Springer.
 38. Biagetti, G., et al., *Human activity monitoring system based on wearable sEMG and accelerometer wireless sensor nodes*. Biomedical engineering online, 2018. **17**: p. 1-18.
 39. Quittmann, O.J., et al., *Normalising surface EMG of ten upper-extremity muscles in handcycling: Manual resistance vs. sport-specific MVICs*. Journal of electromyography and kinesiology, 2020. **51**: p. 102402.
 40. Felici, F. and A. Del Vecchio, *Surface electromyography: what limits its use in exercise and sport physiology?* Frontiers in neurology, 2020. **11**: p. 578504.
 41. Spanu, A., et al., *Dynamic surface electromyography using stretchable screen-printed textile electrodes*. IEEE Transactions on Neural Systems and Rehabilitation Engineering, 2021. **29**: p. 1661-1668.
 42. Campanini, I., et al., *Fundamental concepts of bipolar and high-Density surface EMG understanding and teaching for clinical, occupational, and sport applications: Origin, detection, and main errors*. Sensors, 2022. **22**(11): p. 4150.
 43. Enoka, R.M. and J. Duchateau, *Translating fatigue to human performance*. Medicine and science in sports and exercise, 2016. **48**(11): p. 2228.
 44. Kluger, B.M., L.B. Krupp, and R.M. Enoka, *Fatigue and fatigability in neurologic illnesses: proposal for a unified taxonomy*. Neurology, 2013. **80**(4): p. 409-416.
 45. Enoka, R.M. and D.G. Stuart, *Neurobiology of muscle fatigue*. Journal of applied physiology, 1992. **72**(5): p. 1631-1648.
 46. Noakes, T.D., *Fatigue is a brain-derived emotion that regulates the exercise behavior to ensure the protection of whole body homeostasis*. Frontiers in physiology, 2012. **3**: p. 82.
 47. Allen, D.G., G.D. Lamb, and H. Westerblad, *Skeletal muscle fatigue: cellular mechanisms*. Physiological reviews, 2008. **88**(1): p. 287-332.
 48. Gandevia, S.C., *Spinal and supraspinal factors in human muscle fatigue*. Physiological reviews, 2001. **81**(4): p. 1725-1789.
 49. McCormick, A., C. Meijen, and S. Marcora, *Psychological determinants of whole-body endurance performance*. Sports medicine, 2015. **45**: p. 997-1015.
 50. Inzlicht, M., A. Shenhav, and C.Y. Olivola, *The effort paradox: Effort is both costly and valued*. Trends in cognitive sciences, 2018. **22**(4): p. 337-349.
 51. Borg, G.A., *Psychophysical bases of perceived exertion*. Medicine and science in sports and exercise, 1982. **14**(5): p. 377-381.
 52. Borg, G., *Borg's perceived exertion and pain scales*. 1998: Human kinetics.
 53. Scherr, J., et al., *Associations between Borg's rating of perceived exertion and physiological measures of exercise intensity*. European journal of applied physiology, 2013. **113**: p. 147-155.
 54. Chen, M.J., X. Fan, and S.T. Moe, *Criterion-related validity of the Borg ratings of perceived exertion scale in healthy individuals: a meta-analysis*. Journal of sports sciences, 2002. **20**(11): p. 873-899.
 55. Eston, R., *Use of ratings of perceived exertion in sports*. International journal of sports

- physiology and performance, 2012. **7**(2): p. 175-182.
56. Pageaux, B., *Perception of effort in exercise science: definition, measurement and perspectives*. European journal of sport science, 2016. **16**(8): p. 885-894.
57. Gros Lambert, A. and A.D. Mahon, *Perceived exertion: influence of age and cognitive development*. Sports medicine, 2006. **36**: p. 911-928.
58. Pincivero, D.M., *Older adults underestimate RPE and knee extensor torque as compared with young adults*. Medicine and science in sports and exercise, 2011. **43**(1): p. 171-180.
59. Abbiss, C.R., et al., *Role of ratings of perceived exertion during self-paced exercise: what are we actually measuring?* Sports medicine, 2015. **45**: p. 1235-1243.
60. Marcora, S.M. and W. Staiano, *The limit to exercise tolerance in humans: mind over muscle?* European journal of applied physiology, 2010. **109**: p. 763-770.
61. Eston, R. and J. Williams, *Reliability of ratings of perceived effort regulation of exercise intensity*. British journal of sports medicine, 1988. **22**(4): p. 153-155.
62. Halperin, I. and A. Emanuel, *Rating of perceived effort: methodological concerns and future directions*. Sports Medicine, 2020. **50**: p. 679-687.
63. Meeusen, R., et al., *Prevention, diagnosis and treatment of the overtraining syndrome: Joint consensus statement of the European College of Sport Science (ECSS) and the American College of Sports Medicine (ACSM)*. European Journal of Sport Science, 2013. **13**(1): p. 1-24.
64. Knicker, A.J., et al., *Interactive processes link the multiple symptoms of fatigue in sport competition*. Sports medicine, 2011. **41**: p. 307-328.
65. Taylor, J.L., et al., *Neural contributions to muscle fatigue: from the brain to the muscle and back again*. Medicine and science in sports and exercise, 2016. **48**(11): p. 2294.
66. Halson, S.L., *Monitoring training load to understand fatigue in athletes*. Sports medicine, 2014. **44**(Suppl 2): p. 139-147.
67. Thorpe, R.T., et al., *Monitoring fatigue status in elite team-sport athletes: implications for practice*. International journal of sports physiology and performance, 2017. **12**(s2): p. S2-27-S2-34.
68. Vanhatalo, A., J.H. Doust, and M. Burnley, *Determination of critical power using a 3-min all-out cycling test*. Medicine and science in sports and exercise, 2007. **39**(3): p. 548-555.
69. Black, M.I., et al., *Critical power derived from a 3-min all-out test predicts 16.1-km road time-trial performance*. European journal of sport science, 2014. **14**(3): p. 217-223.
70. Claudino, J.G., et al., *The countermovement jump to monitor neuromuscular status: A meta-analysis*. Journal of science and medicine in sport, 2017. **20**(4): p. 397-402.
71. Gathercole, R., et al., *Alternative countermovement-jump analysis to quantify acute neuromuscular fatigue*. International journal of sports physiology and performance, 2015. **10**(1): p. 84-92.
72. Twist, C. and J. Highton, *Monitoring fatigue and recovery in rugby league players*. International Journal of sports physiology and performance, 2013. **8**(5): p. 467-474.
73. Coutts, A.J., K.M. Slattery, and L.K. Wallace, *Practical tests for monitoring performance, fatigue and recovery in triathletes*. Journal of science and medicine in sport, 2007. **10**(6): p. 372-381.
74. Gescheit, D.T., et al., *Consecutive days of prolonged tennis match play: performance, physical, and perceptual responses in trained players*. International journal of sports

- physiology and performance, 2015. **10**(7): p. 913-920.
75. Bourdon, P.C., et al., *Monitoring athlete training loads: consensus statement*. International journal of sports physiology and performance, 2017. **12**(s2): p. S2-161-S2-170.
 76. Kellmann, M. and K.W. Kallus, *Recovery-stress questionnaire for athletes: User manual*. 2001: Human Kinetics.
 77. Saw, A.E., L.C. Main, and P.B. Gastin, *Monitoring the athlete training response: subjective self-reported measures trump commonly used objective measures: a systematic review*. British journal of sports medicine, 2016. **50**(5): p. 281-291.
 78. Kellmann, M., *Preventing overtraining in athletes in high - intensity sports and stress/recovery monitoring*. Scandinavian journal of medicine & science in sports, 2010. **20**: p. 95-102.
 79. Soligard, T., et al., *How much is too much?(Part 1) International Olympic Committee consensus statement on load in sport and risk of injury*. British journal of sports medicine, 2016. **50**(17): p. 1030-1041.
 80. Schwellnus, M., et al., *How much is too much?(Part 2) International Olympic Committee consensus statement on load in sport and risk of illness*. British journal of sports medicine, 2016. **50**(17): p. 1043-1052.
 81. Kellmann, M., et al., *Recovery and performance in sport: consensus statement*. International journal of sports physiology and performance, 2018. **13**(2): p. 240-245.
 82. An, X. and G.K. Stylios, *A hybrid textile electrode for electrocardiogram (ECG) measurement and motion tracking*. Materials, 2018. **11**(10): p. 1887.
 83. Arquilla, K., A.K. Webb, and A.P. Anderson, *Textile electrocardiogram (ECG) electrodes for wearable health monitoring*. Sensors, 2020. **20**(4): p. 1013.
 84. Alizadeh-Meghrazi, M., et al., *Evaluation of dry textile electrodes for long-term electrocardiographic monitoring*. Biomedical engineering online, 2021. **20**: p. 1-20.
 85. Rajanna, R.R., et al., *Performance evaluation of woven conductive dry textile electrodes for continuous ECG signals acquisition*. IEEE Sensors Journal, 2019. **20**(3): p. 1573-1581.
 86. Zhao, J., et al., *Water-retentive, 3D knitted textile electrode for long-term and motion state bioelectrical signal acquisition*. Composites Science and Technology, 2022. **227**: p. 109606.
 87. Lee, H. and Y. Lee, *Optimal prototype design of dry textile electrode-based compression pants for surface electromyography measurements*. International Journal of Clothing Science and Technology, 2023. **35**(1): p. 120-134.
 88. Jin, C. and Z. Bai, *MXene-based textile sensors for wearable applications*. ACS sensors, 2022. **7**(4): p. 929-950.
 89. Niu, X., et al., *Surface bioelectric dry Electrodes: A review*. Measurement, 2021. **183**: p. 109774.
 90. Eskandarian, L., et al., *Robust and multifunctional conductive yarns for biomedical textile computing*. ACS Applied Electronic Materials, 2020. **2**(6): p. 1554-1566.
 91. Das, P.S., J.W. Kim, and J.Y. Park, *Fashionable wrist band using highly conductive fabric for electrocardiogram signal monitoring*. Journal of Industrial Textiles, 2019. **49**(2): p. 243-261.
 92. Wu, Y., S.S. Mechael, and T.B. Carmichael, *Wearable e-textiles using a textile-centric design approach*. Accounts of Chemical Research, 2021. **54**(21): p. 4051-4064.

93. Zhang, Y., et al., *Effect of Fabric Electrode Surface Coating Medium on ECG Signal Quality under Dynamic and Static Conditions*. Coatings, 2023. **13**(1): p. 108.
94. Xu, X., et al., *Screen printed graphene electrodes on textile for wearable electrocardiogram monitoring*. Applied Physics A, 2019. **125**: p. 1-7.
95. Linz, T., et al., *Contacting electronics to fabric circuits with nonconductive adhesive bonding*. Journal of the Textile Institute, 2012. **103**(10): p. 1139-1150.
96. von Krshiwoblozki, M., et al., *Electronics in textiles—adhesive bonding technology for reliably embedding electronic modules into textile circuits*. Advances in Science and Technology, 2013. **85**: p. 1-10.
97. Zysset, C., et al., *Integration method for electronics in woven textiles*. IEEE Transactions on Components, Packaging and Manufacturing Technology, 2012. **2**(7): p. 1107-1117.
98. Choi, J.-Y. and T.S. Oh, *Contact resistance comparison of flip-chip joints produced with anisotropic conductive adhesive and nonconductive adhesive for smart textile applications*. Materials transactions, 2015. **56**(10): p. 1711-1718.
99. Mehmman, A., et al. *A ball-grid-array-like electronics-to-textile pocket connector for wearable electronics*. in *Proceedings of the 2015 ACM International Symposium on Wearable Computers*. 2015.
100. Subramani, V. and S.K. Gangwal, *A review of recent literature to search for an efficient catalytic process for the conversion of syngas to ethanol*. Energy & fuels, 2008. **22**(2): p. 814-839.
101. Leśnikowski, J., *Research on poppers used as electrical connectors in high speed textile transmission lines*. Autex Research Journal, 2016. **16**(4): p. 228-235.
102. Ozturk, O. and M.K. Yapici, *Surface electromyography with wearable graphene textiles*. IEEE Sensors Journal, 2021. **21**(13): p. 14397-14406.
103. Righetti, X. and D. Thalmann. *Proposition of a modular I2C-based wearable architecture*. in *Melecon 2010-2010 15th IEEE Mediterranean Electrotechnical Conference*. 2010. IEEE.
104. Celin, S. and K. Vasanth, *ECG signal classification using various machine learning techniques*. Journal of medical systems, 2018. **42**(12): p. 241.
105. Übeyli, E.D., *Adaptive neuro-fuzzy inference system for classification of ECG signals using Lyapunov exponents*. Computer methods and programs in biomedicine, 2009. **93**(3): p. 313-321.
106. Pan, J. and W.J. Tompkins, *A real-time QRS detection algorithm*. IEEE transactions on biomedical engineering, 1985(3): p. 230-236.
107. Chua, T.W. and W.W. Tan, *Non-singleton genetic fuzzy logic system for arrhythmias classification*. Engineering Applications of Artificial Intelligence, 2011. **24**(2): p. 251-259.
108. Haseena, H.H., A.T. Mathew, and J.K. Paul, *Fuzzy clustered probabilistic and multi layered feed forward neural networks for electrocardiogram arrhythmia classification*. Journal of Medical Systems, 2011. **35**: p. 179-188.
109. Donoso, F.I., et al., *Atrial activity selection for atrial fibrillation ECG recordings*. Computers in biology and medicine, 2013. **43**(10): p. 1628-1636.
110. Fang, S.-C. and H.-L. Chan, *QRS detection-free electrocardiogram biometrics in the reconstructed phase space*. Pattern Recognition Letters, 2013. **34**(5): p. 595-602.
111. Yang, H., et al., *Spatiotemporal differentiation of myocardial infarctions*. IEEE Transactions on Automation Science and Engineering, 2013. **10**(4): p. 938-947.

112. Gutta, S. and Q. Cheng, *Joint feature extraction and classifier design for ECG-based biometric recognition*. IEEE journal of biomedical and health informatics, 2015. **20**(2): p. 460-468.
113. Afkhami, R.G., G. Azarnia, and M.A. Tinati, *Cardiac arrhythmia classification using statistical and mixture modeling features of ECG signals*. Pattern Recognition Letters, 2016. **70**: p. 45-51.
114. Nejadgholi, I., M.H. Moradi, and F. Abdolali, *Using phase space reconstruction for patient independent heartbeat classification in comparison with some benchmark methods*. Computers in biology and medicine, 2011. **41**(6): p. 411-419.
115. Chui, K.T., et al., *An accurate ECG-based transportation safety drowsiness detection scheme*. IEEE Transactions on Industrial Informatics, 2016. **12**(4): p. 1438-1452.
116. Castroflorio, T., et al., *Use of electromyographic and electrocardiographic signals to detect sleep bruxism episodes in a natural environment*. IEEE journal of biomedical and health informatics, 2013. **17**(6): p. 994-1001.
117. Li, Q., C. Rajagopalan, and G.D. Clifford, *Ventricular fibrillation and tachycardia classification using a machine learning approach*. IEEE Transactions on Biomedical Engineering, 2013. **61**(6): p. 1607-1613.
118. Mak, J.N., Y. Hu, and K.D. Luk, *An automated ECG-artifact removal method for trunk muscle surface EMG recordings*. Medical engineering & physics, 2010. **32**(8): p. 840-848.
119. Oresko, J.J., et al., *A wearable smartphone-based platform for real-time cardiovascular disease detection via electrocardiogram processing*. IEEE Transactions on Information Technology in Biomedicine, 2010. **14**(3): p. 734-740.
120. Mar, T., et al., *Optimization of ECG classification by means of feature selection*. IEEE transactions on Biomedical Engineering, 2011. **58**(8): p. 2168-2177.
121. Zhang, Z., et al., *Heartbeat classification using disease-specific feature selection*. Computers in biology and medicine, 2014. **46**: p. 79-89.
122. Gowri, T., et al. *Adaptive powerline interference removal from cardiac signals using Leaky based normalized higher order filtering techniques*. in *2013 1st International Conference on Artificial Intelligence, Modelling and Simulation*. 2013. IEEE.
123. Rahman, M.Z.U., et al., *An efficient cardiac signal enhancement using time–frequency realization of leaky adaptive noise cancelers for remote health monitoring systems*. Measurement, 2013. **46**(10): p. 3815-3835.
124. SALMAN, M.N., et al., *ADAPTIVE NOISE CANCELLERS FOR CARDIAC SIGNAL ENHANCEMENT FOR IOT BASED HEALTH CARE SYSTEMS*. Journal of Theoretical & Applied Information Technology, 2017. **95**(10).
125. Tadejko, P. and W. Rakowski. *Mathematical morphology based ECG feature extraction for the purpose of heartbeat classification*. in *6th International Conference on Computer Information Systems and Industrial Management Applications (CISIM'07)*. 2007. IEEE.
126. Fujita, N., A. Sato, and M. Kawarasaki. *Performance study of wavelet-based ECG analysis for ST-segment detection*. in *2015 38th International Conference on Telecommunications and Signal Processing (TSP)*. 2015. IEEE.
127. Zidelmal, Z., et al., *QRS detection based on wavelet coefficients*. Computer methods and programs in biomedicine, 2012. **107**(3): p. 490-496.
128. Bayasi, N., et al., *Low-power ECG-based processor for predicting ventricular arrhythmia*.

- IEEE Transactions on Very Large Scale Integration (VLSI) Systems, 2015. **24**(5): p. 1962-1974.
129. Fang, C., et al., *EMG-centered multisensory based technologies for pattern recognition in rehabilitation: state of the art and challenges*. Biosensors, 2020. **10**(8): p. 85.
 130. Zhao, S., et al., *Wearable physiological monitoring system based on electrocardiography and electromyography for upper limb rehabilitation training*. Sensors, 2020. **20**(17): p. 4861.
 131. Ahmadizadeh, C., M. Khoshnam, and C. Menon, *Human machine interfaces in upper-limb prosthesis control: A survey of techniques for preprocessing and processing of biosignals*. IEEE Signal Processing Magazine, 2021. **38**(4): p. 12-22.
 132. Tapia, C., O. Daud, and J. Ruiz-del-Solar, *EMG signal filtering based on independent component analysis and empirical mode decomposition for estimation of motor activation patterns*. Journal of Medical and Biological Engineering, 2017. **37**: p. 140-155.
 133. Wu, Q., et al., *Classification of EMG signals by BFA-optimized GSVCM for diagnosis of fatigue status*. IEEE Transactions on Automation Science and Engineering, 2016. **14**(2): p. 915-930.
 134. Avian, C., et al., *Estimating finger joint angles on surface EMG using manifold learning and long short-term memory with attention mechanism*. Biomedical Signal Processing and Control, 2022. **71**: p. 103099.
 135. Gupta, A., K.L. Mudie, and P.J. Clothier, *The reliability of determining the onset of medial gastrocnemius muscle activity during a stretch-shorten-cycle action*. Journal of Electromyography and Kinesiology, 2014. **24**(5): p. 588-592.
 136. Zhang, X. and P. Zhou, *Sample entropy analysis of surface EMG for improved muscle activity onset detection against spurious background spikes*. Journal of Electromyography and Kinesiology, 2012. **22**(6): p. 901-907.
 137. Liu, J., et al., *Robust muscle activity onset detection using an unsupervised electromyogram learning framework*. PloS one, 2015. **10**(6): p. e0127990.
 138. Too, J., et al., *A new competitive binary grey wolf optimizer to solve the feature selection problem in EMG signals classification*. Computers, 2018. **7**(4): p. 58.
 139. Yousif, H.A., et al., *Assessment of muscles fatigue during 400-meters running strategies based on the surface EMG signals*. Journal of Biomimetics, Biomaterials and Biomedical Engineering, 2019. **42**: p. 1-13.
 140. Bukhari, W., et al., *Study of K-nearest neighbour classification performance on fatigue and non-fatigue EMG signal features*. International Journal of Advanced Computer Science and Applications, 2020. **11**(8): p. 41-47.
 141. Kim, H., J. Lee, and J. Kim, *Electromyography-signal-based muscle fatigue assessment for knee rehabilitation monitoring systems*. Biomedical engineering letters, 2018. **8**: p. 345-353.
 142. Chapman, M., et al., *Perceptual, mechanical, and electromyographic responses to different relative loads in the parallel squat*. The Journal of Strength & Conditioning Research, 2019. **33**(1): p. 8-16.
 143. Whittaker, R.L., M.W. Sonne, and J.R. Potvin, *Ratings of perceived fatigue predict fatigue induced declines in muscle strength during tasks with different distributions of effort and recovery*. Journal of Electromyography and Kinesiology, 2019. **47**: p. 88-95.

144. Alam, M.M., A.A. Khan, and M. Farooq, *Effects of vibration therapy on neuromuscular efficiency & features of the EMG signal based on endurance test*. Journal of Bodywork and Movement Therapies, 2020. **24**(4): p. 325-335.
145. Cui, C., et al., *Fatigue and abnormal state detection by using EMG signal during football training*. International Journal of Distributed Systems and Technologies (IJDST), 2021. **12**(2): p. 13-23.
146. 竹中毅, *7th International Conference on Applied Human Factors and Ergonomics (AHFE 2016)*. サービスロジック, 2017. **3**(4): p. 46-46.
147. Wahyunggoro, O. and H. Nugroho, *Adaptive threshold to compensate the effect of muscle fatigue on elbow-joint angle estimation based on electromyography*. Journal of Mechanical Engineering and Sciences, 2018. **12**(3): p. 3786-3796.
148. Goubault, E., et al., *Shoulder electromyography-based indicators to assess manifestation of muscle fatigue during laboratory-simulated manual handling task*. Ergonomics, 2022. **65**(1): p. 118-133.
149. Chai, G., et al. *Study on the recognition of exercise intensity and fatigue on runners based on subjective and objective information*. in *Healthcare*. 2019. MDPI.
150. Hou, X., et al., *Immediate and delayed effects of cupping therapy on reducing neuromuscular fatigue*. Frontiers in bioengineering and biotechnology, 2021. **9**: p. 678153.
151. Park, S.Y. and C.H. Park, *Diagnosis of muscle fatigue using surface electromyography and analysis of associated factors in type 2 diabetic patients with neuropathy: A preliminary study*. International Journal of Environmental Research and Public Health, 2021. **18**(18): p. 9635.
152. Farago, E. and A.D. Chan, *Motion artifact synthesis for research in biomedical signal quality analysis*. Biomedical Signal Processing and Control, 2021. **68**: p. 102611.
153. Raza, A., et al., *Anofed: Adaptive anomaly detection for digital health using transformer-based federated learning and support vector data description*. Engineering Applications of Artificial Intelligence, 2023. **121**: p. 106051.
154. Raza, A., et al., *Designing ECG monitoring healthcare system with federated transfer learning and explainable AI*. Knowledge-Based Systems, 2022. **236**: p. 107763.
155. Hopenfeld, B., *Multiple channel electrocardiogram QRS detection by temporal pattern search*. bioRxiv, 2021: p. 2021.08. 15.456413.
156. Duan, N., et al., *Classification of multichannel surface-electromyography signals based on convolutional neural networks*. Journal of Industrial Information Integration, 2019. **15**: p. 201-206.
157. Liu, C., et al., *Signal quality assessment and lightweight QRS detection for wearable ECG SmartVest system*. IEEE Internet of Things Journal, 2018. **6**(2): p. 1363-1374.
158. Castillo-Atoche, A., et al., *Energy efficient framework for a AIoT cardiac arrhythmia detection system wearable during sport*. Applied Sciences, 2022. **12**(5): p. 2716.
159. Sun, X., et al., *Hybrid spatiotemporal models for sentiment classification via galvanic skin response*. Neurocomputing, 2019. **358**: p. 385-400.
160. Saha, S., et al., *Chirplet transform - based machine - learning approach towards classification of cognitive state change using galvanic skin response and photoplethysmography signals*. Expert Systems, 2022. **39**(6): p. e12958.
161. Hopenfeld, B., *Peak Space Motion Artifact Cancellation Applied to Textile Electrode Waist*

- Electrocardiograms Recorded During Outdoors Walking and Jogging*. bioRxiv, 2022: p. 2022.01.07.475456.
162. Hopfenfeld, B., *Segment Based Pattern Analysis Reveals a Persistent Regular Rhythm in the Motion Artifact Record of the MIT-BIH Noise Stress Test Database*. bioRxiv, 2022: p. 2022.10.18.512701.
163. *Xiaomi Mijia Cardiogram T-Shirt: Smart T-Shirt with ECG Measurement*. 2020 [cited 2023 21 February]; Available from: <https://xiaomiplanets.com/xiaomi-mijia-cardiogram-t-shirt-2/>.
164. *Athos Shirt*. 2021 [cited 2023 21 February]; Available from: <https://wearables.com/collections/athos/products/athos-shirt>.
165. *SMART SHIRT, SMARTER TRAINING*. 2016 [cited 2023 21 February]; Available from: <https://www.tymewear.com/>.
166. Gouw, A.H., et al., *Is the Tyme Wear Smart Shirt Reliable and Valid at Detecting Personalized Ventilatory Thresholds in Recreationally Active Individuals?* International Journal of Environmental Research and Public Health, 2022. **19**(3): p. 1147.
167. Bonaldi, R., *Electronics used in high-performance apparel—Part 2/2*, in *High-Performance Apparel*. 2018, Elsevier. p. 285-306.
168. *Hexoskin Health Sensors & AI*. 2012 [cited 2023 21 February]; Available from: <https://www.hexoskin.com/>.
169. Zaman, S.u., et al., *Smart E-Textile Systems: A Review for Healthcare Applications*. Electronics, 2022. **11**(1): p. 99.
170. *WHOOP | Unlock Your Potential*. [cited 2023 9.4]; Available from: <https://join.whoop.com/>.
171. *Wearable X - Digital Yoga Pants Nadi X*. [cited 2023 9.4]; Available from: <https://dressx.com/products/ar-digital-yoga-pants-wearable-x>.
172. Lyons, N.R., et al., *Washable garment-embedded textile electrodes can measure high quality surface EMG data across a range of motor tasks*. IEEE Sensors Journal, 2023.
173. Sriraam, N., A. Srinivasulu, and V. Prakash, *A Low-Cost, low-power flexible single lead ECG textile sensor for continuous monitoring of Cardiac Signals*. IEEE Sensors Journal, 2023.
174. Tao, X., et al., *Bluetooth Low Energy-Based Washable Wearable Activity Motion and Electrocardiogram Textronic Monitoring and Communicating System*. Advanced Materials Technologies, 2018. **3**(10): p. 1700309.
175. Ankhili, A., et al., *Comparative study on conductive knitted fabric electrodes for long-term electrocardiography monitoring: silver-plated and PEDOT: PSS coated fabrics*. Sensors, 2018. **18**(11): p. 3890.
176. Zhang, K., et al., *Skin Conformal and Antibacterial PPy-Leather Electrode for ECG Monitoring*. Advanced Electronic Materials, 2020. **6**(8): p. 2000259.
177. Lo, L.-W., et al., *Stretchable sponge electrodes for long-term and motion-artifact-tolerant recording of high-quality electrophysiologic signals*. ACS nano, 2022. **16**(8): p. 11792-11801.
178. Eskandarian, L., et al., *3D-Knit Dry Electrodes using Conductive Elastomeric Fibers for Long - Term Continuous Electrophysiological Monitoring*. Advanced Materials Technologies, 2022. **7**(7): p. 2101572.
179. Zalar, P., et al., *Screen-Printed Dry Electrodes: Basic Characterization and Benchmarking*.

- Advanced Engineering Materials, 2020. **22**(11): p. 2000714.
180. Huang, Y., et al., *A novel wearable flexible dry electrode based on cowhide for ECG measurement*. Biosensors, 2021. **11**(4): p. 101.
 181. Das, P.S. and J.-Y. Park, *A flexible touch sensor based on conductive elastomer for biopotential monitoring applications*. Biomedical Signal Processing and Control, 2017. **33**: p. 72-82.
 182. Cheng, X., et al., *Soft surface electrode based on PDMS-CB conductive polymer for electrocardiogram recordings*. Applied Physics A, 2019. **125**(12): p. 876.
 183. Sharma, P., et al., *Multiwall Carbon Nanotube/Polydimethylsiloxane Composites-Based Dry Electrodes for Bio-Signal Detection*. IEEE Journal on Flexible Electronics, 2024. **3**(3): p. 108-114.
 184. Tadesse, M.G., et al., *3D printing of NinjaFlex filament onto PEDOT: PSS-coated textile fabrics for electroluminescence applications*. Journal of Electronic Materials, 2018. **47**: p. 2082-2092.
 185. Song, K., et al., *A combination of logical judging circuit and water-resistant ultrathin film PEDOT: PSS electrode for noninvasive ECG measurement*. Discover Nano, 2024. **19**(1): p. 45.
 186. Maithani, Y., B. Mehta, and J. Singh, *PEDOT: PSS-treated laser-induced graphene-based smart textile dry electrodes for long-term ECG monitoring*. New Journal of Chemistry, 2023. **47**(4): p. 1832-1841.
 187. Li, G., et al., *Robust, self - adhesive, and low - contact impedance polyvinyl alcohol/polyacrylamide dual-network hydrogel semidry electrode for biopotential signal acquisition*. SmartMat, 2023: p. e1173.
 188. Li, G., et al., *Polyvinyl alcohol/polyacrylamide double-network hydrogel-based semi-dry electrodes for robust electroencephalography recording at hairy scalp for noninvasive brain-computer interfaces*. Journal of Neural Engineering, 2023. **20**(2): p. 026017.
 189. Li, G., et al., *Towards real-life EEG applications: Novel superporous hydrogel-based semi-dry EEG electrodes enabling automatically 'charge-discharge'electrolyte*. Journal of Neural Engineering, 2021. **18**(4): p. 046016.
 190. Li, G.-L., et al., *Review of semi-dry electrodes for EEG recording*. Journal of Neural Engineering, 2020. **17**(5): p. 051004.
 191. Li, G., et al., *Towards emerging EEG applications: A novel printable flexible Ag/AgCl dry electrode array for robust recording of EEG signals at forehead sites*. Journal of Neural Engineering, 2020. **17**(2): p. 026001.
 192. Murciego, L.P., et al., *A Novel Screen-Printed Textile Interface for High-Density Electromyography Recording*. Sensors, 2023. **23**(3): p. 1113.
 193. Li, B.M., et al., *Influence of armband form factors on wearable ECG monitoring performance*. IEEE Sensors Journal, 2021. **21**(9): p. 11046-11060.
 194. Xu, X., et al., *Washable and flexible screen printed graphene electrode on textiles for wearable healthcare monitoring*. Journal of Physics D: Applied Physics, 2020. **53**(12): p. 125402.
 195. Bu, Y., M.F.U. Hassan, and D. Lai, *The embedding of flexible conductive silver-coated electrodes into ECG monitoring garment for minimizing motion artefacts*. IEEE Sensors Journal, 2020. **21**(13): p. 14454-14465.

196. Lam, E., et al., *Exploring textile-based electrode materials for electromyography smart garments*. Journal of Rehabilitation and Assistive Technologies Engineering, 2022. **9**: p. 20556683211061995.
197. Nigusse, A.B., B. Malengier, and L. Van Langenhove, *Development and Evaluation of a Wearable ECG Monitoring System*. Engineering Proceedings, 2024. **52**(1): p. 9.
198. Fink, P.L., et al., *Development and wearer trial of ECG-garment with textile-based dry electrodes*. Sensors and Actuators A: Physical, 2021. **328**: p. 112784.
199. Yang, K., et al., *Waterproof and durable screen printed silver conductive tracks on textiles*. Textile Research Journal, 2013. **83**(19): p. 2023-2031.
200. Ojstršek, A., L. Jug, and O. Plohl, *A review of electro conductive textiles utilizing the dip-coating technique: their functionality, durability and sustainability*. Polymers, 2022. **14**(21): p. 4713.
201. Colli Alfaro, J.G. and A.L. Trejos, *Design and fabrication of embroidered textile strain sensors: An alternative to stitch-based strain sensors*. Sensors, 2023. **23**(3): p. 1503.
202. Gunnarsson, E. and F. Seoane, *Three-lead in vivo measurement method for determining the skin-electrode impedance of textile electrodes: A fast, accurate and easy-to-use measurement method suitable for characterization of textile electrodes*. Textile Research Journal, 2023. **93**(21-22): p. 5124-5139.
203. Franke, T.P., F.J. Backx, and B.M. Huisstede, *Lower extremity compression garments use by athletes: why, how often, and perceived benefit*. BMC Sports Science, Medicine and Rehabilitation, 2021. **13**: p. 1-14.
204. Lozo, M., et al., *Designing compression of preventive compression stockings*. Journal of Engineered Fibers and Fabrics, 2021. **16**: p. 15589250211060406.
205. Reza, M.S., et al., *Electrospun Rubber Nanofiber Web-Based Dry Electrodes for Biopotential Monitoring*. Sensors, 2023. **23**(17): p. 7377.
206. Jose, M., et al., *Fully printed, stretchable and wearable bioimpedance sensor on textiles for tomography*. Flexible and Printed Electronics, 2021. **6**(1): p. 015010.
207. Kralikova, I., B. Babusiak, and M. Smondrk, *Measurement of the conductive fabric contact impedance for bioelectrical signal acquisition purposes*. Measurement, 2023. **217**: p. 113005.
208. Goyal, K., D.A. Borkholder, and S.W. Day, *A biomimetic skin phantom for characterizing wearable electrodes in the low-frequency regime*. Sensors and Actuators A: Physical, 2022. **340**: p. 113513.
209. Kim, S., S. Lee, and W. Jeong, *EMG measurement with textile-based electrodes in different electrode sizes and clothing pressures for smart clothing design optimization*. Polymers, 2020. **12**(10): p. 2406.
210. Alizadeh-Meghrazi, M., et al., *Evaluation of dry textile electrodes for long-term electrocardiographic monitoring*. Biomedical engineering online, 2021. **20**(1): p. 1-20.
211. Goyal, K., D.A. Borkholder, and S.W. Day, *Dependence of Skin-Electrode Contact Impedance on Material and Skin Hydration*. Sensors, 2022. **22**(21): p. 8510.
212. Thakor, N., J. Webster, and W. Tompkins, *Optimal QRS detector*. Medical and Biological Engineering and Computing, 1983. **21**: p. 343-350.
213. Li, Q., R.G. Mark, and G.D. Clifford, *Robust heart rate estimation from multiple asynchronous noisy sources using signal quality indices and a Kalman filter*. Physiological

- measurement, 2007. **29**(1): p. 15.
214. Castro, I.D., et al., *Evaluation of a multichannel non-contact ECG system and signal quality algorithms for sleep apnea detection and monitoring*. Sensors, 2018. **18**(2): p. 577.
215. Li, G., S. Wang, and Y.Y. Duan, *Towards conductive-gel-free electrodes: Understanding the wet electrode, semi-dry electrode and dry electrode-skin interface impedance using electrochemical impedance spectroscopy fitting*. Sensors and Actuators B: Chemical, 2018. **277**: p. 250-260.
216. Goyal, K. and S.W. Day, *Factors Affecting Wearable Electrode Performance and Development of Biomimetic Skin Phantom*. 2023.
217. Besomi, M., et al., *Consensus for experimental design in electromyography (CEDE) project: Electrode selection matrix*. Journal of Electromyography and Kinesiology, 2019. **48**: p. 128-144.
218. Makowski, D., et al., *NeuroKit2: A Python toolbox for neurophysiological signal processing*. Behavior research methods, 2021: p. 1-8.